UNIVERSITY OF SOUTHAMPTON

FACULTY OF ENGINEERING, SCIENCE & MATHEMATICS

OPTOELECTRONICS RESEARCH CENTRE

HIGH-POWER TWO-MICRON FIBRE-BULK HYBRID LASERS

by

Amin Abdolvand

Thesis submitted for the degree of Master of Philosophy

November 2004

UNIVERSITY OF SOUTHAMPTON

ABSTRACT

FACULTY OF ENGINEERING, SCIENCE & MATHEMATICS
OPTOELECTRONICS RESEARCH CENTRE

Master of Philosophy

HIGH POWER TWO-MICRON FIBRE-BULK HYBRID LASERS

by Amin Abdolvand

The design of high-power efficient solid-state lasers with good output beam quality has long been a general goal of many researchers within the solid-state laser community. Progress towards the realization of such solid-state lasers has mainly been limited by poor brightness and limited choice of operating wavelengths of the optical sources available to pump such lasers.

This thesis presents the results of an investigation into a new approach for power and brightness scaling of two-micron solid-state lasers. The strategy described in this thesis is based on reduction of heat generation and heat loading within the laser medium. This was achieved by employing a fibre-bulk hybrid scheme; where a high-power diode-pumped double-clad fibre laser is used to end pump a bulk solid-state laser. Thus, the work described here is split into two related research areas.

The first area of research was devoted to the construction of a high-power, tunable two-micron source based on thulium(Tm)-doped silica fibre. The result was a tunable Tm fibre laser that produced a maximum output power of 10.5W at a wavelength of 1921nm for 44W of launched diode power at 790nm. The output of the laser was tunable over a wavelength range of 215nm from 1855nm to 2070nm at multi-watt power levels, and over 150nm from 1860nm to 2010nm at output power levels in excess of 9W.

In this part of the research results for the first wavelength-combined Tm-doped silica fibre laser system with maximum output power of 14W on four lines at wavelengths, 1926nm, 1957nm, 1980nm and 2000nm, have also been presented. The aim of this work was to explore a new concept for power scaling in fibre lasers. The beam-combined system was tunable over a range of 200nm from 1900nm to 2100nm at multi-watt power levels, and over a range of 120nm, from 1900nm to 2020nm, at power levels in excess of 10W. Beam propagation factors, M^2, of the beam-combined laser system were equal to; $M_x^2 \approx 4.9$ and $M_y^2 \approx 4$, in the *x*-*z* and *y*-*z* planes, respectively. Potential sources of degradation in beam quality of the system were also investigated.

In the second part of the research a high-power tunable Tm-doped silica fibre laser was used to end-pump a Ho:YAG crystal. Ho:YAG has been chosen due to its robust thermo-mechanical properties and favourable spectroscopic characteristics. Highly efficient room-temperature operation of a Ho:YAG laser has been demonstrated. 5.2W of output at 2097nm in a near diffraction-limited beam from a Ho:YAG laser was achieved using 9.1W of incident pump power from a Tm-doped silica fibre laser at 1905nm. The slope efficiency with respect to incident pump power (80%) was close to the theoretical maximum taking into account the pump absorption efficiency, resonator losses and output coupling loss. The optical-to-optical efficiency of the laser was 57%. Room-temperature laser operation of Ho:YAG lasers with different Ho^{3+} concentrations was also investigated. The design and performance of these lasers for highly efficient continuous-wave operation is briefly discussed.

List of Contents

Appendices

List of Tables

List of Figures

Acknowledgements

During the course of the research presented here I have been helped by many people at the Optoelectronics Research Centre (ORC). I am, and will be, eternally grateful to all of them for their help, support and encouragement.

In particular my sincere thanks must go to my supervisor, Professor Andy Clarkson, who contributed so much to help me with his interest, ideas, encouragement and enthusiasm.

I must also express my deep gratitude to Dr. Deyuan Shen with whom I have worked especially closely on several aspects of the work.

Many thanks to the rest of the Optical Physics Group, Dr. Tim Kendall (former member), Dr. Ian Musgrave (former member), Enzo Matera (former member), Dr. Pu Wang, Dr. Martin O'Connor, Dr. Jacob Mackenzie, Dr. Collin Sones, Dr. Valery Philippov, Professor Rob Eason, Professor David Hanna, and also Laurence Cooper from the fibre fabrication group. They have helped me throughout in many different ways and I am very grateful to them all.

I would also like to express my thanks and gratefulness to the secretaries of the ORC. Special mention must go to Mrs Eve Smith who has kindly helped me on innumerable occasions.

Many thanks must go to the technical stuff of the ORC, specially Simon Butler and Chris Nash. I am very grateful to them both.

Thanks are due to EPSRC and QinetiQ/Dstl for supplying the research grant.

And finally but most importantly I would like to thank my wife, Natalie and my daughter, Diana, for support, encouragement and willingly offered sacrifices during the time we spent in England. I love you dearly.

Chapter 1

Introduction and General Aims

In this chapter a review of solid-state lasers operating in the two-micron spectral region, and some of their applications are discussed. The demands and progresses toward power scaling of two-micron solid-state lasers are also described. General aims and the motivation for the research presented in this thesis are then presented. In the final section of this chapter an overview of the thesis is given.

1.1. Overview of Mid-infrared solid-state lasers

Mid-infrared solid-state laser sources have many applications in the areas of medicine, communications and laser radar or lidar (Light Detection And Ranging). For many of these applications the wavelength, pulse energy, and pulse duration of the laser source are of primary importance [Measure92]. These requirements as well as the size, reliability, ease-of-use and efficiency, limit the choice to solid-state or CO_2 gas lasers. Eye-safety is another advantage offered by laser sources operating in this spectral region. This is due to the fact that in the visible region all the laser light entering the human eye is focused to a spot of a few μm size on the retina, while light in the region of 1.4μm to ~2.2μm is absorbed at the cornea before it reaches the retina. At wavelengths in the near-infrared region only a part of the light is absorbed. From here on the term "eyesafe wavelength" will be used for wavelengths from ~1.4μm to ~2.2μm.

Table 1.1 gives a summary of some of the transitions of rare-earth ions in the eyesafe-wavelength region, which have been utilised for laser operation. All of

the transitions given here have been demonstrated in lasers pumped by near-infrared diode lasers (Ho^{3+} lasers co-doped with Tm^{3+} and/or in an intracavity configuration and Er^{3+} at 1.5μm co-doped with Yb^{3+}).

Laser Host	**λ, nm**	**Reference**
Nd^{3+}:YAG	1444	[Kretschmann97]
Er^{3+}:Glass	1535	[Laporta93]
Er^{3+}:YAG	1623	[Kubo92]
Er^{3+}:YLF	2810	[Dergachev03]
Tm^{3+}:YVO_4	1870	[Hauglie-Hanssen94]
Tm^{3+}:YAG	2013	[Kmetec94, Bollig98, Lai00]
Ho^{3+}:YLF	2067	[McGuckin92]
Ho^{3+}:YAG	2091, 2097	[Storm90, Bollig98, Budni00]

Table 1.1: Typical lasers using rare-earth-ion transitions in the eyesafe wavelength region.

Although the 1.4μm transition of Nd:YAG and the 1.9μm transition in Tm:YVO_4 make these lasers attractive for some medical applications [Kretschmann97, Hauglie-Hanssen94], however for certain types of surgery a short water-absorption length is required, which favours Er^{3+} laser around 2.8μm [Jensen96, Dergachev03], where water has an absorption length of the order of a few μm. Tm^{3+} lasers operating near 2μm can be very efficient due to the two-for-one cross-relaxation process, which can excite two thulium ions into the upper laser level for each absorbed pump photon [Shaw94].

The main application of interest for this work is 2μm lasers suitable for atmospheric lidar. Except for the Er^{3+} lasers near 1.5μm and the Tm^{3+} and Ho^{3+} lasers operating between 2.0μm and 2.1μm, the atmospheric absorption is too strong to allow efficient transmission over several kilometres for all the other lasers listed in the table 1.1 and so are not suited for long distance remote sensing. Er:glass lasers are difficult to operate at high end-pumped power levels because of the poor thermal properties of glass.

Nd:YAG and CO_2 lasers have extensively been used as the source for lidar systems. The Nd:YAG systems used for lidars, emitting at 1064nm, are not eye-safe. This disadvantage can be overcome by using the Nd laser as a source for nonlinear frequency conversion schemes to the mid-infrared however, at the

expense of complexity of the system. CO_2 lidar systems require a cooled detection system and gas supplies have to be replenished to increase their life time.

Table 1.2 shows the double-pass extinction in clear air for a number of potential atmospheric lidar sources. The double pass extinction is given as the returning backscattered signal for lidars which must traverse twice the air path length. From table 1.2 it can be seen that the Ho:YAG and Tm:YAG lasers output wavelengths have a longer atmospheric extinction length as compare to the CO_2 emission.

Laser Host	**λ, nm**	**Extinction, dB/km**
Tm^{3+}:YAG	2013	1.3
Tm^{3+}:(Lu,Y)AG	2022	0.8
Ho^{3+}:YAG	2091	0.5
CO_2	10591	2.7

Table 1.2: Double-pass extinction in clear air for some potential atmospheric lidar sources [Henderson93].

The long upper level lifetime of Tm and Ho, 10.9ms and 7.2ms, respectively [Fan88], offers the potential for high-energy (cw-pumped) Q-switched operation as required for many lidar applications. In addition, the Ho:YAG emission sits in a region of the atmospheric absorption spectrum that has fewer absorption features than other lasers operating at 2μm. An informative review of the use of solid-state lasers in lidar systems at 2μm, is given by [Henderson93].

However, while 2μm solid-state lasers hold the potential to become excellent sources for lidar systems, several problems have been faced in the development of efficient, high-power 2μm solid-state lasers. These problems will be addressed in the next section.

1.2. 2μm solid-state lasers

In the previous section, it was seen that the two most attractive materials for lidar applications are thulium at 2μm and holmium at 2.1μm. Table 1.3 gives data, which illustrates the relative spectroscopic properties of Tm^{3+} and Ho^{3+} in YAG relative to another promising candidate for lidar applications, Nd:YAG. The

lasing wavelength as well as the higher emission cross section of Ho:YAG favours this material to the 2.01μm transition of Tm:YAG.

Material	**Ho^{3+}:YAG**	**Tm^{3+}:YAG**	**Nd^{3+}:YAG**
Wavelength, nm	2097	2013	1064
$\sigma_{stimulated\ emission}$, cm^2	$1.5x10^{-20}$	$2x10^{-21}$	$3x10^{-19}$
Saturation Fluence, Jcm^{-2}	10	50	0.6
Upper laser level life time, ms	7.2	10.9	$230x10^{-3}$

Table 1.3: Selected laser parameters of Ho:YAG and Tm:YAG compared with Nd:YAG.

As it can be seen from table 1.3, the stimulated emission cross sections in Ho:YAG and Tm:YAG are more than an order of magnitude smaller than that of Nd:YAG at 1064nm, which leads to lower gain. Another problem is the high saturation fluence of these materials [Koechner99]. This is due to the fact that for efficient extraction of stored energy a laser must operate at an intracavity fluence comparable to or greater than the saturation fluence. This in turn increases the risk of damage to laser components. Furthermore, the laser transition for Tm and Ho terminate in the ground state level of the ion, resulting in a quasi-three level laser system. Therefore, significant pump power must be absorbed just to bring the laser crystal to transparency.

Singly doped holmium lasers cannot be efficiently pumped with high-power near-infrared diode bars [Fan88]. One way to solve this problem with holmium lasers is by using diode pumping with both thulium and holmium doped into the same rod. In this way a thulium ion could absorb one pump photon at ~785nm. The excited thulium ion interacts with another thulium ion in the ground state, and this results in two excited thulium ions. However this happens if the concentration of Tm ions is high enough. This excitation carries on through the crystal by the ion-ion interaction, until an excited thulium ion interacts with a holmium ion. The excitation of the Ho ions then contributes to the population inversion which drives the laser. Therefore one pump photon can actually provide two excited Ho ions, improving the quantum efficiency. However, this form of excitation has some disadvantages. There is thermal equilibrium between the excited Ho and Tm ions. The energy transfer process between the two ions has a finite timescale, and so not

all of the expected excitation density is available when the Ho laser is Q-switched. There are also other undesirable energy transfer mechanisms. Essentially strong upconversion effects in Tm^{3+}-Ho^{3+} co-doped lasers have so far prevented their extensive use in lidar applications [Fan88]. One example where upconversion is less severe is in the case of the Tm,Ho:YLF crystal. For example, pulse energies of up to 6mJ have been reported with pumping by a single cw 20W diode bar [Finch95]. However, the upconversion losses are very sensitive to temperature and because of that Q-switched operation required the cooling of the rod to a temperature as low as –63°C. In addition, YLF is much more fragile than YAG, leading to an increased likelihood of thermal fracture when pumped at high power levels. One important disadvantage of Ho in YLF is that the operating wavelength around 2065nm has a significantly higher atmospheric propagation loss due to molecular absorption and scattering as well as aerosol absorption than the 2091nm line in Ho:YAG [Henderson93]. The upconversion effects in Tm,Ho:YAG and thermal problems with Tm,Ho:YLF have led many researchers to return to singly doped Tm lasers as sources for lidar applications [Wagener95, Grund97, Honea97, Lai00]. The thulium laser can work with diode pumping at 785nm. This can yield a highly efficient process whereby for every pump photon absorbed at 785nm, the laser can produce two laser photons. This process, commonly called "Two-for-one" cross-relaxation, is an inter-ionic $Tm^{3+} \rightarrow Tm^{3+}$ process that, as briefly discussed, has many advantages not only in regard to pumping efficiency but also with the thermal loading of the laser. However, the lower gain associated with thulium lasers bring with them their own challenges. Still, output powers as high as 115W in an end-pumped configuration [Honea97] and 120W in a side-pumped scheme [Lai00] have been achieved.

Upconversion problems associated with Tm,Ho co-doped lasers can be avoided by using an intracavity pumping scheme with thulium and holmium ions separated in two different rods in the same cavity [Stoneman92, Bollig98]. Recently Budni *et. al.* demonstrated 19W Ho:YAG laser intracavity pumped by a diode-pumped Tm:YLF laser. The diode-to-holmium optical-optical conversion efficiency achieved was 18% [Budni00]. Also lately Dergachev *et. al.* reported an

efficient Ho:YLF laser end-pumped by a diode-pumped Tm:YLF laser. That laser produced 21W cw power and 37mJ of pulse energy in the Q-switched regime at 2.06μm [Dergachev03]. However, in the mentioned approach further power scaling, and more importantly, further brightness scaling is limited by the brightness scalability of the thulium pumped lasers themselves due to the effects of thermal loading. A further drawback of these approaches is that there is limited scope for flexibility in pump wavelength making it difficult to precisely match it with the holmium absorption maximum and to explore the use of other Ho-doped crystals, which also have some attractive spectroscopic properties [Walsh98].

The next section presents an attractive solution to these problems and represents the motivation for this research.

1.3. 2μm fibre-bulk hybrid laser

Demands in power and brightness scaling of 2μm solid-state lasers have been presented in the previous section. One attractive and efficient solution to these problems is to use a high-power Tm-doped silica fibre laser operating in the 1.85-2.1μm region with good output beam quality to pump Ho:YAG and/or other promising holmium doped crystals in a fibre-bulk hybrid scheme.

The fibre laser offers a high brightness pump source and can be efficiently pumped by high-power diode bars. Its wavelength can be tuned to match an absorption transition of the bulk laser, by using a grating. The heat input to the bulk laser can be minimized by in-band pumping, setting the pump wavelength very close to the emission wavelength. Heat generation can be further reduced by using long lengths of crystal with low concentration and hence minimising upconversion effects owing to the good output beam quality of the fibre. The quasi-three level transition of the bulk materials require intense pumping. This in fact is offered by the fibre laser. Hence the fibre-bulk hybrid scheme provides the combined wavelength flexibility and high brightness offered by high-power fibre lasers and high pulse energies that can be extracted from the conventional bulk lasers. Therefore, the best attributes of both are used.

1.4. Overview of thesis

This chapter discussed the general aims and motivation for research towards power and brightness scaling in 2μm solid-state lasers. The idea behind the 2μm fibre-bulk hybrid laser was also briefly discussed. Chapter 2 will discuss the demands of power scaling in end-pumped solid-state lasers. Features of bulk and fibre lasers in the context of power scaling will also be presented and discussed. The thesis has then been divided into two related parts.

The first part is devoted to high-power, two-micron fibre lasers. Chapter 3 reports work conducted on developing a high-power tunable Tm-doped silica fibre laser. The aim was to develop a pump source for various high-power Ho^{3+}:YAG lasers. Chapter 4 presents work carried out to explore a route for power scaling in Tm-doped silica fibre lasers.

The second part is dedicated to two-micron fibre-bulk hybrid lasers. Chapter 5 presents the spectroscopic characteristics of Ho^{3+} ions in YAG. It also reports highly efficient cw operation of a Ho:YAG laser end-pumped by a Tm-doped silica fibre laser. Conclusions and suggestions for future work are then given in chapter 6.

1.5. References

[Bollig98] C. Bollig, W.A. Clarkson, R.A. Hayward, D.C. Hanna, "Efficient high power Tm:YAG laser at 2μm end-pumped by a diode-bar", Optics Communications , Vol.154(1-3), pp.35-38(1998).

[Bollig98] C. Bollig, R.A. Hayward, W.A. Clarkson, D.C. Hanna, "2W Ho:YAG laser intracavity pumped by a diode-pumped Tm:YAG laser", Optics Letters, vol.23(22) pp.1757-9(1998).

[Budni00] P.A. Budni, M.L. Lemons, J.R. Mosto, and E.P. Chicklis, "High-Power/High-Brightness Diode-Pumped 1.9um Thulium and Resonantly Pumped 2.1um Holmium Lasers,", IEEE Journal of quantum Electronics, vol. 6(4), pp. 629-634 (2000).

[Dergachev03] A. Dergachev, P. Moulton, "Tunable CW Er:YLF diode-pumped laser,", ASSP 2003 San Antonio USA 2-6 Feb 2003 MA2.

[Dergachev03] A. Dergachev, P. Moulton, "High-power, high-energy diode-pumped

Tm:YLF-Ho:YLF laser,", *ASSP 2003* San Antonio USA 2-6 Feb 2003 PD10.

[Fan88] T.Y. Fan, G. Hubber, R.L. Byer and P. Mitzscherlich, "Spectroscopy and diode laser pumped operation of Tm,Ho:YAG, ", IEEE Journal of quantum Electronics, vol. 24(6), pp. 924-933 (1988).

[Finch95] A. Finch and J.H. Flint, "Diode-pumped 6mJ repetively Q-switched Tm,Ho:YLF laser," in Conference on lasers and Electro-Optics, vol.15 of 1995 OSA Technical Digest Series, p.232 (OSA, 1995)

[Hauglie94] C. Hauglie-Hanssen and N. Djeu, "Further investigation of a 2μm Tm:YVO_4 laser, " IEEE Journal of quantum Electronics, vol. 30(2), pp. 275-279 (1994).

[Henderson93] S.W. Henderson, P.J.M. Suni, C.P. hale, S.M. Hannon, J.R. Magee, D.L. Burns and E.H. Yuen, "Coherent laser radar at 2 um using solid-state lasers," IEEE Transactions on Geoscience and Remote Sensing, vol.31 (1), pp.4-15 (1993).

[Honea97] E. C. Honea, R.J. Raymond, S.B. Sutton, J.A. Speth, S.C. Mitchell, J. A. Skidmore, M. A. Emanuel and S. A. Payne, "115W Tm:YAG Diode-pumped Solid-State Laser," IEEE J. Quantum Electron, 33 (9), 1592 (1997)

[Grund97] C.J. Grund, S.A. Cohn and S.D. Mayer, "The high resolution Doppler lidar: Boundary layer measurements applications and performance," in 9^{th} conference on coherent laser radar, pp.308-311 (1997)

[Jensen96] T. Jensen, A. Diening, G. Huber and B.H. T. Chai, "Investigation of diode-pumped 2.8um Er:$LiYF_4$ lasers with various doping levels," Optics Letters, vol.21(8), pp. 585-587(1996).

[Kmetec94] J. D. Kmetec, T. S. Kubo, T. J. Kane and G.J. Grund, "Laser performance of diode-pumped Thulium-doped $Y_3Al_5O_{12}$, $(Y,Lu)_3Al_5O_{12}$ and $Lu_3Al_5O_{12}$ crystals," Optics Letters, vol. 19(3), pp. 186-188(1994).

[Koechner99] W. Koechner, Solid-State Laser Engineering, Springer-Varlag, Berlin Heidelberg, 1999)

[Kretschmann97] H.M. Kretschmann, F. Heine, V.G. Ostroumov and G. Huber, "High-power diode-pumped cw Nd^{3+} lasers at wavelengths near 1.44um ", Optics Letters, vol.22(7), pp.466-468(1997).

[Kubo92] T.S. Kubo and T.J. Kane, "Diode-pumped lasers at five eyesafe wavelengths," IEEE Journal of quantum Electronics, vol. 28(4), pp. 1033-1040 (1992).

[Lai00] K.S. Lai, P.B. Phua, R.F. Wu, E. Lau, S.W. Toh, B.T. Toh and A. Chug, "120W continuous-wave diode-pumped Tm:YAG laser," Optics Letters, vol.25 (21), pp.1591-1593 (2000).

[Laporta93] P. Laporta, S. Taccheo, S. Longhi, O. Svelto and G. Sacchi, "Diode-pumped microchip Er-Yb:glass laser," Optics Letters, vol. 18(15), pp. 1232-1234(1993).

[McGuckin92] B.T. McGuckin and R.T. Menzies, " Efficient cw diode-pumped Tm,Ho:YLF laser with tunability near 2.067um,", IEEE Journal of quantum Electronics, vol. 28(4), pp. 1025-1028 (1992).

[Measure92] Measures R.M., 1992, Laser Remote Sensing: Fundamentals and Applications (Krieger Publishing Company, Malabar, Florida.

[Shaw94] L.B. Shaw, R.S. Chang and N. Djeu, "Measurment of up-conversion energy transfer probabilities in Ho:YAG and Tm:YAG,", Phys. Rev. B, vol. 50, pp. 6609-6619 (1994).

[Stoneman92] R.C. Stoneman and L. Esterowitz, "Intracavity-pumped 2.09um Ho:YAG laser," Optics Letters, vol.17 (10), pp.736-736 (1992)

[Storm90] M.E. Storm, "Single-mode lasing of Ho:Tm:YAG at 2.091um in a monolithic crystal,", in Advanced Solid State Lasers, edited by H.P. Jenssen and G. Dube, vol. 6 of OSA Proceedings, pp. 140-143 (OSA, 1990).

[Wagener95] T.J. Wagener, N. Demma, J.D. Kmetec and T.S. Kubo, "2um lidar for laser based remote sensing: Flight demonstration and application survey," IEEE Aerospace and Electronics Systems magazine, vol. 10(2), pp. 23-28 (1995)

[Walsh98] B.M. Walsh, N.P. Barnes and B. DiBartolo, "Branching rations, cross-section and radiative lifetimes of rare earth iones in solids: Application to Tm^{3+} and Ho^{3+} ions in $LiYF_4$," J. Appl. Phys., 83, 2772-2787 (1998).

Chapter 2

Review of Elements of Power-Scaling in End-Pumped Solid-State Lasers: Crystal versus Fibre

Research on scaling of the output power and brightness of diode laser end-pumped solid-state lasers has, for a long time, occupied many researchers within the laser community. This was mainly due to the high efficiency, reliability and compactness of these sources. In this chapter the fundamental problems of power and brightness scaling in end-pumped solid-state lasers are discussed. In the context of power scaling, bulk and fibre lasers are compared. Throughout this chapter problems and demands associated with power and brightness scaling of these lasers and some of the strategies that are currently in use in the literature to meet these demands are discussed. This chapter also provides the essential theoretical background for the rest of this thesis.

Here and throughout the thesis, “power-scaling” is generally intended to mean increasing the output power of a laser whereas “brightness-scaling” is intended to mean increasing the output power of a laser whilst maintaining good beam quality (near diffraction-limited output).

2.1. Bulk lasers

In the past two decades solid-state laser technology has been revolutionised due to the rapid improvement of diode-laser pump sources [Byer88]. This was due to higher spectral and spatial brightness offered by diode laser sources compared to

conventional lamp sources. Consequently it became possible to demonstrate good laser performance of several transitions in rare-earth ions at room temperature that performed poorly or not at all under lamp pumping. Examples of these include: 2.1μm transition in Ho^{3+} [Hemmati89 and McGuckin92], near 2.0μm in Tm^{3+} [Kemetec94], 1.5μm in Er^{3+} [Hutchinson92] and 1.0μm in Yb^{3+} [Lacovara91]. These transitions are commonly referred to as "quasi-three-level" transitions. All the laser transitions investigated in this work have a quasi-three-level scheme. Hence, first a detailed study of quasi-three-level lasers is presented. Conditions for efficient room-temperature laser operation on these transitions is also discussed.

Whilst the advantages of diode-pumping have enabled the development of many solid-state laser devices, designing a high power laser with good beam quality has proved to be a rather difficult task. The main obstacle is thermal effects in the laser medium. These effects and strategies to reduce them are the subject of the second part of this section.

2.1.1. Quasi-three level laser behaviour

In a quasi-three-level laser transition the lower laser level is in the ground-state multiplet. This means that the lower laser level is only a few hundred wavenumbers (cm^{-1}) above the ground state. Thus, the lower laser level can be significantly populated in thermal equilibrium at room temperature, since kT is $207cm^{-1}$ at $300K$ (where k is the Boltzman constant $\sim 1.38054 \times 10^{-23}$J/K and T is the temperature of the host material in Kelvin). This population is as a result of a rapid thermal relaxation satisfying a Boltzman distribution between levels. This relaxation rate is much faster than any other rates that are typical in solid-state lasers and thus leads to the quasi-thermal equilibrium approximation for relative population of Stark levels, crystal field splittings, within the lower laser level manifold [Hall84, Byer88]. Thus the relative populations of Stark levels can be treated as if they are in thermal equilibrium with each other at all times. An idealized quasi-three-level laser transition is shown in figure 2.1.

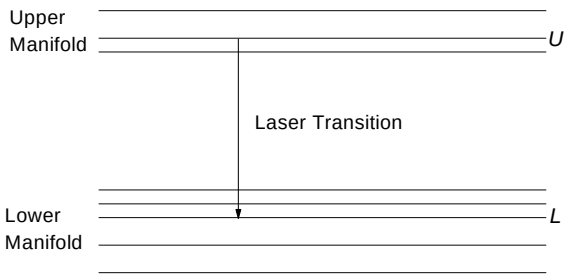

Figure 2.1: Upper and lower manifolds of an idealized quasi-three-level laser.

Upper and lower manifolds are each split by a crystal field. The fraction of the total number of ions in the level *L* of the lower manifold can be determined by

$$f_L = \frac{\exp(-E_{lL} / kT)}{Z_l} \qquad (2.1)$$

where

$$Z_l = \sum_{i=1}^{m} \exp(-E_{li} / kT) \qquad (2.2)$$

f_L is the fractional population within the level *L*, E_{lL} is the energy of the level *L*, *kT* is the thermal energy (*k* is the Boltzman constant and *T* is the temperature of the host in Kelvin), Z_l is the partition function of the lower manifold, and E_{li} are the energies of the levels in the lower manifold which has m levels [Fan87]. f_U, is the fractional population of the level *U* within the upper manifold can be likewise found by calculating the partition function over the levels of the upper manifold.

2.1.1.1. Laser gain

Population inversion in the laser medium is the essential condition for laser gain [Koechner99], and means that the population density of the upper laser level is greater than that of the lower level. If we assume that N_2 and N_1 are the total population densities of the upper and lower manifolds of the laser transition (see figure 2.1), then for laser gain on the transition between levels *U* and *L* we have

$$f_U N_2 > f_L N_1 \qquad (2.3).$$

Thus, the minimum fraction of the population in the upper manifold, PU_{min}, required to obtain population inversion in laser medium is given by

$$PU_{\min} = \frac{N_2}{N_1 + N_2} = \frac{f_L}{f_L + f_U} \qquad (2.4).$$

For example in the ${}^5I_7 \rightarrow {}^5I_8$ transition of Ho^{3+} in YAG near 2.1μm at 300*K*, 13% of the population needs to be in the upper manifold in order to attain population inversion (see chapter 5).

2.1.1.2. Threshold

The threshold pump power for an end-pumped quasi-three-level laser, when Gaussian pump and cavity mode intensity profiles are assumed, is given by [Fan87]

$$P_{th} = \frac{\pi h \nu_P (w_L^2 + w_P^2)}{4\eta_{abs}\eta_{p-q}(f_L + f_U)\sigma\tau}\left(2N_t f_L \sigma\ell + T + L\right) \qquad (2.5)$$

where w_p and w_L are the Gaussian beam radii for the pump beam and laser cavity mode respectively and ν_{p} is the pump frequency. σ and τ are the atomic cross section of the laser transition and the lifetime of the upper manifold, respectively, and f_{U} and f_{L} are the fractional population of the Stark levels, which constitute the upper and lower laser level. *T* and *L* are the output coupler transmission and the resonator loss and ℓ is the laser rod length. N_t is the concentration of active ions in the laser host, and $\eta_{p\text{-}q}$ is the pump quantum efficiency that is the average number of ions in the upper manifold created per absorbed pump photon. η_{abs} is the pump absorption efficiency that is the fraction of incident pump radiation absorbed over the length of the laser rod and for no pump-induced ground-state-depletion [Krupke90] is given by

$$\eta_{abs} = 1 - \exp(-\alpha\ell) \qquad (2.6)$$

where α is the absorption efficiency.

In contrast, the threshold pump power for an end-pumped four-level laser where the lower laser level is a few *kT* above the ground state and thus can be considered unpopulated in thermal equilibrium, is given by [Fan87, Risk88].

$$P_{th} = \frac{\pi h\nu_P (w_L^2 + w_P^2)}{4\eta_{abs}\eta_{p-q}\sigma\tau}(L + T). \qquad (2.7)$$

Comparison of equations 2.5 and 2.7 shows that the threshold pump power for quasi-three-level lasers has an additional term, $2f_L\sigma N_t\ell$ and an inverse proportional relationship to the term (f_L+f_U). The term $2f_L\sigma N_t\ell$ in equation 2.5 is equal to the round-trip absorption at the laser wavelength for the laser medium in thermal equilibrium due to the finite lower laser level population. It is often called "re-absorption loss". Thus in order to reduce the power required for reaching the population inversion in the quasi-three-level lasers, one has to reduce the re-absorption loss. It can be seen that in $f_L\sigma N_t\ell$, the additional loss is proportional to the fractional population of the lower laser level $f_L N_t$, and the length of the laser rod ℓ.

It is also worth noting that as the fractional populations of the upper and lower laser levels in equation 2.5, f_U and f_L, tend towards the four-level case, i.e. $f_U \to 1$ and $f_L \to 0$, the quasi-three level laser threshold, equation 2.5, reduces to equation 2.7.

2.1.1.3. Slope efficiency

Differential quantum efficiency or slope efficiency is the change in the number of stimulated output photons per unit change in the number of pump photons above threshold. The slope efficiency for an end-pumped four-level laser, for example the 1.064μm laser transition in Nd:YAG, is given by [Clarkson98]

$$\eta_s = \left(\frac{T}{T+L}\right)\left(\frac{\nu_L}{\nu_P}\right)\eta_{abs}\eta_q\eta_{PL} \qquad (2.8)$$

where ν_P and ν_L are the pump and lasing frequencies respectively and η_q is the pumping quantum efficiency that is the fraction of absorbed pump photons which lead to subsequent excitation in the upper laser level. The factor η_{PL} depends on the overlap between the pump and laser modes and the ratio of the intracavity intensity to the saturation intensity. η_{PL} tends to 1 at high pump powers where intracavity intensity is much higher than the saturation intensity.

For pump powers above but near threshold the slope efficiency of quasi-three-level lasers is more complicated than four-level lasers due to the re-absorption loss in the laser medium. This results in a slope efficiency that is lower than that in four-level lasers where there is no loss for insufficient pump regions. In order to analyse the slope efficiency of quasi-three-level lasers near threshold one should take into account the spatial distribution of the pump region along with the mode matching ratio throughout the active medium [Risk88]. However, a few times above threshold, quasi-three-level lasers can be nearly as efficient as four-level lasers. This is due to the fact that a larger volume of the laser rod is sufficiently pumped to overcome the lower laser level population and thus no longer causes a loss to the lasing mode.

2.1.2. Power-scaling in end-pumped Bulk lasers

The main obstacles in designing a high-power solid-state laser with good beam quality are thermal effects within the laser medium. In this section, I first review the importance of thermal effects in end-pumped solid-state lasers and then briefly review some of the strategies that have so far been used for power scaling in these lasers. It has to be pointed out that here the review is restricted to end-pumped edge-cooled rods with cylindrical geometry similar to those used in this work. The advantage of edge cooling is the relative ease of its employment, however it has the disadvantage of strong thermal lensing due to predominantly radial heat flow in the laser rod.

2.1.2.1. Thermal effects

In solid-state lasers, the pumping process not only enables the required population inversion for laser action, but also produces heat in the active medium. This is mainly due to the quantum defect heating in the active medium, i.e. the energy difference between the pump and emitted photons [Koechner99].

In addition, there are a number of other mechanisms, energy-transfer-upconversion (most pronounced under non-lasing conditions), non-radiative decays (from the pump level to the upper laser level and from the lower laser level to the ground level) which can produce extra heat inside the crystal [Clarkson98]. Also, the non-uniform spatial distribution of the pump light inside the laser medium causes a spatial variation in heat loading density and therefore temperature. The spatial variation in temperature, and hence internal stress within the laser medium leads to the following detrimental effects in laser performance:

a) Laser beam distortion due to thermal lensing (caused by a change in refractive index due to spatial change in rod temperature),
b) Depolarisation loss due to stress-induced birefringence,
c) Laser rod end-face bulging due to thermally induced stress,
d) Stress-induced fracture of the laser rod.

There are a number of factors such as thermo-optical and thermo-mechanical properties of a laser medium, laser medium geometry, pumping geometry, heat sink arrangement and resonator geometry that determine the degree to which these effects are detrimental to laser performance.

a) Thermal lensing

An important thermal effect in end-pumped lasers is the change in rod temperature. In end-pumped solid-state lasers efficient operation requires small focus pump beam sizes which results in a very high pump deposition density and hence a high local thermal loading in the laser medium. This leads to strong thermal lensing, since the parabolic temperature profile in the rod cause a

corresponding variation in the refractive index (*dn/dT*). A parabolic index profile acts as a spherical lens. However, the refractive index profile of the lens depends on the transverse intensity profile of the pump beam and hence the thermal lens can be highly aberrated. This aberrated thermal lens results in increased diffraction loss for the oscillation mode and hence reduces the brightness of the laser output. The aberrated thermal lens can also make resonator design difficult, as the thermal lens focal lengths can be as short as a few rod lengths [Siegman86].

An analytical expression for the aberrated thermal lens has been derived by Clarkson et. al. [Clarkson98]. This was an extension of a theory given by Innocenzi et. al. [Innocenzi90] for the radially varying thermal lens focal length, $f_{th}(r)$, for an end-pumped edge-cooled laser rod by a pump beam with a Gaussian intensity profile. For the sake of completeness the main results of the theory for a pump beam with Gaussian intensity profile are presented here. Here it was intended to restrict the discussion to a pump beam with Gaussian intensity profile due to its high on-axis intensity, which leads to both a strong and highly aberrated thermal lens. It is worth noticing that it has already been shown that a pump beam with more uniform transverse intensity profile, “Top-hat” profile, rather than the Gaussian beam leads to a much less aberrated thermal lens [Clarkson98].

For a Gaussian pump beam profile the radially varying thermal lens focal length is given by [Clarkson98]

$$f_{th}(r) = \frac{2r^2 f_{th}(0)}{w_P^2\left[1-\exp\left(\frac{-2r^2}{w_P^2}\right)\right]} \qquad (2.9)$$

where $f_{th}(0)$ is the focal length on axis at $r = 0$ and is given by

$$f_{th}(0) = \frac{\pi K_c w_P^2}{P_P \gamma \eta_{abs}\left(dn/dT\right)} \qquad (2.10)$$

where r is the radius from the pump beam axis, w_p is the pump beam size, K_c is the thermal conductivity of the laser material, P_p is the incident pump power, η_{abs} is the fraction of incident pump power that is absorbed, dn/dT is the change in

refractive index with respect to change in temperature and γ is the fraction of absorbed pump power converted to heat (if the pumping quantum efficiency is unity and there are no deleterious upconversion or excited-state absorption processes, then under lasing conditions γ is approximately equal to the quantum defect, i.e. $\gamma = 1 - (\lambda_P / \lambda_L)$ [Koechner99]).

The power of the thermal lens (in diopters) is inversely proportional to the thermal lens focal length. Thus the shorter the thermal lens focal length the more detrimental the effects of the aberrated thermally induced lens become.

b) Stress induced birefringence

The lensing contribution of the thermally induced stress in a cylindrical laser rod is different for light polarized parallel and perpendicular to the principal axes of the stress tensor. The principal axes of the stress tensor, and hence the resulting indicatrix, are orientated radially and tangentially everywhere in the rod. These radial and tangential components of thermally induced stress lead to a birefringence in the laser rod. Stress induced birefringence is particularly a problem where a preferred polarization for the laser output is required. This is known as depolarisation of the linearly polarized beam or depolarisation loss [Clarkson98, Koechner99]. Naturally birefringent hosts, for example YLF, see a reduction in this effect due to the fact that the natural birefringence is stronger than this induced effect.

There are a number of techniques for reducing the effects of stress-induced birefringence in end-pumped solid-state lasers. An informative review of the problem is given in Hanna et. al. [Hanna99].

c) Laser rod end-face bulging

The thermally induced expansion of the laser rod can cause bulging of the rod end-faces which provides a further complication to thermal lensing. In general this effect has a relatively smaller impact on the beam distortion in the laser rod as compare to thermal lensing. However, the relative extent to which this effect is detrimental to the laser performance strongly depends on the thermo-optical properties of the laser material and heat sink arrangement. For example, due to

YLF's negative change in refractive index with change in temperature, the thermal lens focal length can partially offset the lensing effect caused by end-face bulging.

d) Stress-induced fracture of the laser rod

A laser rod will fractured when the thermally induced stress exceeds the tensile strength of the laser material. This catastrophic failure can form an upper limit to the maximum power that the laser can be scaled to. The extent to which this effect is detrimental to laser performance strongly depends on the thermo-mechanical properties of the laser material. In general, the laser material can be characterised by a "Thermal Shock" parameter in W/cm. For instance, the thermal shock parameter for YAG is ~7.9 while for YLF it reduces to approximately 1.6 and for glass ~ 1 [Koechner99].

2.1.2.2. Power-scaling strategies

A vast number of strategies have so far been used for power-scaling in end-pumped solid-state lasers. Some of them fall into one of the following categories:

a) Reduction of heat generation and heat loading in the laser material,
b) Improvements in pump beam parameters,
c) Compensation of thermal effects by novel resonator designs and alternative approaches.

Each of these strategies will briefly be discussed here.

a) Reduction of heat generation and heat loading in the laser material

The first, and the most obvious source of heat generation within the laser medium is the fraction of pump light converted to heat, referred to as the pump quantum defect heating. For a given laser material, this can be reduced by operating on a laser transition which terminates in the ground level manifold and by pumping into the upper manifold of the transition. This can result in a very

small fraction of pump power causing heat generation within a laser medium, and thus reduce the degradation in laser beam quality and depolarisation loss (see section 2.1.2.1 and also [Clarkson98]). However, such a pumping scheme may not be entirely favourable from a spectroscopic point of view and thus would require further considerations to improve the absorption efficiency of the pump light in the laser material. This can be done, for instance, by using a small pump beam size and/or long laser rod. It is worth noting that this strategy is restricted to laser transitions where the pump and laser wavelengths are close, or for upconversion pumped lasers, i.e. lasers which emit at frequencies higher than that of the pump light [Whitley91, Heine94].

In a given laser material, there are also other heat generation routes such as energy transfer upconversion (ETU) [Guy98] and concentration quenching [Brown98]. Using a longer laser rod with lower ion concentration could serve to significantly reduce the heat dissipation due to these effects [Abdolvand03]. It has to be pointed out that heat dissipation due to upconversion processes is the source of main concern for Q-switched lasers and lasers with a high threshold. This is due to the fact that upconversion processes are more pronounced in the non-lasing condition [Clarkson98].

The mentioned routes for reducing heat generation within the laser medium emphasise the need for a high-power pump source with good beam quality. This would allow the pump beam to be focused to a small beam size while minimising divergence of the pump beam throughout a long laser rod. Progress towards the improvement of highly elliptical output beam from high-power diode laser sources is a subject of the next section.

a) Improvements in pump beam parameters

The output from a diode-bar is typically highly elliptical with beam quality factors differing considerably for orthogonal planes. In the plane perpendicular to the array the beam quality factor M_y^2 is 1, while in the plane parallel to the array the beam quality factor, M_x^2, depends on the length of the array and can be much larger. For instance, a commercially available 20W cw diode-bar at 790nm has

beam quality factors of M_x^2 ~2000 and M_y^2~1 in orthogonal planes. This not only restricts the shape of the pump profile but also the minimum spot size.

The minimum waist spot size, w_{min}, for a Gaussian beam when focused by a thin lens is approximated by [Svelto98]

$$w_{\min} = \frac{2\lambda f M^2}{\pi D} \qquad (2.11)$$

where f and D are the focal length and diameter of the lens, respectively, M^2 and λ are the beam quality factor and wavelength of the incident beam.

If we focus a collimated beam from a diode-bar operating at 790nm with M^2 values of 2000 and 1 in orthogonal planes by a lens with 40mm focal length and diameter of 30mm, the result would be a beam with minimum spot size of ~1.4mm by ~1μm in the two planes. Such a pump beam would result in an extremely aberrated and strong thermal lens inside the laser rod. It will also reduce the laser efficiency and increase the threshold, and hence would make the resonator design demanding.

This problem, to some extent, has been solved by the development of novel beam shaping and focusing schemes using lenses, fibre-optics, mirrors and other optics [Wang01]. In particular the two-mirror beam shaper, which has been invented by Clarkson and Hanna [Clarkson96] is one example of these techniques. This technique allows reconfiguration of the highly aberrated beam from typical high-power diode lasers to a beam with nearly equal beam quality factor in orthogonal planes without a significant loss in brightness. Typically the resulting M^2 values are equal to ~70 in the both orthogonal planes. This allows tight focusing of the pump beam inside the laser rod, and hence efficient end-pumped operation for many low-gain and quasi-three-level laser transitions.

b) Compensation of thermal effects by novel resonator designs and alternative approaches

Research within the laser community for power scaling in solid-state lasers without compromising beam quality has led to many novel laser configurations. Side-pumped “zig-zag” slab lasers [Rutherford00], side-pumped rod lasers

[Konno01], thin disk lasers [Brauch95], double-clad planar waveguide lasers [Shepherd01] are examples of these configurations. Whilst some of these schemes improve the brightness scalability of solid-state lasers compared to the traditional end-pumped designs, they often increase complexity and reduce flexibility of the lasers. For instance, in the thin disk approach, face-cooling of a laser disk results in axial heat flow in the laser disk. This significantly decreases the strength of the thermal lens. However, in order to minimise radial heat flow in the laser disk the high aspect ratio of pump beam size to disk thickness is required. Generally for high power operation, the thickness of the laser disk is not sufficient to absorb a significant fraction of the pump power from a single-pass and thus the pump has to be reflected to multi-pass the laser disk [Erhard01]. Therefore, this limits the applicability of this approach to the laser materials with short absorption length for the pump light.

In contrast with end-pumped solid-state lasers, double-clad planar waveguides can be coupled almost directly with diode-bars. However, the gain region is correspondingly asymmetric, and it becomes difficult to extract the power in a good quality beam. The lack of guiding in one of the dimensions makes it difficult to improve the brightness of the waveguide output.

Nevertheless, there are many situations where end-pumping of solid-state lasers is preferred due to its relative simplicity, flexibility in resonator design and potential for efficient operation on quasi-three-level laser transitions. To overcome the problems of brightness scaling in end-pumped solid-state lasers a number of approaches have been reported including the use of aspheric lenses as compensators [Tidwell92, Wyss02] and various resonator designs [Clarkson98, Koechner99].

One powerful alternative to the end-pumped bulk laser is a fibre laser. A fibre laser can be considered as an extremely elongated laser rod. Double-clad fibre lasers make excellent high-power cw laser sources with exceptional beam quality at many wavelengths [Limpert03, Clarkson03, Platonov02]. Fibre lasers are discussed in the next part of this chapter.

2.2. Fibre lasers

The fibre or guided-wave laser has a history almost as long as that of the laser itself [Snitzer61, Koester64]. However, interest in the potential advantages of guided-wave gain media was only quickened in the past two decades. This was due to the advent of high-quality single mode rare-earth doped silica fibres with low propagation losses resulting in the demonstration of efficient lasing and amplification in silica fibres [Poole85, Mears85]. An essential feature of the rare-earth-doped fibre is that the active ion is doped into a guided core. This is usually chosen to have a diameter of a few micrometers, so that the fibre is monomode due to the fact that at the lasing wavelength only the lowest order mode can propagate. Thus the problems of transverse mode control, which are characteristic of bulk lasers, are removed. Reduced cavity mode volume in fibres, offered by the guided-wave geometry, also reduces the pump power needed to reach the threshold. Low threshold pump powers, however, do not imply that the fibre lasers are necessarily low power devices and indeed it has been demonstrated that powers in excess of hundreds of watts with excellent beam quality are achievable from diode-pumped fibre lasers [Liem04, Limpert03, Platonov02]. Also, due to the high gains in doped fibres, which could be achieved for low pump powers, efficient laser operation on quasi-three-level transitions and transitions with low quantum efficiency and weak absorption could be obtained.

In addition, problems of heat dissipation, which are characteristic of bulk lasers, are removed in fibre lasers. This is due to the fact that heat can be dissipated over the long length of fibre, and it has only a short distance to travel towards the outer surface of the fibre.

However, in fibre lasers the combination of small core sizes and long device lengths leads to low thresholds for nonlinear effects such as stimulated Brillouin scattering (SBS), which in turn can limit the maximum output power [Agrawal95]. In addition, fibre lasers suffer from the disadvantage that the relative small core area limits the energies which can be extracted in a Q-switched operation [Renaud01]. This can be solved by using larger multimode cores, but at the expense of poorer beam quality.

Another obstacle for power scaling in fibre lasers is more basic. High output power requires high input power. In order to end-pump a monomode core with a small dimension one has to use an essentially diffraction-limited pump beam. However, beam quality of high-power diode lasers are far from being diffraction-limited. The solution to this problem has been via the use of cladding-pumping [Po89, Po93], however at the expense of greatly extending the length of the gain medium. This might reduce the efficiency of the laser unless the fibre can be fabricated with sufficiently low propagating losses in the core and inner cladding. Here, first the principles of fibre laser design and operation are reviewed and then the problems and demands of power scaling in fibre lasers are addressed.

2.2.1. Background

The type of fibre that is considered here consists of a region of refractive index, n_{core}, which is surrounded by a material of lower refractive index, $n_{cladding}$ (Figure 2.2). We assume the fibre to have a step-index-profile and a core diameter of 2a (Figure 2.3). It is fabricated by having a usually cylindrical core of glass enclosed in an appropriate cladding glass.

If the propagation of light in the fibre is considered in simple ray tracing terms, then the light that will be guided down the centre of the core will do so by total internal reflection at the core/cladding interface. For this to occur the angle of incidence at the interface, θ (for angle definitions see figure 2.1), must be greater than the critical angle, θ_c, where

$$\theta_c = \sin^{-1}\left(n_{clad} \Big/ n_{core} \right) \qquad (2.12).$$

The angle of incidence at the core/cladding, θ, can be related through Snell's Law to angle of incidence, ϕ_i, of the light with the end-face of the fibre. There is a maximum value for ϕ_i, known as the acceptance angle, ϕ_{max}, for light to enter the core and still be guided where,

$$\phi_{\max} = \sin^{-1} \frac{n_{core}}{n_0} \sqrt{1 - \left(\frac{n_{clad}}{n_{core}} \right)^2} \qquad (2.13)$$

where n_0 is the refractive index of the medium surrounding the fibre.

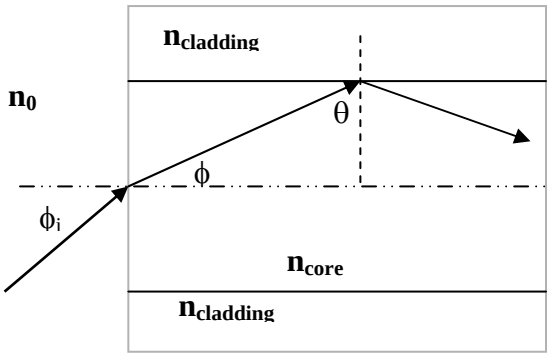

Figure 2.2: Meridional rays of a step-index optical fibre.

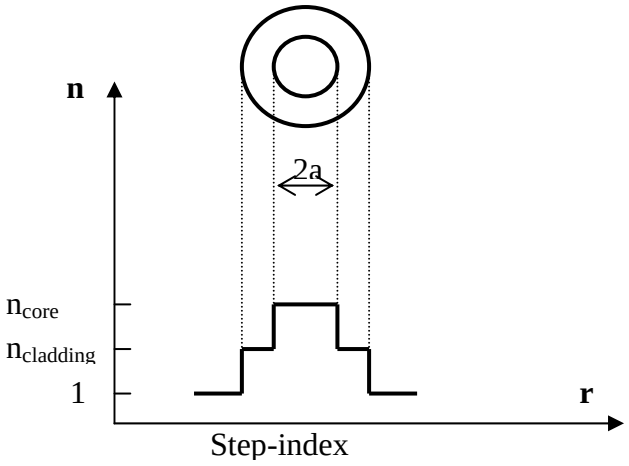

Figure 2.3: Step-index fibre. The fibre is shown end on and the index of refraction profile is displayed.

The numerical aperture, *NA*, of the fibre can be found in terms of the refractive indices of the core and cladding as,

$$NA = n_0 \sin \phi_{\max} = n_{core} \sin \theta_t = n_{core} \sqrt{1 - \left(n_{clad} / n_{core} \right)^2} = \\ = \sqrt{n_{core}^2 - n_{clad}^2} \qquad (2.14)$$

Thus, the numerical aperture is proportional to the *sin* of the largest incident angle that the fibre can accept and transmit (it is worth mentioning that the presented results apply to the meridional rays of a fibre and must be modified for skew rays in an optical fibre).

It is usual to define a quantity, referred to as the normalized frequency or V-number, that provides an indication of the number of modes of propagation that are supported at a particular wavelength in the fibre. The V-number can be written in terms of the fibre characteristics as [Snyder83]

$$V = \frac{2\pi}{\lambda} aNA \qquad (2.15)$$

where λ is the wavelength of the light in vacuum, *a* is the core radius and *NA* is the numerical aperture of the fibre.

For a fibre to be single mode at the particular wavelength, the *V*-number must be less than 2.4. This indicates that only the fundamental mode, LP_{01}, can propagate in the fibre while higher order modes would be cut off [Marcuse77, Marcuse78]. However, in practice, it is found that under about $V \leq 1.7$, light is not guided well in the fibre mainly due to the fact that the bending loss becomes significant [Neumann88]. If more than one mode at the wavelength can propagate then the fibre is called multi-mode and the V-number is larger than 2.4.

For a multi-mode fibre the intensity distribution function is often approximated as a top-hat function of radius *a*, with uniform intensity distribution across the core [Digonnet85]. However, for single mode operation the intensity function, *I(r)*, can be approximated by a Gaussian distribution and is given by [Snyder83]

$$I(r) = \frac{2}{\pi w^2} \exp\left(\frac{-2r^2}{w^2}\right) \qquad (2.16)$$

where *w* is the spot size given by

$$w = a \Big/ \left(\ln V\right)^{1/2} \qquad (2.17)$$

and a is the core radius.

2.2.1.1. Gain

The most remarkable features of fibre lasers and amplifiers are the very high gain that can be achieved for modest pump power, and the very low pump power that is needed to saturate the pump transition. Both these features are due to the guide-wave geometry that reduce the cavity mode volume via the small dimensions, approximately a few microns, of the active core.

The first consequence of high gain in fibres is that it makes diode laser pumping of these devices extremely feasible. In fact, demonstration of the first end-pumped fibre laser with relatively low threshold and high slope efficiency was the second major development in the field of fibre lasers [Stone73].

Its second consequence leads to the fact that fibre lasers are very much tolerant to losses. This can give greater freedom of design in fibre laser resonators compared to bulk lasers where the inclusion of lossy elements in the cavity leads to higher thresholds. In fact in fibre lasers it is possible to achieve oscillation from the bare, uncoated fibre ends. It is possible to suppress this oscillation by a number of ways. For instance by immersing the fibre ends in index-matching liquid, antireflection coating, or by purposely angle polishing ends [Koester64]. However, the complete suppression of feedback is difficult, and even if it was possible, single pass gain in fibres is enough to lead to a process known as ASE (Amplified Spontaneous Emission). This is a situation where photons spontaneously emitted at one end of the fibre are amplified on a single pass to an intensity that sufficiently depletes the gain. In chapter 3 we will see how ASE affects the performance of a tunable Tm-doped silica fibre laser.

2.2.1.2. Threshold

In a single-mode fibre, the transverse dimensions of both pump w_p and laser w_L beams are comparable to the core radius a. Thus both w_p and w_L are much smaller than corresponding typical values for a bulk laser. From equations 2.5 and 2.7, for a quasi-three-level and four-level laser, respectively, the threshold pump power

P_{th} is seen to be proportional to (w_p^2 + w_L^2). Thus threshold pump power in fibre laser is expected to be much smaller than in a bulk laser. Consequently in fibre lasers, low threshold laser operation can be achieved even for an active media of low radiative quantum efficiency and hence of short lifetime.

2.2.1.3. Slope efficiency

From expression 2.8, it can be seen that the slope efficiency for both a four-level and a quasi-three-level laser is independent of the upper state lifetime and depends only on pump efficiency η_q. Therefore in fibres, it is possible to achieve high slope efficiency even for a transition with low radiative quantum efficiency (i.e. the fraction of ions in the upper level which decay through radiation on the laser transition), and hence unpromising from the point of view of bulk laser, if the pump efficiency approaches 1 ($\eta_q \to 1$).

2.2.2. Power-scaling in end-pumped fibre lasers

Conventional end-pumped single-mode fibres require a diffraction-limited pump source for efficient pumping. However, high-power diode lasers have poor beam quality and hence cannot be launched into the end of the fibre core. The solution to this problem was provided by cladding pumping. First proposed in the 1970s [Maurer74, U.S. Patent 3.808.549], the concept allowed the efficient conversion of output radiation from a broad-stripe semiconductor laser diode into a single mode emission of fibre laser [Kafka89 U.S. Patent 4.829.529, Po93]. In the simple double-clad fibre design (Figure 2.4), the rare-earth doped core lies within a lower index inner cladding that in turn lies within an outer cladding. The pump light can be either end-launched or side-launched into the inner cladding. In side-launched case multiple pumps can be used along the fibre and hence uniform pump distribution along the fibre and high output powers are achievable [Gapontsev94 U.S. Patent 5.999.673, Goldberg99]. Indeed a reliable Yb^{3+}-doped fibre laser based on a side-pump technique with output power as high as 135W in a single mode has recently been reported [Platonov02]. However, here we restrict our

discussion to end launching. The pump light launched into the inner cladding is guided by the interface between the cladding and its outer cladding and thus gets efficiently absorbed into the doped core. The result is a laser output with excellent beam quality from the core.

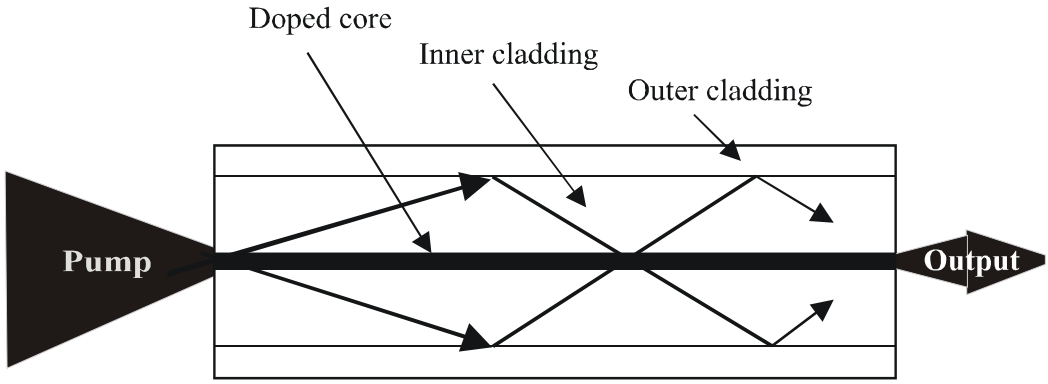

Figure 2.4: Scheme of cladding-pumped fibre laser.

However, in cladding pumping the core's effective absorption coefficient is smaller than the true absorption coefficient by a factor roughly equal to the ratio of the inner-cladding area to the core area. Therefore, for a given doped-core, fibre length must be respectively increased to allow efficient absorption of pump light. This length increase depends on the core/cladding area ratio, and on the design of the fibre profile, but it is typically >10 times. In a quasi-three level laser transition, where ground-state-absorption (GSA) is substantial, this length increase results in a increase in reabsorption loss and hence increase in threshold. This makes cladding pumping not very effective for these transitions.

Thus, in a cladding-pumped fibre laser efficient brightness conversion of multimode diode to monomode lasing can be achieved, if propagation losses of the pump light in the inner cladding and the lasing mode in the core are not greatly increased by an increase in fibre length. Therefore, in order to achieve high laser efficiency it is important to optimise the coupling of the pump radiation from the inner cladding to the core. This can be obtained by determining the optimised condition for available cladding shapes. Obviously, the ideal situation is that the pump remains uniform along the fibre, so that the initial effective

absorption coefficient is maintained. Figure 2.5 shows the typical structures for double clad fibres. One of the most common inner cladding shapes is the rectangular shape. It has already been reported that a rectangular inner cladding optimises coupling as it provides a convenient shape for coupling in laser diode pump power: This, in turn, minimises the area of the first cladding and thus the required fibre length due to increase in absorption [Muendel96, Liu96].

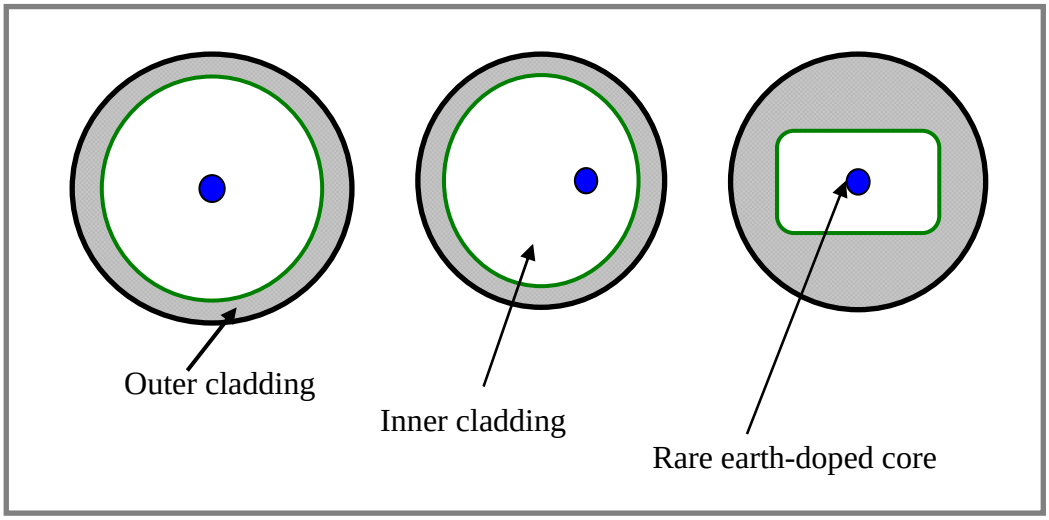

Figure 2.5: Typical structures of cladding pumped fibre lasers.

This is due to the fact that in this case the paths of rays inside the inner cladding scan the whole cross section of it and have the possibility of emerging anywhere after crossing the doped core. Therefore, the absorbable power ratio of rectangular double clad fibres is normally considered to be high. Also the design in which the core in slightly offset from the centre of the cladding has proved to improve the pump absorption efficiency. This is due to the fact that the helical path skew rays in the fibre have a larger possibility of emerging at a farther position from the centre region [Liu96].

Another important design consideration is the *NA* of the cladding. Ideally it should be as large as possible to capture as much of the pump light as possible. However, the maximum value for *NA* is generally limited by the maximum available index difference. For double-clad silica fibre lasers, in which the inner

cladding is made of glass and the outer cladding is made of a low-refractive index polymer, high *NA*s (*NA*>0.6) can be achieved [Digiovanni99].

Very recently output power as high as 1.3kW with a near diffraction-limited beam quality, $M^2<1.5$, has been reported from a single fibre [Liem04]. This was due to the use of a low-numerical aperture large-mode-area (LMA) fibre design approach. This design greatly improves power scalability of the fibre lasers due to increase in the core size, typically between 20 to 30μm, and hence considerable reduction of power density in the fibre core. On the other hand, the V-value of the fibre remains relatively small, typically less than 10, due to the use of small numerical aperture of the fibre core (typically around 0.06). Small numerical aperture of the core creates a large discrimination between the lasing modes. This in turn, makes it possible to use bending loss to achieve fundamental mode operation. However, fibre bend loss increases rapidly with increasing mode area. Therefore means of extending the core dimensions with which one can achieve single-mode operation and ways of reducing the bend loss of large-mode-area fibres are critical to further power and brightness scaling in fibre lasers using this approach.

Thus, cladding pumping of fibre lasers in combination with the use of large core size could greatly improve the power scalability of fibre lasers. However, one can expect that using multimode core in fibre lasers, in order to accommodate high powers, could eventually lead to the familiar thermal and mode control problems of bulk lasers. We will discuss this in the following section.

2.2.2.1. Thermal effects

Recently, a lot of work has been published on the question of power scalability of fibre lasers and their degree of immunity to thermal effects [Zenteno93, Davis98, Brown01]. The answers depend on a wide range of parameters, such as the dimension of the fibre cladding and core, the glass composition, the means of heat removal from the cladding surface, the doping level and hence the pump excitation length, the nature of the transition and the energy defect between pump

and laser photon. What is clear however is that fibre lasers due to long length of the device have more immunity to thermal effects than conventional bulk lasers.

Here, we will briefly discuss thermal issues in fibre lasers by comparing the temperature distribution in laser rods and fibres via the equations, which describe the temperature distributions in laser rods and fibres.

For a cylindrical laser rod of radius R (figure 2.6), in which there is a constant and uniform heat dissipation, Q [W/m^3], due to the pumping process, a radial temperature distribution, $T(r)$ is given by [Koechner99]

$$T(r) - T(R) = Q(R^2 - r^2) \Big/ 4K_c \qquad (2.18)$$

where r is the radial distance from the cylinder axis and K_c is the thermal conductivity. Thus, the temperature difference between the centre and the outside surface of the rod is given by [Koechner99]

$$T(0) - T(R) = QR^2 \Big/ 4K_c \qquad (2.19)$$

The equation 2.19 can be written as follow

$$T(0) - T(R) = \left(P \Big/ L\right) \Big/ 4\pi K_c \qquad (2.20)$$

where $P = \pi Q R^2 L$, is the total heat dissipated in a length L of the rod.

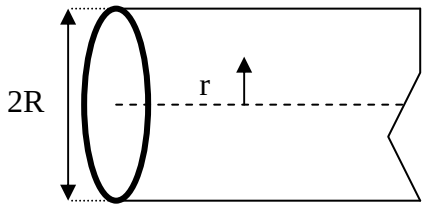

Figure 2.6: Radial temperature profile for a cylindrical rod with uniform heat dissipation throughout the cylinder.

As it can be seen the temperature difference is dependent only on the heat dissipated per unit length and not on the radius of the rod. The temperature gradient generates stress due to the differential expansion with a maximum value at the surface of the rod given by [Koechner99]

$$\sigma_{\max} = \frac{2^{1/2}\alpha E}{8(1-\gamma)\pi K}(P/L) \qquad (2.21)$$

where α is the thermal coefficient of expansion, E is Young's modulus and γ is Poisson's ratio. It can be seen that the stress depends on the heat dissipated per unit length and not on the radius.

Similar equations can be derived for the case of a longitudinally pumped fibre having a doped core of radius R` (where pumping is confined) lying within the cladding region of radius R (Figure 2.7). Considering a uniform pump beam profile the temperature profile is given by [Kishida79, Alcock86]

$$T(r) - T(R') = {Q(R'^2 - r^2)}\Big/{4K_c} \qquad \text{for r<R`} \qquad (2.22)$$

and

$$T(r) - T(R') = -\frac{QR'^2}{2K_c}\ln\left(\frac{r}{R'}\right) \qquad \text{for R`<r<R} \qquad (2.23)$$

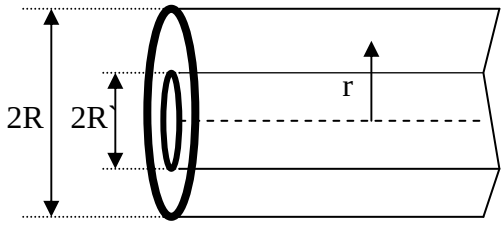

Figure 2.7: Example of longitudinally pumped fibre laser where uniform heat dissipation, Q, confined to the central cylindrical region of radius R`. There is no dissipation in the region R`<r<R.

Hence the temperature difference between the centre and the surface ($r = R$) is [Alcock86]

$$T(0) - T(R) = \left(\frac{QR'^2}{4K_c} \right) \left(1 + 2\ln\left(\frac{R}{R'} \right) \right) \qquad (2.24)$$

And thus the stress at the outer surface is given by [Zenteno93]

$$\sigma_{\max} = \left[\frac{2^{1/2} \alpha E Q R'^2}{8\pi(1-\gamma)K_c} \right] \left[2 - (R'/R)^2 \right] \qquad (2.25)$$

Thus for high power operation in end-pumped fibre lasers, it can be seen from equation 2.25 that for $R` << R$ the maximum stress is twice that of the uniformly pumped rod with the same heat dissipation. Furthermore by comparing 2.20 and 2.24 it can be noted that in the case of longitudinal pumping the temperature difference is greater by a factor of $[1+2\ln(R/R`)]$.

However in fibre lasers, but not in bulk lasers, one can always, in principle, increase the length so that the power absorbed per unit length is small enough to reduce the thermally induced stress. On the other hand while by using a low-doped fibre of longer length the thermal problems can be removed there still remains the question of what power limit the fibre can withstand before nonlinear or other detrimental processes occur. Nonlinear effects are the subject of the next section.

Another limitation is the small surface area of the fibre which can lead to significant absolute temperature rise of the fibre. This occurs if one relies on free convection in air for heat removal. This temperature rise could reduce fluorescence efficiency if conductive cooling is not provided. This can particularly be a problem in double clad fibres due to the different thermal properties of the inner cladding and the outer jacket (outer cladding) of the fibre. In the next chapter the effect of cooling on performance of Cladding-pumped Tm^{3+}-doped silica fibre laser is experimentally investigated.

2.2.2.2. Nonlinear effects

Silica glass is a fairly weak nonlinear material due to its inversion symmetry. Thus a wide variety of nonlinear phenomena in silica-based optical fibres arise mainly from the third-order nonlinear susceptibility χ^3. Thus one can expect that pump power thresholds for observation of nonlinear processes in optical fibres should in principle be several order of magnitudes larger than in traditional materials. However, the efficiency of nonlinear effects in fibres is determined by the waveguide geometry of fibres. This is due to the fact that in general the efficiency of nonlinear processes is determined not only by the nonlinear coefficient, but also by the product of the pump power density and the interaction length. Thus in fibres the combination of long length of the device and the fact that the effects of diffraction are compensated by the refraction in the reflecting cladding, compensate the small nonlinear coefficient of silica glass. This reduces the threshold for observation of nonlinear processes, such as Stimulated Brillouin Scattering (SBS) and Stimulated Raman Scattering (SRS), in silica fibres. This is in contrast with the situation in nonlinear bulk media, nonwaveguide media, where the product of the pump power density and the interaction length solely depends on the pump power [Sevelto98].

2.3. Summary

Quasi-three-level bulk laser and fibre laser theory have been discussed in brief. The problems of power scaling in end-pumped bulk lasers and fibre lasers have also been discussed. In the context of power scaling, efforts have been made to compare bulk and fibre lasers.

2.4. References

[Abdolvand03] A. Abdolvand, D. Y. Shen, L. J. Cooper, R. B. Williams and W. A. Clarkson, “Ultra-efficient Ho:YAG laser end-pumped by a cladding-pumped Tm-doped silica fibre laser,”, in technical digest of Advanced Solid-State Photonics (ASSP), San Antonio, Texas, Paper: MA7 (2003).

[Agrawal95] G. P. Agrawal, "Nonlinear Fibre Optics," Academic, New York (1995).

[Alcock86] I. P. Alcock, A. I. Ferguson, D. C. Hanna and A.C. Tropper, "CW oscillation of a monomode neodymium-doped fiber laser at 0.9μm on the $^4F_{3/2} \rightarrow {}^4I_{9/2}$ transition," Optics. Commun., vol. 58, pp. 405-408 (1986).

[Brauch95] U. Brauch, A. Giesen, M. Karszewski, C. Stewen and A. Voss, "Multiwatt diode-pumped Yb:YAG thin disk laser continuously tunable between 1018 and 1053nm,", Opt. Lett. Vol. 20, pp. 713 (1995).

[Brown98] D. C. Brown, "Heat, Fluorescence, and stimulated-emission power densities and fractions in Nd:YAG,", IEEE Trans. Quantum Electron., Vol.34, pp.560 (1998).

[Brown01] D. C. Brown, H. J. Hoffman, "Thermal, Stress, and Thermo-Optical effects in high avrage power double-clad silica fibre lasers," IEEE J. Quantum Electronics, vol. 37, pp. 207-217 (2001).

[Budni00] P. A. Budni, M.L. Lemons, J.R. Mosto, and E.P. Chicklis, "High-Power/High-Brightness Diode-Pumped 1.9um Thulium and Resonantly Pumped 2.1um Holmium Lasers,", IEEE Journal of quantum Electronics, vol. 6(4), pp. 629-634 (2000).

[Byer88] R. L. Byer, "Diode-pumped solid-state lasers,", Science, vol. 239, pp.749 (1988).

[Clarkson96] W. A. Clarkson and D.C. Hanna, "Two-mirror beam-shaping technique for high-power diode bars,", Opt. Lett., Vol. 21, pp. 375 (1996).

[Clarkson98] W. A. Clarkson and D.C. Hanna, "Resonator design considerations for efficient operation of solid-state lasers end-pumped by high-power diode-bar,", Kluwer Academic Publisher, Dordrecht/Boston/London (1998).

[Clarkson03] W. A. Clarkson, A. Abdolvand, D. Y. Shen, R. B. Hayward, L. J. Cooper, R. B. Williams and J. Nilsson, "High power two-micron fibre lasers," SPIE Proceedings on Gas and Chemical Lasers - High Power Lasers Conference 2002 (Invited).

[Davis98] M. K. Davice, M. J. F. Digonnet, R. H. Pantell, "Thermal effects in doped fibres," J. Lightwave Technology, vol. 16, pp. 1013-1022 (1998).

[Digiovanni99] D. j. Digiovanni, M. H. Muendel, "High-power fibre lasers," Opt. Photon News, vol. 10, pp. 26 (1999).

[Digonnet85] M. F. G. Digonnet, C. J. Gaeta, Applied Optics, vol. 24, pp. 333 (1985).

[Erhard01] S. Erhard, J. Gao, A. Giesen, K. Contag, A.A. Lagatsky, A. Abdolvand, N.V. Kuleshov, J. Aus der Au, G.J. Spuhler, F. Brunner,

R. Paschotta, U. Keller, “High power Yb:KGW and Yb:KYW thin disk laser operation, ”, OSA TOPS Vol. 56, pp. 333-334 (2001).

[Fan87] T.Y. Fan and R. L. Byer, “Modelling and cw operation of a quasi-three-level 946nmm Nd:YAG laser,”, IEEE J. Quantum Electron. Vol. 23, pp. 605 (1987).

[Fan87] T.Y. Fan and R. L. Byer, “Continues wave operation of a room temperature, diode laser-pumped, 946nm Nd:YAG laser,”, Opt. Lett. Vol. 12, pp. 809 (1987).

[Gapontsev96] V. Gapontsov, U. S Patent 5999673 (1994).

[Goldberg99] Goldberg, Opt. Lett. Vol. 24, pp. 673 (1999).

[Guy98] S. Guy, C.L. Bonner, D. P. Shepherd, D. C. Hanna, A. C. Tropper and F. Ferrand, “High-Inversion densities in Nd:YAG: upconversion and Bleaching,”, IEEE J. of Quantum. Electron., Vol. 34, pp. 900 (1998).

[Hall84] D. W. hall, M. J. Weber and R. T. Brundage, “Fluorescence line narrowing in neodymium laser glasses,”, J. Appl. Phys. Vol. 55, pp. 2642 (1984).

[Hanna99] D. C. Hanna and W. A. Clarkson, “A review of diode-pumped lasers: Advances in Lasers and Applications,”, SUSSP 52 : Bristol and Philadelphia Institute of Physics Publishing, pp.1-17 (1999).

[Heine94] F. Heine, E. Heuman, T. Danger, T. Schweitzer, G. Huber and B.H.T. Chai, “Green upconversion continues wave Er:YLF laser at room tempreture,”, Appl. Phys. Lett., Vol. 65, pp.383 (1994).

[Hemmati89] H. Hemmati, “2.07mm cw diode-laser pumped Tm,Ho:YLF room temperature,”, Opt. Lett. Vol. 14, pp. 345 (1989).

[Hutchinson92] J. A. Hutchinson and T. H. Allik, “Diode array-pumped Er, Yb: Phosphate glass laser,”, Appl. Phys. Lett. Vol. 60, pp. 1424 (1992).

[Innocezi90] M. E. Innocezi, H.T Yura, C. L. Fincher and R.A. Fields, “Thermal modeling of continues wave end-pumped solid-state lasers,”, Appl. Phys. Lett. Vol. 56, pp. 1831 (1990).

[Kafka89] J. Kafka, U. S Patent, 4829529 (1989).

[Kishida79] S. kishida, K. washio, S. Yoshikawa, “CW oscillation in Nd:phosphate glass,”, Appl. Phys. Lett., vol. 34, pp. 273-275 (1979).

[Kmetec94] J. D. Kmetec, T. S. Kubo, T. J. Kane and G.J. Grund, “Laser performance of diode-pumped Thulium-doped $Y_3Al_5O_{12}$, $(Y,Lu)_3Al_5O_{12}$ and $Lu_3Al_5O_{12}$ crystals,” Optics Letters, vol. 19(3), pp. 186-188(1994).

[Krupke90] W. F. Krupke and L.L. Chase, "Ground-state depleted solid-state lasers, principles, characteristics and scaling,", Optical and Quantum Electron., Vol. 22, pp.1 (1990).

[Koechner99] W. Koechner, Solid-State Laser Engineering, Springer-Varlag, Berlin Heidelberg, 1999.

[Koester64] C. J. Koester and E. Snitzer, "Amplification in a fibre laser," Appl. Opt. Vol. 3**, pp.** 1182-1186 (1964).

[Konno01] K. Konno, S. Fujikawa and K. Yasui, in Technical digest of Advanced Solid-State Lasers, pp. 9 (2001).

[Lacovara91] P. Lacovara, H. K. Choi, C. A. Wang, R. L. Aggarwal and T. Y. Fan, "Room temperature diode-pumped Yb:YAG laser, ", Opt. Lett. Vol. 16, pp. 1089 (1991).

[Liem04] A. Liem, J. Limpert, H. Zellmer, A. Tünnermann, "1.3KW Yb-doped fibre laser with excellent beam quality,", in Conference on lasers and Electro-Optics, CLEO/America, San Francisco, Post deadline paper: CPDD2 (2004).

[Limpert03] J. Limpert, A. Liem, H. Zellmer, A. Tunnerman, "Continues-wave ultra high brightness fibre laser systems,", in technical digest of Advanced Solid-State Photonics (ASSP), San Antonio, Texas, Post deadline paper: PD1 (2003).

[Liu96] A. Liu, K. Ueda, "The absorption characteristics of circular, offset, and rectangular double-clad fibers", Optics Communications 132, Elsevier Eds., pp. 511-518 (1996).

[Marcuse77] D. Marcuse, Bell. Sys. Tech. Jour., vol. 56, pp. 5 (1977).

[Marcuse78] D. Marcuse, "Gaussian approximation of the fundomental modes of graded-index fibres," J. Opt. Soc. Amer., vol. 68, pp. 103-109 (1978).

[Maurer74] D. Maurer, U. S Patent 3808549 (1974).

[Mears85] R. J. Mears, L. Reekie, S. B. Poole and D. N. Payne, Elect. Lett., vol. 21, pp. 736 (1985).

[Mears86] R. J. Mears, L. Reekie, S. B. Poole and D. N. Payne, Elect. Lett., vol. 22, pp. 159 (1986).

[McGuckin92] B. T. McGuckin and R.T. Menzies, " Efficient cw diode-pumped Tm,Ho:YLF laser with tunability near 2.067um,", IEEE Journal of quantum Electronics, vol. 28(4), pp. 1025-1028 (1992).

[Neumann88] E. G. neuman, "Single-Mode Fibres,", Vol. 57, Springer series in Optical Science, Springer-Vertalg (1988)

[Muendel96] M. H. Mundel, "Optimal inner cladding shapes for double-clad fibre lasers," in *Conference on lasers and Electro-Optics*, vol. 9 of *1996 Technical Digest Series*, p. 209 (Optical society of America, 1996).

[Platonov02] N. S. Platonov, D. V. Gapontsov, V.P. Gapontsov and V. Shumilin, "135W cw fibre laser with perfect single mode output", *in Conference on Lasers and Electro-Optics* (Optical Society of America, Washington, D.C., 2002), postdeadline paper CPDC3.

[Po89] H. Po, E. Snitzer, R. Tumminelli, L. Zenteno, F. Hakimi, N. M. Cho and T. Haw, "Double clad high brigthnee Nd fiber laser pumped by GaAlAs phased array," Presented at the Opt. Fibre Commun. Conf., paper PD7 (1989).

[Po93] H. Po, J.D. Cao, B. M. Laliberte, R.A. Minns, R.F. Robinson, B.H. Rockney, R.R. Tricca and Y.H Zhang, Electron. Lett., Vol. 29, pp. 1500 (1993).

[Poole85] S. B. Poole, D. N. Payne and M. E. fermann, Electron. Lett., vol. 21, pp. 737 (1985).

[Renaud01] C. C. Renaud, H. l. Offerhause, J. A. Alvares-Charves, J. Nilsson, W. A. Clarkson, P. W. Turner, D. J. Richardson and A. B. Grudinin, IEEE J. of Quantum Electron., vol. 37, pp. 199 (2001).

[Risk88] W. P. Risk, "Modelling of longitudinally pumped solid-state lasers exhibiting reabsorption losses,", J. Opt. Soc. Am. B, Vol. 5, pp. 1412 (1988).

[Rutherford00] T. S. Rutherford, w. M. Tulloch, E. K. Gustafson and R.L. Byer, Trends in Optics and Photonics-Advanced Solid-State Lasers, Vol.34, pp.16 (2000).

[Svelto98] O. Sevelto, "Principles of Lasers,", Plenum Press, New York, 1998.

[Shepherd01] D. P. Shepherd, S. J. Hetrick, C. Li, J. I. Mackenzie, R. J. Beach, S. C. Mitchell and H. E. Meissner, "High-power planar dielectric waveguide lasers,", Journal of Physics D-Applied Physics, Vol. 34(16), pp.2420 (2001).

[Siegman86] A. Siegman, "Lasers,", University Science Books , 1986.

[Snitzer61] E. Snitzer, Phys. Rev. Lett., vol. 7, pp. 444 (1961).

[Snyder83] A. W. Snyder and J. D. Love, "Optical waveguide theory,", Chapman and Hall, 1983.

[Stone73] J. Stone and C. Burrus, Appl. Phys. Lett. Vol. 23, pp. 388 (1973).

[Tidwell92] S. C. Tidwell, J. F. Seamens, m.S. Bowers and A. Cousins, "Scaling of cw diode-end-pumped Nd:YAG lasers to high average powers,", IEEE J. Quantum Electron. Vol. 28, pp.997 (1992).

[Wang01] P. Y. Wang, "Beam-shaping optics delivers high-power beams,",Laser Focus World, December 2001.

[Whitley91] T. J. whaitley, C.A. Millar, R. Wyatt, M.C. Brierly and D. Szebesta, "Upconversion pumped green lasing in erbium doped flurozirconate fibre,", Electron Lett., Vol.27, pp. 1785 (1991).

[Zenteno93] L. Zenteno, "High-power Double-clad fiber lasers," Journal of Lightwave Technology, vol. 11, pp. 1435-1446 (1993).

Part I

High-Power Tunable 2μm Fibre Lasers

Chapter 3

High-Power Tunable Cladding-pumped Tm^{3+}-doped Silica Fibre Laser

3.1. Introduction

In chapter 2 it was shown that fibre lasers provide an attractive alternative to bulk lasers. This is due to the fact that in fibre lasers the heat generated due to the laser pumping cycle can be dissipated over the long length of fibre thus minimising the risk of thermally induced damage. The output beam quality from a fibre is determined by the waveguiding properties of the active ion doped core that can easily be tailored to produce a single-spatial-mode output. We've also seen that high power diode lasers with poor beam quality, thus unsuitable for direct end launching into the fibre core can however be efficiently used to end-pump fibre lasers via the elegant technique, referred to as cladding–pumping [Po89, U.S. Patent 4815079]. On the other hand, a further advantage that fibre lasers offer is the potential for broad wavelength tunability owing to the broad transition linewidths in glass hosts.

In this context high-power fibre lasers operating in the 2μm spectral region with applications in the areas such as remote sensing, medicine and free space communications are of specific interest. One strategy for power scaling in the 2μm region is to employ a cladding-pumped Tm-doped silica fibre laser. Tm-doped silica fibre lasers have proved to be efficient and compact sources for high-power continuous-wave two-micron radiation [Jackson98, Hayward2000]. This is

due to their broad pump absorption band (figure 3.1) at the operating wavelength of commercially available high-power diode lasers.

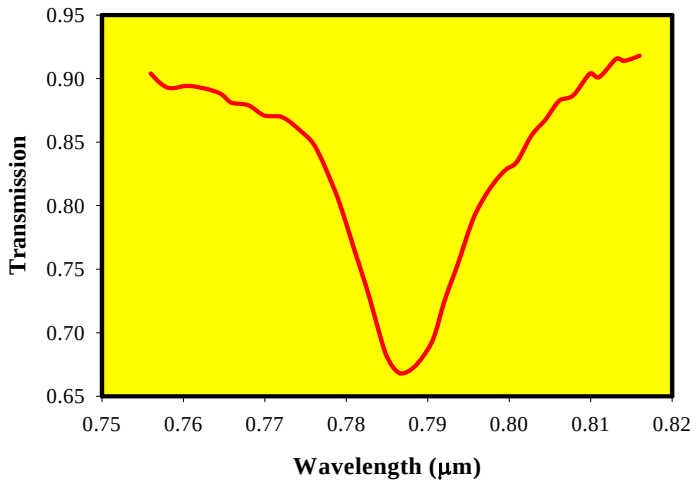

Figure 3.1: Broad pump absorption band centred on 787-790nm [Clarkson01].

Indeed the first demonstration of laser action in a Tm^{3+}-doped fibre laser was in silica, on the $^3F_4 \rightarrow {}^4H_6$ (figure 3.2) transition at ~1.9μm, by pumping into the $^3H_4$ level [Hanna88]. Rapid multiphonon decay from this level leads to efficient population of $^3F_4$.

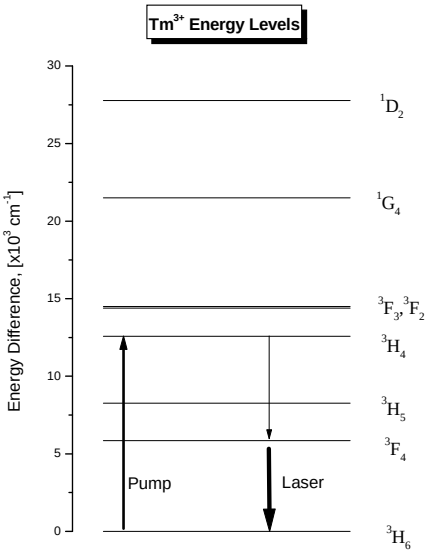

Figure 3.2: Tm^{3+} Energy Levels and the most promising pump and lasing transition.

Low threshold, efficient operation has been achieved on this transition, including diode-pumped operation and widely tunable operation [Hanna88, Hanna90, Jackson98, Hayward2000]. The wide tuning range is due to the broad emission linewidth of the two-micron transition ($^3F_4 \rightarrow {}^4H_6$) of Tm^{3+} ions in silica glass, which spans a wavelength range from ~1700 to ~2100nm. Figure 3.3 shows the broad emission spectrum of Tm-doped silica fibre.

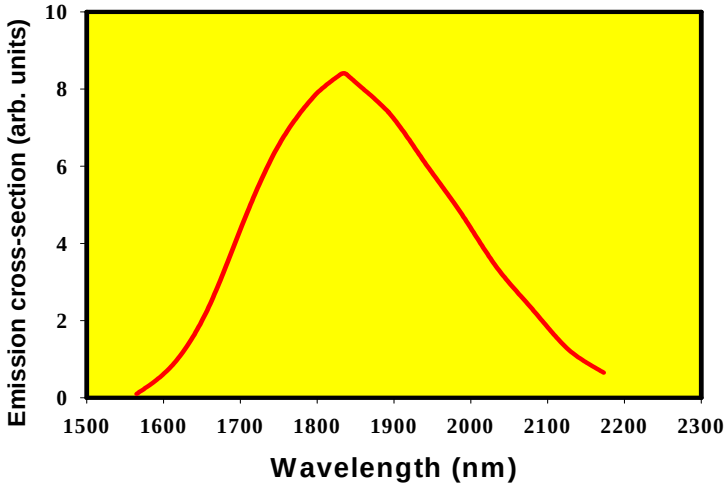

Figure 3.3: Very broad emission spectrum of Tm: silica fibre (>300nm) [Clarkson01].

In this chapter, a high-power cladding-pumped Tm-doped silica fibre laser with a maximum output power of 10.5W at 1921nm with an operating wavelength tunable over 215nm from 1855 to 2070nm is described.

3.2. Fibre geometry and experimental set-up

The Tm^{3+}-doped aluminate silica fibre used in this work was pulled from a preform fabricated in-house using the standard modified chemical vapour deposition and solution-doping technique [Townsend87]. The resulting preform had a thulium concentration of ~2.2% by weight, which equates to ~1.72×10^{20} ions/cm^{-3} or ~22000ppm. The resulting fibre had a thulium-doped alumino-silicate core (n=1.46) surrounded by a pure silica inner-cladding (n=1.45) with non-circular shape. This was achieved by milling two flats inclined at the small angle with respect to each other on the circular preform before pulling the fibre. This in

turn served to improve absorption of the diode pump light by preventing skew rays from following paths that avoid the core. The final fibre had an inner core diameter of ~20µm with a numerical aperture (*NA*) of 0.12, and an inner cladding with an outer diameter of ~200µm. The latter was coated with a low refractive index (n=1.375) polymer. This results in a calculated numerical aperture for the pump guide of 0.49. The area ratio (A_{core} / A_{clad}) was then 0.011 with only ~4% of the inner cladding area being removed by the preform milling process. Figure 3.4 shows the cross section and geometry of the resulting Tm-doped silica fibre.

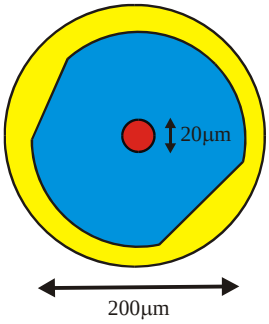

Figure 3.4: Tm: silica fibre's geometry that is used in our experiments.

This design of a double-clad fibre with a relatively small inner cladding dimension and a high *NA* permitted efficient in-coupling of the diode pump sources. This is due to the fact that in general the inner-cladding size should be chosen to minimise the cladding-to-core area ratio in order to maximise pump absorption efficiency per unit length of fibre. However, at the same time it should allow efficient in-coupling of the diode pump source.

One could, in principle, estimate the diameter of the inner-cladding, *d*, required for efficient launching of diode pump light into circular fibre via [Clarkson03]

$$d = \left(2\gamma_w \gamma_{na} M^2 \lambda_p\right) \Big/ \pi \sin^{-1}(NA) \qquad (3.1)$$

where M^2 is the beam quality factor of the pump diode, and γ_w and γ_{na} are the ratios by which the focused pump beam size and far field beam divergence should under fill the inner-cladding diameter and $sin^{-1}NA$ respectively. It is obvious that the values of γ_w and γ_{na} need to be selected to give a high launch efficiency, however without resulting in a significant decrease in pump brightness on launching into the fibre. In practice, choosing $\gamma_w = \gamma_{na} = 1.2$ seems to work well. For a typical diode-bar, the beam quality factor, M^2_x, parallel to the array is ~2000, whereas the beam quality factor, M^2_y, in the orthogonal direction is 1. Thus it is necessary to re-shape the output beam from the diode to roughly equalise the M^2 value in orthogonal planes, however without significantly reducing the brightness.

For the experiment described here two cw diode-bar pump sources at 787-790nm were used. The output beam from each diode-bar was re-shaped by a two-mirror beam shaper, to roughly equalise the beam propagation factors to $M^2 \approx 70$ in orthogonal plans [Clarkson96]. Using equation 3.1, the minimum inner-cladding diameter that could be used was estimated to be ~173μm.

The experimental arrangement used for the tunable Tm-doped fibre laser is shown in figure 3.5. Pump light from beam-shaped diode-bars was launched into opposite fiber ends using thin dichroic mirrors ($t \approx 1$mm) with high reflectivity at the pump wavelength (785-790nm) at 45º and high transmission at the lasing wavelength (1850-2100nm) to allow extraction of the fibre laser output. Thin dichroic mirrors were chosen due to the fact that in general a plane-parallel plate placed in the path of a converging beam introduces astigmatism into it which increases linearly with the plate thickness, t [Andreeva75].

This arrangement allows the use of different lenses for collimating the fibre laser output and focussing the pump, and hence has the advantage that the resonator alignment and pump launching optics can be independently optimised. This arrangement also has the attraction that the pump remains uniform along the fibre and thus the line centre amplified spontaneous emission (see chapter 2) can be suppressed. It allows oscillation to be tuned into the far wings of the laser transition since enough gain can still be accessed in these regions.

The launch efficiency and the effective absorption coefficient for the pump determined, via measurements of transmitted pump power for different lengths, were ~80% and 4.0-4.5 dB/m respectively.

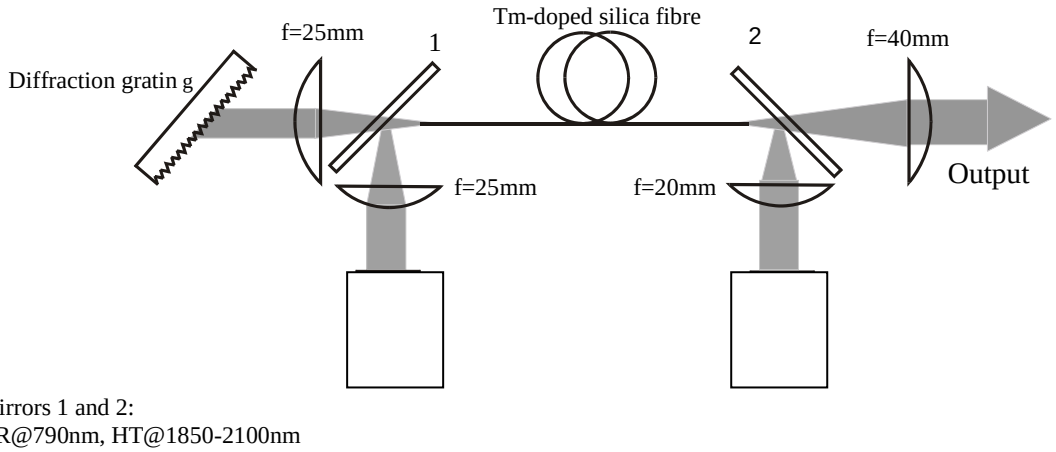

Figure 3.5: Tunable clading-pumped Tm-doped silica fibre laser.

Wavelength tuning was achieved by employing an extended cavity comprising an antireflection-coated Infrasil plano-convex collimating lens of focal length, 25mm, and a simple diffraction grating with 600 lines/mm in the Littrow configuration to provide wavelength selective feedback. The grating was blazed at a wavelength of 1.96μm and had measured reflectivities of 90% (polarised perpendicular to the grooves) and 70% (polarised parallel to the grooves) at 2μm. The fiber-end near the grating was angle-cleaved to suppress broadband feedback from the uncoated face that might otherwise compete with the wavelength-dependent feedback provided by the grating and thus restrict the tuning range. The opposite end of the fiber was cleaved perpendicularly to provide the feedback necessary for laser oscillation. This end of the fiber also acted as the output coupler and, due to its high transmission (~96.5%), dominates over the feedback losses at the grating end of the laser. A somewhat long length of the fibre (~4.7m), slightly longer than the length that would be optimum, was used to

ensure that negligible pump light was transmitted by the fibre as a precaution against damage to opposing diodes.

3.3. Results and discussion

The threshold pump power incident on the pump focussing lens was measured to be ~7.5W (~6W launched), and at the maximum available incident pump power of 55W (corresponding to ~44W launched power) the fibre laser produced a maximum output power 10.5W at 1921nm (see figure 3.6). From figure 3.6 it can be seen that the average slope efficiency with respect to launched pump power at 1921nm is ~29%, but at higher pump powers the slope efficiency increases to ~34%. This suggests that by using higher power diode-bars, it should be possible to achieve a significant increase in optical-to-optical efficiency as well as output power.

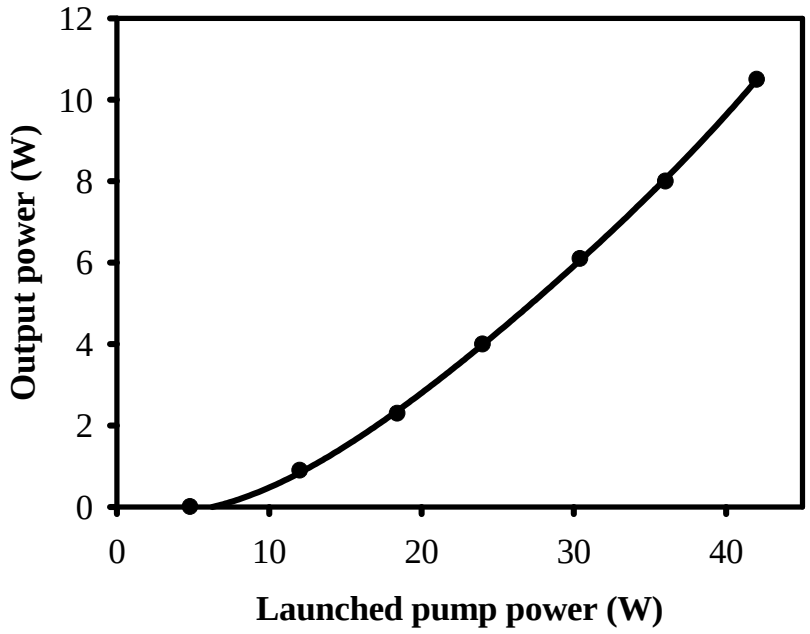

Figure 3.6: Output power versus launched pump power. The experimentally measured points in the graph are only connected (not fitted) for better visibility. The accuracy of power meter in the 2µm spectral region was assessed to be ~± 2%.

The lasing wavelength could be tuned over 215nm from 1855 to 2070nm at multi-watt power levels, and over 150nm from ~1860 to 2010nm at output power

levels in excess of 9W by simply adjusting the diffraction grating angle (see figure 3.7). The bandwidth of the tunable laser output (FWHM) was measured to be ~1nm.

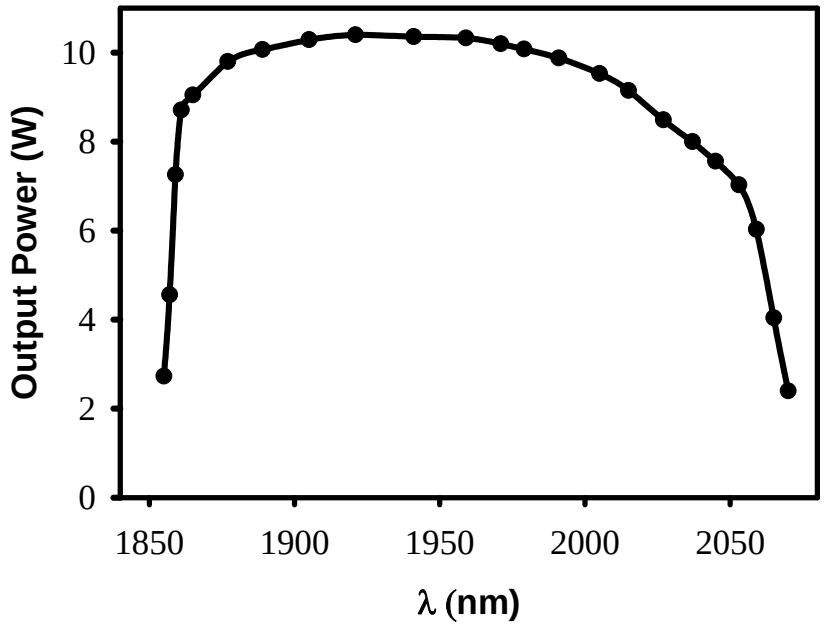

Figure 3.7: Tunable Tm-doped fibre laser output versus wavelength. The experimentally measured points in the graph are only connected (not fitted) for better visibility. The experimental error was assessed to be $\pm$ 3%.

From figure 3.7 it can be seen that the tuning range was sharply limited as we tuned the laser to the shorter wavelengths. This might be due to the higher reabsorption loss at shorter wavelengths. However, in the long wavelength wing where the emission approaches a four level character, involving Stark levels which are above the ground level, gain is achieved for a small population in the upper laser level. Thus the laser is more tunable in the long wavelength wing. In practice, for many of the broad band transitions of rare-earth dopants in glass, the character of the emission can vary from essentially pure 3-level to pure 4-level, (i.e. empty lower laser level) as the emission wavelength goes from line centre to the long wavelength limit [Hanna90].

One of the main limitations of the laser arrangement shown in figure 3.5 is that only simple singlet plano-convex lenses were available for collimating the fibre output at both ends. Thus, due to the effect of spherical aberration, the output

beam quality was degraded to $M^2 \sim 5$, where a plano-convex lens with focal length of 40mm was used to collimate the output power of the fibre laser. Also the feedback efficiency of the external cavity was reduced due to the aberration caused by the plano-convex lens with focal length of 25mm (see section 4.4.1 of chapter 4 for more information on beam quality degradation due to phase aberration, and also [Siegman93, Siegman94]). By taking into account the effect of spherical aberration on beam quality, it was estimated that $M^2 \leq 1.3$ for the fibre output (i.e. before the collimating lens). The use of aberration-corrected lenses should improve the beam quality and, in addition, may help to extend the wavelength tuning range by increasing the feedback efficiency of the external cavity.

During the experiments the main body of the fibre, over 90% of it, was kept immersed in water at a temperature of 12°*C*. This was made possible by use of a water-cooled heat sink which had been designed and built in house (see figure 3.8). As the fibre was in direct contact with water it enabled us to change the temperature of the water circulating around the fibre by simply adjusting the chiller temperature. The tuning curve presented in figure 3.7 is for the best obtained results.

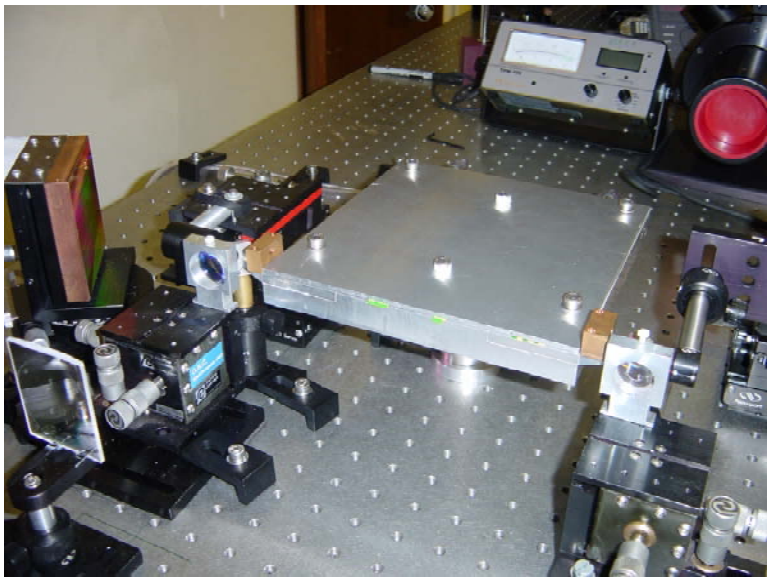

Figure 3.8: Experimental setup with water cooled heat sink.

The idea of active cooling came from the fact that the small surface area of the fibre can lead to a significant absolute temperature rise of the fibre if one only relied on free convection in air and radiation loss for removal of the heat (see chapter 2, section 2.2.2.1, for more details). To further investigate the effect of cooling on the fibre laser performance the following experiment was performed. Tuning range and overall performance of the Tm-doped silica fibre laser in the air at room temperature and in the heat sink at $12°C$ were investigated and compared. The length of the fibre was ~5.4m and the pumping scheme and laser setup in each case was identical to the previous experiment (see figure 3.5).

The output power versus launched pump power for the two cases are shown in figure 3.9. Circles and triangles represent the performance of the fibre cooled with water at $12°C$ and in air at room temperature, respectively. For the fibre cooled at 12°C the threshold pump power launched into the fibre was ~6.2W, and for the maximum launched pump power of ~44W the fibre laser produced a maximum output power of 10.4W at 1981nm, whilst for the fibre in the air the threshold pump power launched into the fibre was higher by 15%, namely ~7.3W. Also in this case for the maximum launched pump power of ~44W the fibre laser produced only a maximum output power of 9.1W at 2001nm. From figure 3.9 it can be seen that while the average slope efficiency with respect to the launched pump power for the cooled fibre at 1981nm is ~29%, for the fibre in the air the average slope efficiency is only 24% at 2001nm.

The tuning range of the fibre laser was also influenced by the cooling process. Figure 3.10 shows the output power versus wavelength for two cases. It can be seen that whilst the fibre was tunable over 190nm in both cases, the centre wavelength shifted towards the shorter wavelength, from 2001nm in the case of non actively cooled fibre to 1981nm in the case of water cooled fibre.

All the observed effects are due to the quasi-three-level nature of the 2μm transition of thulium ions in silica fibres. As we have seen in chapter 2 the common element in quasi-three level laser transitions is that the lower laser levels are in the ground-state multiplet, which means that the lower laser levels are only a few hundred cm^{-1} above the ground state. Thus the lower laser levels have a significant population in thermal equilibrium at room temperature since kT is

$207cm^{-1}$ at 300K. Cooling the quasi-three level laser transition leads to the increase in the population inversion density by reducing the lower laser level population, which in turn leads to the lower threshold and consequently higher efficiency.

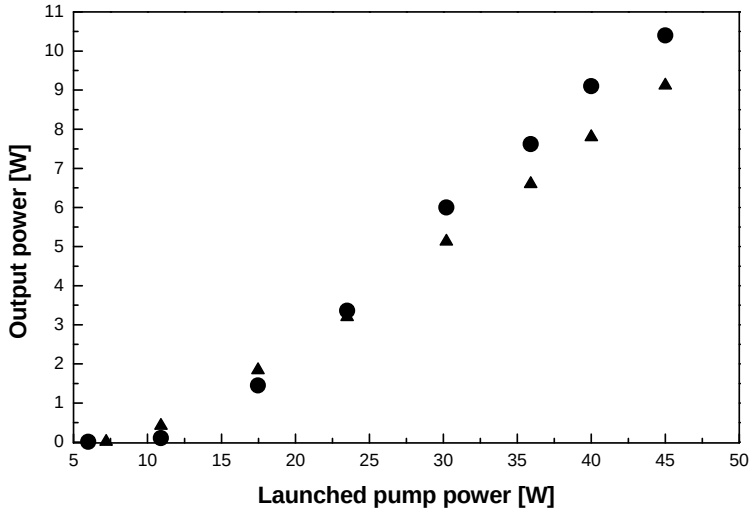

Figure 3.9: Output power versus launched pump power for two cases: fibre cooled at 12°*C* (circles) and fibre in the air at room temperature (triangles).

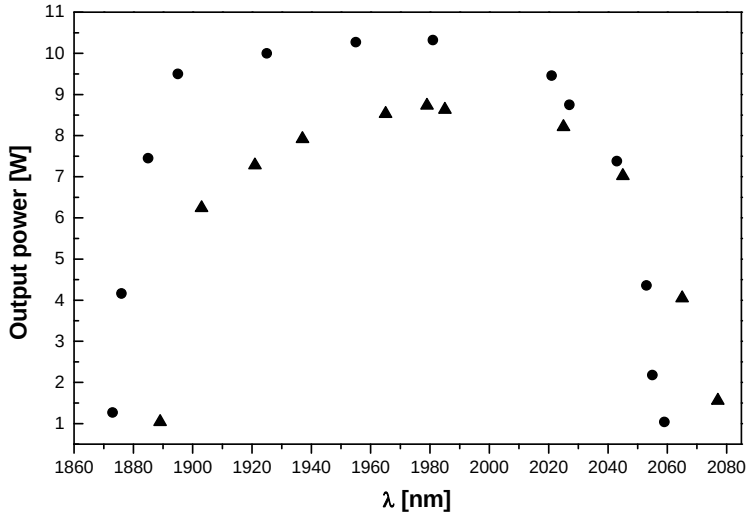

Figure 3.10: Output power versus wavelength for two cases: fibre cooled at 12°*C* (circles) and fibre in the air at room temperature (triangles).

Here in the case of an actively cooled fibre, the cooling effect led to an increase in the population inversion density and hence the reduction in the reabsorption loss, which in turn reduced the threshold. The peak emission shift from 1981nm in the case of an actively cooled fibre to 2001nm for the fibre in air at room temperature can be attributed to a change in Stark level population responsible for the transition in each case. The probable scenario might be as follows: at low temperatures by the effect of cooling the laser transition terminates at lower Stark levels with the consequence of shortening in centre wavelength. As the temperature increases the laser transition terminates at higher Stark levels with the consequence of centre wavelength shift towards the longer wavelength.

3.4. Summary

In this chapter a cladding-pumped Tm-doped silica fibre laser with 10.5W of output power at 1921nm, tunable from 1855 to 2070nm at multiwatt power levels was presented. Also the effect of cooling on the fibre performance was investigated. It was shown that despite the significant advantage that the distributed heat absorption in fibre lasers brings over bulk lasers, heat sinking of these devices would improve their performance by decreasing the lower laser level population. It is worth mentioning that heat sinking of the fibre ends would enable longer term stability, reduced thermally-induced core-end effects and improve performance in a similar way to the rest of the fibre but is difficult to implement.

The author is very grateful to Dr. D. Y. Shen for fruitful discussions and also help during the experiments presented in this chapter.

3.5. References

[Andreeva75] V. D. Andreeva, “Fundamental aberration coefficient of an optical system,” Sov. J. Opt. Tech., vol. 42, pp.321 (1975).

[Clarkson96] W. A. Clarkson, D. C. Hanna, “Two-mirror beam-shaping technique for high-power diode bars,” Opt. Lett. vol. 21, 375-377 (1996).

[Clarkson03] W. A. Clarkson, A. Abdolvand, D. Y. Shen, R. B. Hayward, L. J. Cooper, R. B. Williams and J. Nilsson, “High power two-micron fibre

lasers," SPIE Proceedings on Gas and Chemical Lasers - High Power Lasers Conference 2002 (Invited).

[Clarkson01] W. A. Clarkson, A. Abdolvand, V. Matera, T. M. J. Kendall, D. C. Hanna, J. Nilsson and P. W. Turner, "Spectral beam combining of cladding-pumped Tm-doped silica fibre lasers," Quantum Electronics & Photonics Confrence(QEP-15)/Glasgow, pp.13 (2001).

[Hanna88] D. C. Hanna, R. M. Percival, I. R. Perry, R. G. Smart, P. J. Suni, J.E.Townsend, A.C.Tropper, "Continuous-wave Oscillation of a Monomode Thulium-Doped Fibre Laser," Electron. Lett., vol.24(19) pp.1222-1223(1988).

[Hanna89] D. C. Hanna, M. J. McCarthy, I. R. Perry, P. J. Suni, "Efficient high-power continuous-wave operation of monomode Tm-doped fibre laser at 2µm pumped by Nd:YAG laser at 1.064µm," Electron. Lett., vol.25(20) pp.1365-1366(1989).

[Hanna90] D. C. Hanna, R. M. Percival, R. G. Smart, A. C. Tropper, "Efficient and tunable operation of a Tm-doped fibre laser," *Opt. Commun.*, vol.75 pp.283 (1990)

[Hayward00] R. A. Hayward, W. A. Clarkson, P. W. Turner, J. Nilsson, A. B. Grudinin, D. C. Hanna, "Efficient cladding-pumped Tm-doped silica fibre laser with high power single-mode output at 2µm," Electron. Lett., vol.36(8) pp.711-12(2000).

[IPG Photonics] For more information please visit: www.ipgphotonics.com

[Jackson98] S. D. Jackson and T. A. King, "High-power diode-cladding-pumped Tm-doped silica fibre laser, " Opt.. Lett., vol.23, pp.1462-1464(1998)

[Jenkins76] F. A. Jenkins and H. E. White, "Fundamentals of Optics", 4th edn, McGraw-Hill, new York (1976)

[Po89] H. Po, E. Snitzer, R. Tumminelli, L. Zenteno, F. Hakimi, N. M. Cho and T. Haw, "Double clad high brigthnee Nd fiber laser pumped by GaAlAs phased array," Presented at the Opt. Fibre Commun. Conf., paper PD7 (1989).

[Siegman93] A. E. Siegman, "Analysis of laser beam quality degradation caused by quartic phase aberrations," Appl. Opt., vol. 32, pp. 5893 (1993).

[Siegman94] A. E. Siegman, J. A. Ruff, "Measurement of beam quality degradation due to spherical aberration in a simple lens," Optical and Quantum Electronics, vol. 26, pp. 629-632 (1994).

[Townsend87] J. E. Townsend, S. B. Poole and D. N. Payne, "Solution doping technique for fabrication of rare-earth doped fibre amplifiers," Electronics Letters, vol. 23, pp. 329-331 (1987).

Chapter 4

High-power Wavelength-Combined Cladding-Pumped Tm-doped Silica Fibre Laser

4.1. Introduction

In chapter two it was shown that for power scaling in fibre lasers there are three main issues which need to be addressed: Firstly, the effective core area must be increased to avoid unwanted nonlinear processes and intensity induced damage, whilst maintaining freedom from thermal effects, and also retaining the ability to select a single-spatial-mode. Secondly a practical way for efficiently launching the pump light from multiple high power diode sources into the fibre is needed. Finally a fibre geometry which allows effective removal of waste heat to minimise the risk of thermally-induced damage is also required. In chapter two we have also seen that over the last few years there has been an increase in the research activity directed towards finding solutions to the above problems. However there is clearly going to be an upper limit to the single mode power that can be obtained from a conventional double-clad fibre.

One attractive solution for power and brightness scaling of fibre lasers is to use multiple fibres and beam-combine their outputs using an intracavity diffraction grating. For example, this technique has been recently applied to two Yb-doped silica fibre lasers and an output power of 223mW at ~1μm has been reported [Cook99]. This scheme offers the route for scaling fibre laser powers to very high powers while maintaining the spatial brightness of a single fibre beam [Bochove2002]. In this respect cladding-pumped Tm-doped silica fibre lasers are

of particular interest for power scaling in the 2μm spectral region due to their broad emission spectrum (>300nm), broad absorption band, of up to 20nm with centre at 790nm, and a relatively high lasing efficiency (see chapter 3). A wavelength-combined Tm-doped silica fibre laser system with 14W output power in the 2μm spectral region will now be presented.

4.2. Experimental set-up and results

We explored spectral beam combining of four double-clad Tm-doped silica fibre lasers. The geometry and spectroscopic characteristics of each fibre used in our experiment was identical to the one explained in chapter 3. Our set-up is shown in figure 4.1 and used four double-clad Tm-doped silica fibres of length ~4m.

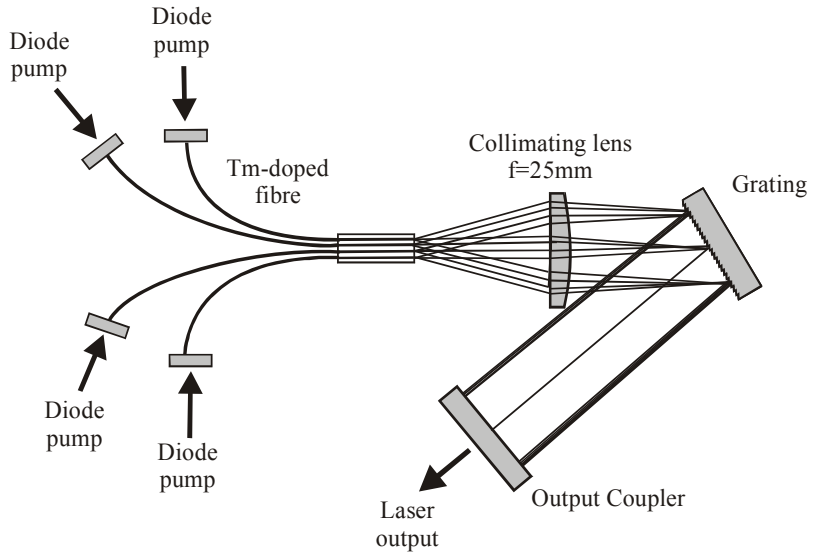

Figure 4.1: Wavelength-combined Tm-doped silica fibre lasers.

Each fibre was butted to a mirror with a high reflectivity at ~1.8-2.1μm and a high-transmission (>94%) at the pump wavelength. Each fibre was end-pumped by a beam-shaped diode-bar with a wavelength in the range of 790-797nm [Clarkson96]. Here also the two- mirror beam shaper allowed the highly elliptical diode-bar output beam to be reformatted with nearly equal beam quality factors in orthogonal planes of ~70, without significantly reducing the output power.

For preliminary experiments the end facets were cleaved perpendicular to the fibre axis (flat-cleaved) and arranged adjacently in a linear array with core-to-core separation of ~200μm (figure 4.2). The outputs from the fibres were collimated with a single 25mm focal length lens and then incident with slightly different angles of incidence on a diffraction grating with 600 lines/mm, and ~80% first-order reflectivity at 1.9μm, positioned 25mm from the lens. The first-order diffracted beam was then incident on a plane output coupler with a reflectivity of ~45% from ~1.8-2.1μm to provide feedback for laser oscillation.

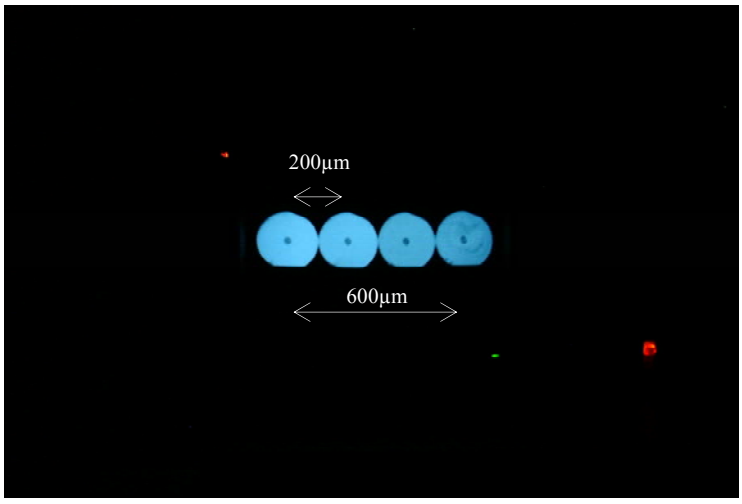

Figure 4.2: Core-to-core arrangement of the fibres in a linear array with core-to-core separation of ~200μm.

The grating is inside the resonator and the fibre-end facet interface is located at the focal plane of the lens so that the beam is collimated at the grating and output coupler. This ensures the spatial overlap of the beams from the fibres. The principle of operation is that the grating selects the operating wavelength of each of the four fibre lasers so as to produce a single combined beam incident on the output coupler, and the flat mirror makes the beams propagate in the direction normal to its surface. Without the grating feedback, the four lasers using only the 3.6% Fresnel reflection for feedback produced a combined output power of approximately 23.6W for a total launched pump power of ~85W. With grating feedback, a maximum combined output power of 11W was achieved on four lines at wavelengths, 1967nm, 1976nm, 1985nm and 1994nm.

Lets consider the diffraction grating equation:

$$m\lambda = \Lambda(\sin\theta + \sin\phi) \quad (4.1)$$

where m is the diffraction order (The integer m in our case was taken to be 1 due to the fact that the grating has been blazed at 1.9μm), Λ is the groove spacing (600 lines/mm), θ is the angle of incident and ϕ is the angle of diffraction.

Using equation 4.1, it can be seen that the wavelength separation $\Delta\lambda$ relates to the focal length f of the collimating lens, core-to-core separation D of the fibres and the dispersion $d\theta/d\lambda$ of the grating, and can be expressed as [Daneu00]

$$D \approx f\frac{d\theta}{d\lambda}\Delta\lambda . \quad (4.2)$$

The grating dispersion is given by

$$\frac{d\theta}{d\lambda} = \frac{1}{\Lambda\cos\theta} \quad (4.3)$$

where θ is the angle of incidence relative to the grating normal. Thus equation 4.2 can be rewritten in a more convenient form as

$$\Delta\lambda \approx \Lambda\frac{D}{f}\cos\theta . \quad (4.4)$$

In this experiment θ was approximately 47.5° and D was equal to 200μm. By adjusting the grating angle, the centre wavelength tuned over a range of 68nm from 1952nm to 2020nm with over 9W output power across the entire range (see figure 4.3).

Figure 4.4 shows the output power as a function of the lunched pump power of the laser with flat-end facet fibres. The power reflected from the grating in zero order was ~3.8W, indicating that a grating with higher first-order reflectivity would allow higher output power.

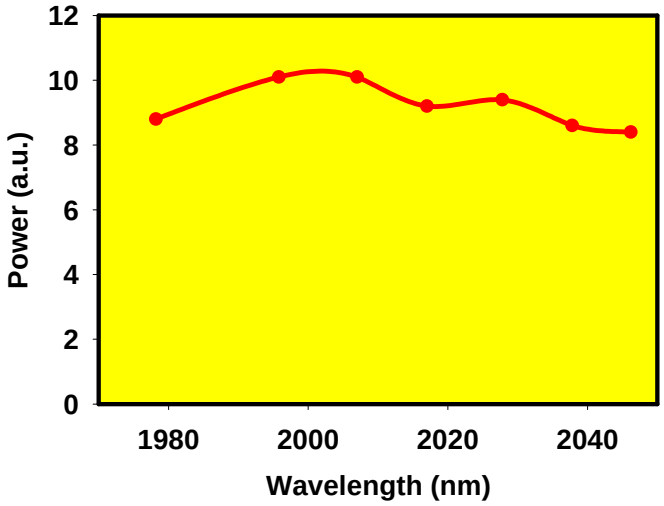

Figure 4.3: Combined output power versus wavelength (flat-cleaved fibre end facets). The experimental error was assessed to be ± 3%.

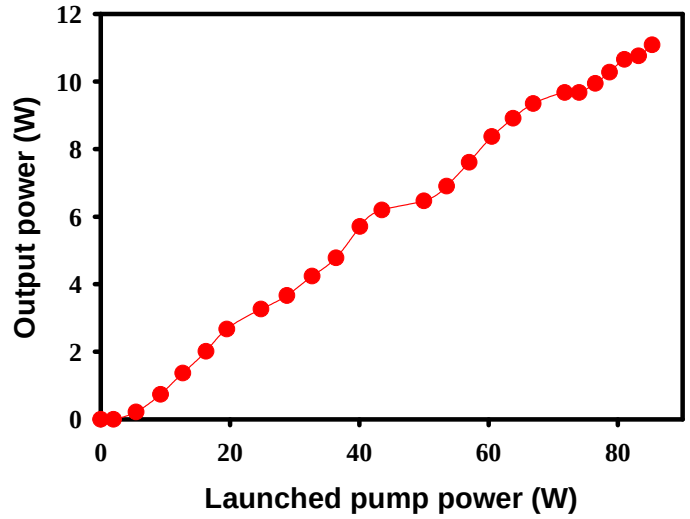

Figure 4.4: Output power as a function of launched pump power for fibres with flat-end facets and 45% reflectivity output coupler. The experimental error was assessed to ± 2%.

In this experiment the tuning range was limited by the onset of lasing from the flat end-facet due to ~3.6% Fresnel reflection when the external cavity feedback falls below this level. Flat end-facets also restricted the choice of output coupler to one with higher transmission than optimum for high output power.

To scale to higher output power and extend the tuning range of the laser the fibre facets were angle-cleaved by ~7° degrees to reduce the effective feedback [Koester64]. The set-up was identical to that used in the previous experiment.

Figure 4.5 shows the cw output power as a function of the launched pump power for two different output couplers. By using an output coupler with ~20% reflectivity in the range ~1.8-2.1μm, a maximum combined output power of 14W was achieved on four lines at wavelengths, 1926nm, 1956nm, 1980nm and 2000nm. In this case the angle of incident θ was approximately 51° and core-to-core separation of the fibres, D, was equal to 600μm. In this experiment the somewhat larger value of D than was the case for fibres with flat-end facets was due to the difficulty in putting fibres with angle-cleaved end-facets together, to maintain the unidirectionality of the beams before the collimating lens.

The power reflected from the grating in zero order was ~1.8W. By adjusting the grating angle, the centre wavelength could be tuned over a range of 200nm from 1900nm to 2100nm with muiltwatt output power across the entire range (see figure 4.6).

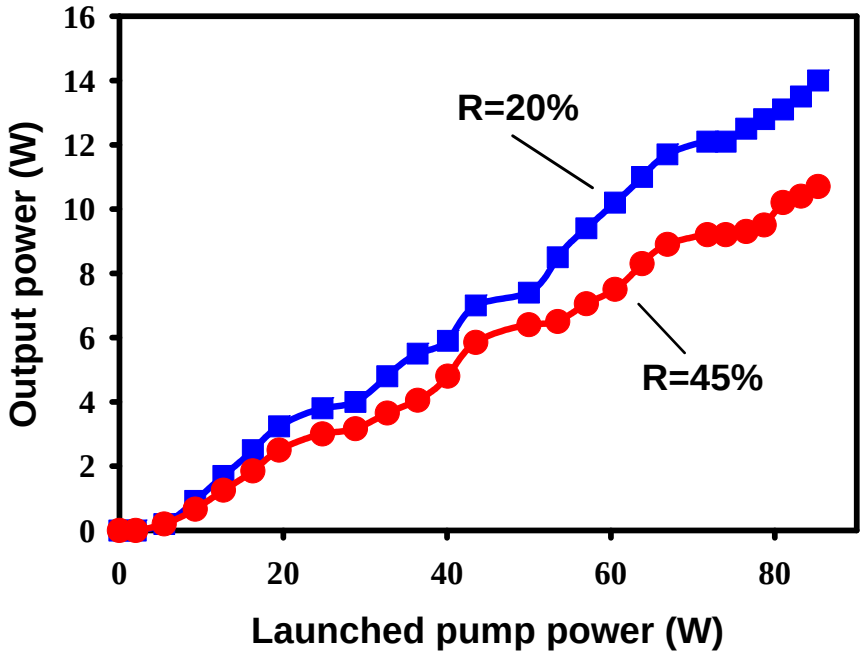

Figure 4.5: Output powers as a function of the launched pump power for two different output couplers (angle-cleaved fibre end-facets). The experimental error for these measurments was assessed to be ± 2%.

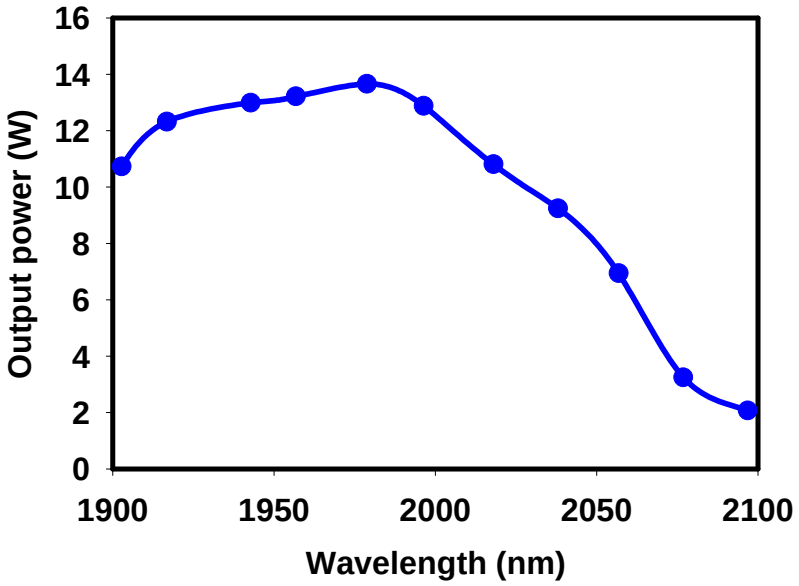

Figure 4.6: Combined output power versus centre wavelength (angle cleaved end facets). The experimental error was assessed to be $\pm 3\%$.

4.3. Beam quality discussion

For the beam-combined system with flat-cleaved fibre end-facets and at the maximum available launched pump power of ~85W, the M^2 beam propagation factors of the beam-combined laser system, was measured using a Merchantek beam scope to be $M_x^2 \approx 4.9$ and $M_y^2 \approx 4$, in the x-z and y-z planes, respectively. This beam quality was similar to what was expected, and measured values of $M_x^2 \approx 4.1$ and $M_y^2 \approx 3.8$, for a single fibre just after the collimating lens (f=25mm) and no external cavity. This is due to spherical aberration caused by the collimating lens as a result of the large numerical aperture (NA=0.12) of the fibre. However, here we consider three potential sources of degradation in beam quality for beam-combined systems, namely: phase aberration of the lens, offset aberration of the lens and heating of the grating. We will further assess the contribution of each of these sources in degradation of beam quality of our system in the following sections.

4.3.1. Analysis of beam quality degradation due to phase aberration of the lens

In general, an imperfect optical element, for example an uncorrected simple lens, can add quartic phase distortion to an incident wavefront and degrade the transverse beam quality. According to Siegman et. al. [Siegman93, Siegman94], a laser beam with a Gaussian intensity profile and Gaussian spot size *w,* and initial beam quality factor M_i^2, after propagating through a lens of focal length *f* which produces a phase distortion $\Delta\varphi(w)$ of the form

$$\Delta\varphi(w) = \frac{2\pi}{\lambda}\left(\frac{w^2}{2f} - C_4 w^4\right) \qquad (4.5)$$

will suffer a degradation in the beam quality with a resultant beam quality factor M_f^2 being given by

$$M_f^2 = \sqrt{\left(M_i^2\right)^2 + \left(M_q^2\right)^2} \qquad (4.6)$$

where M_q^2 is due to the quartic phase aberration and is given by

$$M_q^2 = \left(\frac{w}{w_q}\right)^4 \qquad (4.7)$$

with a critical width w_q which is given by

$$w_q = \left(\frac{\lambda}{2^{1.5}\pi C_4}\right)^{0.25} \qquad (4.8)$$

and *w* is the Gaussian spot size of the laser beam just before the lens, λ is the wavelength of the incident light. Here C_4 is the quartic phase aberration coefficient, or in other words spherical aberration coefficient, and for a thin lens can be written in the following form [Siegman93]

$$C_4 = \frac{1}{32n(n-1)f^3}\left[\frac{n^3}{n-1} + (3n+2)(n-1)p^2 + \frac{n+2}{n-1}q^2 + 4(n+1)pq\right] \quad (4.9a)$$

$$= C_{4f} \Big/ f^3 \quad (4.9b)$$

where n is the refractive index of the lens material and C_{4f} is a dimensionless factor that helps to rewrite equation 4.8 in a more convenient and useful form as follows

$$w_q = \left(\frac{f^3\lambda}{2^{1.5}\pi C_{4f}}\right)^{0.25} \quad (4.10)$$

In equation 4.9a, the quantities p and q are called the position and shape factors of a thin lens, respectively. The shape factor, q, for the thin lens is given by [Siegman93]

$$q = \frac{R_2 + R_1}{R_2 - R_1} \quad (4.11)$$

where R_1 and R_2 are the curvatures of the first and second surfaces of the thin lens. The case $q=0$ corresponds to a symmetric lens, and the case $q=\pm 1$ correspond to plano-curved or curved-plano lenses.

The parameter p is given by [Siegman93]

$$p = \frac{2f}{S} - 1 \quad (4.12a)$$

$$= 1 - \frac{2f}{S''} \quad (4.12b)$$

where S and S'' represent the object and image distance from the lens, respectively. The case $p=0$ corresponds to an object and its image lying at a distance $2f$ on each side of the lens. The value $p=1$ corresponds to an object at the focal plane of the lens and the image at infinity. Similarly, $P=-1$ corresponds to an object at infinity and the image at the focal plane of the lens. From equation 4.12,

it can be seen that when an object and its image are real then $p^2 \leq 1$ and thus spherical aberration cannot be zero.

From equation 4.9a it can be seen that the quartic phase aberration coefficient, C_4, of a thin lens depends on its position and shape factors and also on the material of the lens. For a given position factor, the value of the shape factor which minimises the spherical aberration is given by the condition

$$\frac{\partial C_4}{\partial q} = 0 \qquad (4.13)$$

Thus, we obtain

$$q_{\min} = -2p\frac{n^2-1}{n+2}. \qquad (4.14)$$

Substituting equation 4.14 into equation 4.9a, we obtain the corresponding minimum spherical aberration

$$C_{4\min} = -\frac{1}{32f^3}\left[\left(\frac{n}{n-1}\right)^2 - \frac{np^2}{n+2}\right]. \qquad (4.15)$$

According to equation 4.9a, for a given value of p, C_4 as a function of q follows a parabola with a vertex lying at (q_{min}, C_{4min}).

For the CaF_2 plano-convex lens used in our experiment with $n \approx 1.42$, and f=25mm and its planar side towards the focal point of the laser beam (p=1 and q=-1), the dimension-less factor, C_{4f}, calculated via equation 4.9 was ≈ 0.41. Using the following, known and estimated values: fiber core diameter $\approx 20\mu m$, NA=0.12, f=25mm , λ=2000nm, , $M_i^2 \approx 1.3$, C_{4f}=0.41, we estimated (see equations 2.15, 2.17 and 2.11) the Gaussian spot size of the laser beam on the collimating lens to be $w \approx 2.38$mm, whilst the calculated value for critical beam size, w_q, was 1.72mm (for this calculation equation 4.10 is used). This implies that there will be an observable degradation in beam quality due to aberration. Using equations 4.6, 4.7 and 4.8 it was possible to calculate the degradation in beam quality, caused by quartic phase aberration of the lens, and was found to be $M_q^2 \approx 3.76$. This results in a calculated value for the final beam quality, $M_f^2 \approx 3.98$, which is in reasonable agreement with the measured M^2 values of $M_x^2 \approx 4.1$ and

$M_y^2 \approx 3.8$ in the *x*-*z* and *y*-*z* planes, respectively, for a single fibre laser just after the collimating lens (*f*=25mm).

It is, however, possible to improve the beam quality of the system by simply improving the fibre design, for instance by reducing the *NA* of the core. This would serve to reduce the beam size on the collimating lens, below and/or fairly close to the critical beam size, and hence reducing the demands on lens design. However, in the context of power scaling, it is desirable to use a longer focal length collimating lens in order to reduce the wavelength separation of the fibre lasers. This would serve to allow more fibre lasers to be beam-combined (this will be considered in more detail in section 4.4). Thus it is very important to see if there is any practical way to improve brightness scalability of the system by reducing the effect of spherical aberration caused by the lens. Since spherical aberration of a thin lens varies as f^{-3}, indeed it is possible to make it small for a combination of lenses having focal lengths of different signs.

For example, the overall focal length of ~18cm can be achieved by using a combination of an equi-convex lens with radii of curvature 9.24cm and –15.51cm and focal length of ~14cm, and a negative meniscus with radii of curvature –9.56cm and –15.31cm and focal length of ~-60cm, all made of CaF_2.

For a thin lens with a refractive index $n \approx 1.42$ (CaF_2 lens as used in our experiment), equations 4.9a, 4.14 and 4.15 reduce to

$$C_4 = \frac{-1}{19f^3}\left(6.81 + 2.62p^2 + 8.14q^2 + 9.68pq\right) \quad (4.16a)$$

$$q_{\min} = -0.59p \quad (4.16b)$$

$$C_{4\min} = \frac{-1}{32f^3}\left(11.43 - 0.41p^2\right) \quad (4.16c)$$

respectively. The shape factor of the lenses are given by q_1=0.25 and q_2=4.32 (see equation 4.11). If consider that a parallel beam of light is incident on the first lens (equi-convex lens), then the position factor for this lens would be equal to, p_1= –1. Substituting for f_1, p_1 and q_1 into equation 4.16a, we find that the spherical aberration for the first lens is $C_4 \approx -1.44 \times 10^{-4}$ cm^{-3}. On the other hand, since the second lens (negative meniscus) focuses the beam at a distance of 18cm, its

position factor is given by $p_2 = 1-(2f_2 \div 18)$ (see equation 4.12b) or p_2=7.66. Substituting for f_2, p_2 and q_2 into equation 4.16a, we find that the spherical aberration for the second lens is $C_4 \approx 1.54\times\ 10^{-4}$ cm^{-3}. As it can be seen this value is almost equal in magnitude but opposite in sign to the corresponding coefficient for the first lens. Figure 4.8 shows a rough scheme of the proposed doublet design for the lens system.

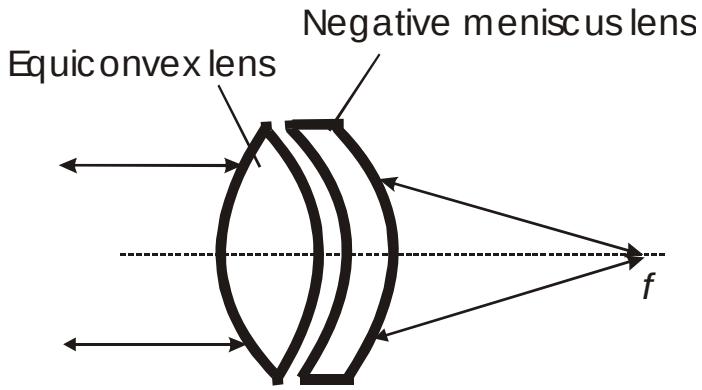

Figure 4.8: Proposed doublet design to correct for spherical aberration.

A design of this kind can also serve to improve the feedback from the grating. It is particularly important in tunable schemes like the one described in chapter 3 (see figure 3.5).

4.3.2. Analysis of beam quality degradation due to off-axis lens aberration

In beam-combined systems, one should also consider the effect of offset of a lens aberration on beam quality. Generally linear decentre can occur if two beams are combined. The beam quality degradation due to decentre , $M^2_{decentre}$, of two incoherently combined beams, two combined beams at different wavelengths, is given by [Zorabedian03]

$$M^2_{decentre} = \sqrt{1+\left(\frac{\Delta}{w}\right)^2} \qquad (4.17)$$

where Δ is the linear decentre and w is the spot size of the input beam at the collimating lens, with the assumption that the spot size is identical for the two beams. Taking Δ to be 400µm in our case (see fig. 4.2) and $w \approx 2.4$mm, results in $M^2_{decentre} \approx 1.01$, which obviously is a negligible degradation in beam quality.

However, in order to experimentally study the effect of off-axis aberration, the beam quality factor of one fibre in an external cavity after the output coupler as a function of lens position in the x direction (transverse to the propagation direction) was measured. For beam quality measurements a coherent ModeMaster was used. The results are shown in figure 4.9, and confirm that degradation in beam quality is negligible for lens offset $\leq \pm 500\mu m$ from the centre of the collimating lens.

Thus, off-axis aberration turns out to be a negligible source of degradation in the beam quality of the beam-combined laser, but clearly needs to be considered in the design of higher power beam-combined laser systems where many fibres are spectrally beam combined.

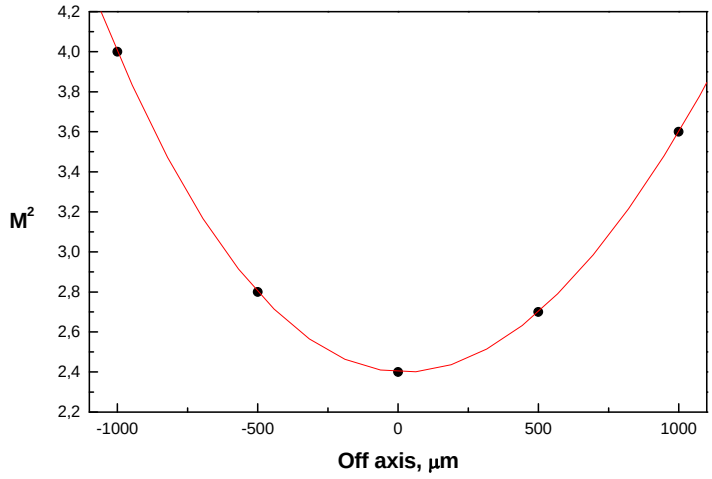

Figure 4.9: M_r^2 as a function of lens movement in off axis. The line in the graph is the best fit to the measured points.

4.3.3. Analysis of beam quality degradation due to heating of the grating

Another potential source of degradation in beam quality for beam-combined systems, which should certainly be considered, is heating of the grating. This is due to the fact that the heating of the grating with consequence of bulging of its surface can act as a thermal lens and thus result in the further degradation of beam quality, and hence put an upper limit on brightness scalability of beam–combined systems. However, the solution to this problem, which should be considered for design of an ultra high power beam-combined system, is to use a grating with a metal substrate for good thermal management via heat sinking.

In order to asses the contribution of heating of the grating in beam quality degradation of the beam combined system the following experiment was performed; the beam quality factor of one fibre in an external cavity (using R=45% output coupler) was measured and compered with the M^2 value for the beam combined system. When the external cavity consisting of one fibre laser was producing the maximum output power of 3.1W at 2μm, the M_r^2 value was measured after the output coupler to be 2.4. This value is roughly two times less than the measured value for the beam combined system of $M_x^2 \approx 4.9$ and $M_y^2 \approx 4$, in the x-z and y-z planes, respectively (see section 4.3). This reveals that heating of the grating is one of the main sources of degradation in beam quality for the beam combined system.

4.4. Power scalability discussion

Wavelength beam combined systems with an external cavity offer a route towards power scaling of fibre lasers. A rough estimation using equation 4.2 shows that it is possible to beam combine up to 100's of fibre lasers. For example, taking D=3cm, and f=25cm, and $d\theta/d\lambda$ of 2 rad/μm, results in $\Delta\lambda$ of 60nm. This would, in principle, allow up to 150 fibres with centre-to-centre spacing of 200μm to be beam combined.

4.5. Summary

In this chapter, a simple way for power scaling in fibre lasers was described, and was demonstrated what is believed to be the first spectral beam-combined Tm-doped silica fibre laser operating in the 2μm wavelength region. An angle-cleaved end-facet was used to extend the tuning range of the laser and allowed higher output power to be achieved via the use of a higher transmission output coupler. A maximum combined output power of 14W was achieved on four lines at wavelengths, 1926nm, 1956nm, 1981nm and 2001nm. By simply adjusting the grating angle, the centre wavelength tuned over a range of 200nm from 1900nm to 2100nm with muiltwatt output power across the entire range. The M^2 beam propagation factors of the spectrally beam-combined laser, measured using a Merchantek beam scope, were $M_x^2 \sim 4.9$ and $M_y^2 \sim 4$. Different causes of beam quality degradation were discussed. With a simple change in fibre design, reducing the core NA, and/or a reasonable level of correction for spherical aberration, and also using a metal substrate grating it should be possible to improve the overall beam quality of the system.

With a longer focal length collimating lens and a larger aperture grating, the wavelength separation of the fibre lasers can be reduced; allowing more lasers to be wavelength-combined. This scheme offers the potential for scaling of fibre laser powers. Such multiwatt tunable fibre laser sources could find application in areas where high-power broadband operation in the eyesafe spectral region is required.

The author would like to acknowledge Mr. T. M. J. Kendall and Mr. V. Matera (guest undergraduate student from the university of Milan, Italy) for their help in obtaining the experimental results presented in section 4.2 of this chapter. Only the results of the section 4.2 have been used by Mr. Matera in his diploma thesis (M.Sc. in engineering), which was submitted to the university of Milan in Autumn 2001.

4.6. References

[Bochev02] E. J. Bochove, "Theory of spectral beam combining of fibre lasers," IEEE J. of Quantum Electronics, vol. **38**, pp. 432-445 (2002).

[Clarkson96] W. A. Clarkson, D. C. Hanna, "Two-mirror beam-shaping technique for high-power diode bars," Opt. Lett., vol. 21, pp. 375-377 (1996).

[Cook99] C. C. Cook and T. Y. Fan, "Spectral Beam Combining of Yb-doped Fiber Lasers in an External Cavity," OSA Trends in Optics and Photonics, Advanced Solid-State Lasers 26, 163-166 (1999).

[Daneu00] V. Daneu, A. Sanchez. T. Y. Fan, H. K. Choi, G. W. Turner, C. C. Cook, "Spectral beam combining of a broad-strip diode laser array in an external cavity," Opt. Lett., vol. 25 (6), pp. 405- 407 (2000).

[Koechner99] W. Koechner, "Solid-State Laser Engineering," Springer-Varlag, Berlin Heidelberg, 1999, pp. 413-417.

[Koester64] C. J. Koester and E. Snitzer, "Amplification in a fibre laser," Appl. Opt., vol. 3**,** pp. 1182-1186 (1964).

[Siegman93] A. E. Siegman, "Analysis of laser beam quality degradation caused by quartic phase aberrations," Appl. Opt., vol. 32, pp. 5893 (1993).

[Siegman94] A. E. Siegman, J. A. Ruff, "Measurement of beam quality degradation due to spherical aberration in a simple lens," Optical and Quantum Electronics, vol. 26, pp. 629-632 (1994).

[Zorabedian03] P. Zorabedian, "Software tool boosts beam analysis efficiency," Laser Focus world, pp. 63-66, November 2003.

Part II

Highly-Efficient 2µm Fibre-Bulk Hybrid Lasers

Chapter 5

Ultra-efficient Ho:YAG Laser End-Pumped by a Cladding-Pumped Tm-doped Silica Fibre Laser

5.1. Introduction

Diode-pumped solid-state lasers operating in the eye-safe 2μm spectral region have received rising interest due to their applications in remote sensing. Ho:YAG in this respect is an attractive alternative to Tm:YAG, since its lasing wavelength (typically 2091 or 2097nm) coincides with a wavelength region with excellent atmospheric transmission [Henderson93], thus avoiding the need for wavelength tuning. However, singly doped holmium lasers cannot be efficiently pumped with high-power near-infrared diode bars and therefore have to be co-doped with Tm^{3+} which can be pumped by high-power diodes. The Ho^{3+} is thereby excited by energy transfer from the excited Tm^{3+} ions. Unfortunately, a strong up-conversion effect in Tm^{3+}-Ho^{3+} co-doped lasers has prevented their general use in lidar applications [Henderson93]. This is due to the fact that severe upconversion losses can result in significant shortening of the effective lifetime of the upper laser level and hence reduce efficiency [Fan88, Rustad96]. Recently, attention has been focussed on using singly-doped Ho:YAG crystals and pumping 'in-band' by diode-pumped Tm-doped bulk lasers [Budni2000]. This approach has the advantages that upconversion losses are much lower and quantum defect heating in Ho:YAG is greatly reduced, leading to fairly high lasing efficiencies. However, thermal effects in the Tm-doped bulk laser put an upper limit on the output power.

Another drawback of this approach is that there is limited scope in the flexibility of the pump wavelength making it difficult to precisely match to the peak absorption of Ho^{3+} in YAG at 1905nm.

One attractive solution is to use a cladding-pumped Tm-doped silica fibre laser as the pump laser for Ho:YAG. As it was seen, in the first part of the thesis, cladding-pumped fibre lasers benefit from a geometry that allows relatively simple thermal management and hence offer the potential for scaling to very high power levels. The combination of high output power, good beam quality and wide wavelength tunability suggests that cladding pumped fibre lasers would be ideal pump sources for many Tm and Ho-doped bulk lasers. Preliminary experiments on Tm-doped fiber laser pumping of a Ho:YAG laser yielded a maximum output power of ~0.5*W* and a slope efficiency with respect to incident pump power of ~37% [Barnes01].

In this chapter, first the spectroscopic characteristics of Ho:YAG will be reviewed, and then a highly efficient room-temperature Ho:YAG laser, end-pumped by a cladding-pumped Tm-doped silica fibre laser, with >5*W* TEM_{oo} output and an ~80% slope efficiency with respect to incident pump power will be presented.

5.2. Spectroscopy of Ho:YAG

5.2.1. The Ho^{3+} Ion

The Holmium ion Ho^{3+} is a member of the trivalent rare earth ions. The Ho^{3+} ion has ten electrons in the 4f subshell, screened from external fields by two electronic subshells with larger radial extension ($5s^2 5p^6$).

5.2.2. Energy levels

Figure 5.1 shows many of the energy levels of Ho^{3+} in Yttrium Aluminium Garnet ($Y_3 Al_5 O_{12}$ or YAG). The energy levels are split into discrete Stark levels by the influence of the crystal field of the host. The Stark levels of each energy

level are closely spaced and the energy transfer between them is in the order of *ps* (10^{-12}s) [Kaminskii81]. The main manifolds of interest to us are the $^5I_8$ and $^5I_7$, the ground state manifold and upper laser manifold, respectively.

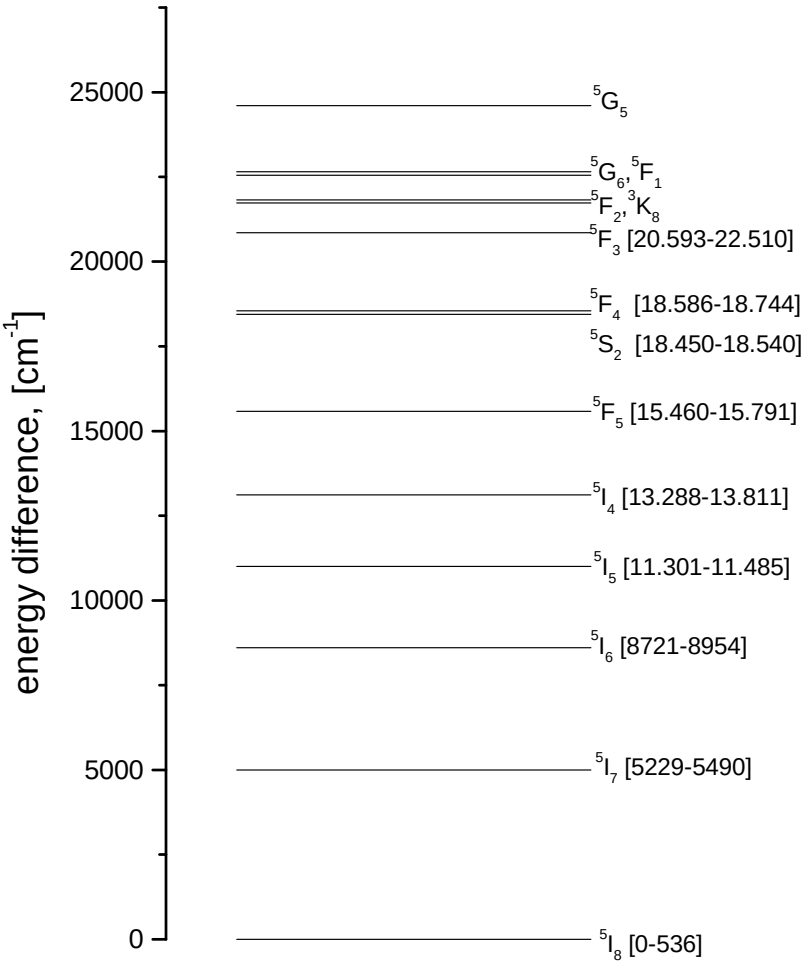

Figure 5.1: Energy-level diagram of Ho^{3+} in YAG. The data used from [Gruber91].

5.2.3. Fractional population of the laser manifolds

Table 5.1 contains a list of the Stark levels of the four bottom energy levels and their Boltzman factors at 20°C. The ground state manifold is split into 17 Stark levels with energies from 0 to 536cm^{-1}. For a temperature greater than 0°*K* the number of ions in the ground state will be a Boltzman distribution with the fraction of the total number of ions in that state (see chapter 2, section 2.1.1). The

upper laser Stark level is the 5th Stark level of the $^5I_7$ manifold and the lower laser Stark level is the 17th of the $^5I_8$ manifold for emission at 2097nm.

Stark level	$^5I_8$		$^5I_7$		$^5I_6$		$^5I_5$	
	E [cm^{-1}]	***f***	***E [cm^{-1}]***	***f***	***E [cm^{-1}]***	***f***	***E [cm^{-1}]***	***f***
1	0	0.157	5229	0.108	8721	0.110	11301	0.0124
2	4	0.154	5232	0.106	8726	0.107	11311	0.118
3	41	0.128	5243	0.100	8735	0.102	11322	0.112
4	51	0.122	5249	0.0970	8741	0.0994	11328	0.109
5	138	0.0795	5303	0.0748	8745	0.0974	11332	0.107
6	145	0.0768	5312	0.0715	8763	0.0892	11355	0.0953
7	151	0.0746	5320	0.0688	8773	0.0849	11382	0.0835
8	160	0.0714	5341	0.0620	8819	0.0678	11391	0.0799
9	399	0.0221	5352	0.0588	8844	0.0599	11422	0.0686
10	418	0.0201	5375	0.0525	8854	0.0571	11477	0.0524
11	448	0.0174	5395	0.0476	8869	0.0530	11485	0.0504
12	457	0.0166	5404	0.0455	8940	0.0374		
13	498	0.0136	5418	0.0425	8954	0.0349		
14	506	0.0131	5455	0.0355				
15	520	0.0122	5490	0.0299				
16	531	0.0116						
17	536	0.0113						

Table 5.1: Stark level energies in cm^{-1} and Boltzman factors for 20°C of the first four manifolds of Ho:YAG. Data was taken from [Gruber91].

Table 5.2 contains the Boltzman factors for the 5th Stark level of the $^5I_7$ manifold and the 17th Stark level of the $^5I_8$ manifold, measured at different temperatures. From equation 2.5, in chapter 2, it can be seen that the threshold of quasi-three-level lasers is proportional to the ratio of the lower laser level to the upper laser level Boltzman population fraction, namely f_L / f_U. From table 5.2 it can be calculated that this fraction increases from 0.1077 to 0.1566 (i.e. by 69%), for a temperature change from –20°C to 25°C. This suggests that strong thermal loading and as a consequence of that a change in Boltzman fractional population can have a significant effect on the performance of these lasers.

Temperature	-20°C	0°C	20°C	25°C	100°C
Boltzman factor for 5th Stark level of the $^5I_7$	0.0752	0.0750	0.0748	0.0747	0.0739
Boltzman factor for 17th Stark level of the $^5I_8$	0.0081	0.0097	0.0113	0.0117	0.0172

Table 5.2: $^5I_7$ and $^5I_8$ fractional Boltzman populations for a range of temperatures in Celsius [Gruber91].

5.2.4. Absorption and Emission spectra

Figure 5.2 shows the absorption spectrum and figure 5.3 shows the emission spectrum of Ho:YAG in the range of 1.8 to 2.2μm for the transition between the $^5I_8$ ground state and the $^5I_7$ manifold. According to the absorption spectrum the absorption peak is located at 1905nm. Thus the upper pump Stark level is the 4th Stark level of the $^5I_7$ manifold while the ground state pump level is the first Stark level of the $^5I_8$ manifold (see table 5.1).

Most Ho:YAG lasers operate at the 2097nm or 2091nm however some of them operate at 2123nm owing to the more favourable ratio of upper to lower (f_U/ f_L) Boltzman population factors or because of wavelength-dependent losses in the cavity. The wavelength of interest to us was the 2097nm line. From the absorption spectrum, the atomic cross-section σ was calculated to be 13.1×10^{-20}cm^2 (it is also given in [NASA02]). The atomic cross-section calculation was based on the fact that the atomic cross-section σ of the transition is the same for the absorption and the emission processes [Payne92].

The effective absorption cross-section σ_{abs} is then given by the atomic cross section σ multiplied with the Boltzman factor f_L of the lower Stark level of the transition

$$\sigma_{\text{abs}} = f_L\ \sigma . \qquad (5.1)$$

In the same way the effective emission cross section σ_{em} is given by σ multiplied with the Boltzman factor f_U of the upper Stark level of the transition:

$$\sigma_{\text{em}} = f_U\ \sigma \qquad (5.2)$$

Thus, according to table 5.1 the effective emission cross-section of the 2097nm line is only 0.98×10^{-20}cm^2 because of the relatively low Boltzman population of the upper Stark level (f_U=0.0748). Also Payne et. al. [Payne92] gave a measured effective emission cross-section value of 0.98×10^{-20}cm^2 for 2097nm line in Ho:YAG at 22°C.

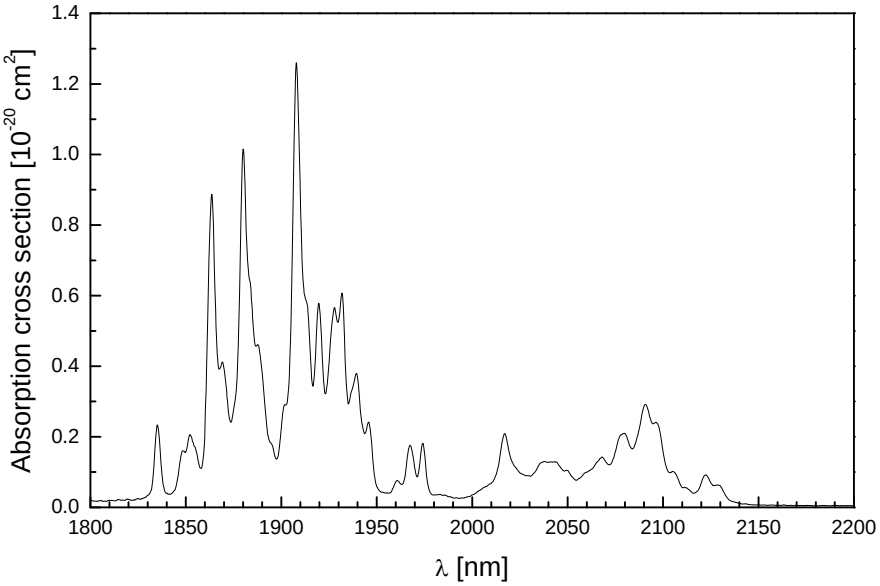

Figure 5.2: Absorption spectrum of Ho^{3+} in YAG at 22°C measured with 0.2nm resolution in a 2% doped 5mm length Ho:YAG rod [NASA02].

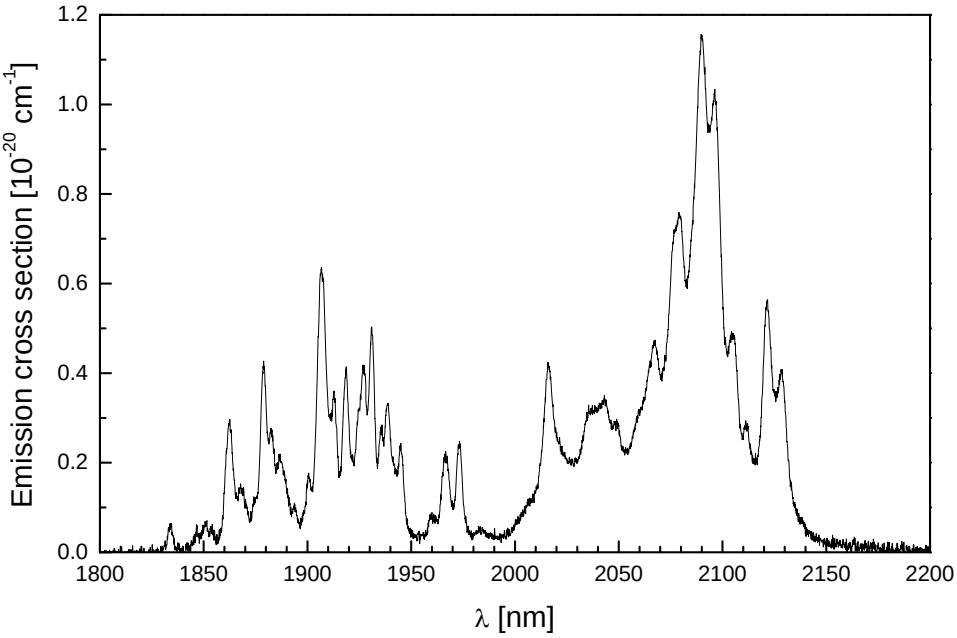

Figure5.3: Emission spectrum of Ho^{3+} in YAG at 22°C measured with 0.1nm resolution in a 2% doped 5mm length Ho:YAG rod [NASA02].

5.2.5. Discussion

From the absorption spectrum shown in figure 5.2 it can be seen that Ho:YAG has several relatively strong absorption lines near 1.9μm. However, high power diode bars operating at 1.9μm are not yet readily available, so power scaling via this approach is not possible [Nabors95].

The only absorption within the wavelength range of readily available high-power diode lasers is at 880nm into the $^5I_5$ level, but the absorption cross section at this wavelength is very small (0.05×10^{-20} cm^2) and because of the short lifetime of the $^5I_5$ and the $^5I_6$ levels (440ns and 45μs, respectively) no cross-relaxation process takes place [Basiev96]. One way that laser designers have overcome this problem with holmium lasers is by using diode pumping and a sensitisation scheme. Both holmium and thulium are doped into the same rod. This form of scheme brings with it its own problems [Rustad96, Fan88, Henderson93, and also see chapter 1]. On the other hand, singly doped Ho:YAG exhibits strong upconvesion process into the $^5I_6$ level (figure 5.4) [Shaw94]. At the high dopant levels required to efficiently absorb a diode-laser pump, up-conversion could substantially shorten the effective energy storage time. Upconversion-rate measurements by Shaw et al [Shaw94] yielded upconversion parameters of 0.12, 0.27 and 0.5×10^{-17}cm^3/s for 0.5, 1 and 2(at.)% doped Ho:YAG, respectively. It is worth mentioning that these values are fairly close to the measured values given by Barnes et. al. [Barnes03]. It has to be pointed out that heat dissipation due to upconversion processes is the source of main concern for Q-switched lasers and lasers with a high threshold. This is due to the fact that upconversion processes are more pronounced in non-lasing condition [Clarkson98].

However, in a pumping arrangement which does not require a very short absorption length, when the pump light has a good beam quality, the holmium concentration can be reduced to small values, because Ho:YAG lasers pumped near 2μm do not rely on any cross-relaxation processes (two for one cross-relaxation processes are an attractive feature of Tm:YAG laser). Hence, with a small dopant concentration of holmium in YAG, energy storage should be very efficient and high-energy Q-switched pulses can be expected, even under cw-pumping. This is due to the fact that the lifetime of the $^5I_7$ level of Ho^{3+} in YAG is

7.2ms and gives the potential for high energy storage of cw-pumped Q-switched lasers.

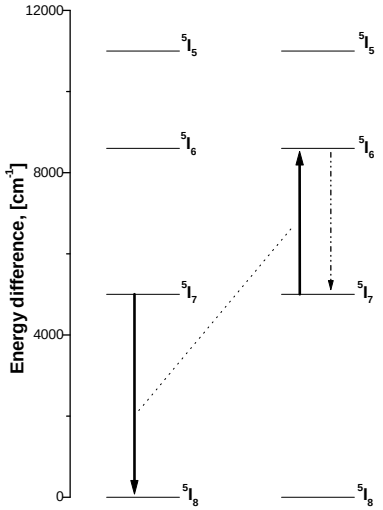

Figure 5.4: Upconversion in singly-doped Ho:YAG.

On the other hand, the relatively high emission cross-section is also a great advantage from the threshold and overall efficiency points of view. It has also important practical implications for the Q-switched operation of the laser [Payne92]. For efficient energy extraction the intracavity fluence should be at least comparable to the saturation fluence $\boldsymbol{F}_{sat,}$ which is, for a quasi-three-level, given by [Beach95]

$$F_{sat} = \frac{h\nu}{(1 + f_L / f_U)\sigma_{em}} \qquad (5.3)$$

$\boldsymbol{F}_{sat}$ is 7.9 J/cm^2 for the 2097nm transition of Ho:YAG. The damage threshold for many optical components and coating is specified at 20-40 J/cm^2 for pulses in the order of 100ns pulse length. For comparison the saturation fluence in Tm:YAG is 50J/cm^2 which means that for efficient energy extraction from a Q-switched Tm:YAG laser a strong design effort is required to ensure that the laser beam is large at all optical components. The risk is still high in Ho:YAG lasers, however,

efficient energy extraction should be possible without operating so close to the damage limit of the optical components.

5.2.6. Summary

Thus, spectroscopic studies of the Ho:YAG indicates that in a pumping arrangement which does not require a very short absorption length, that is a pump beam with good beam quality, the holmium concentration can be reduced to small values, since Ho:YAG lasers pumped around 2μm do not rely on any cross-relaxation process. These and many other attractive features such as; small quantum defect heating, reduced thermal loading and increased energy storage which in turn would result in efficient and high-energy Q-switched pulses, can be offered by in-band pumping of Ho:YAG. In-band end-pumping of Ho:YAG by a Tm^{3+}-doped silica fibre laser is what is explored in the next part of this chapter.

5.3. Ultra-efficient cw operation on Ho:YAG

5.3.1. Introduction

One of the main disadvantage of quasi-three-level lasers as compared to four-level lasers is their reabsorption loss due to the significant population in the lower laser level at room temperature. This leads to a number of deleterious effects, including increased laser threshold and reduced slope efficiency. However, by increasing the pump intensity to overcome the lower laser absorption, highly efficient laser operation can be achieved [Fan87, Lacovara91]. In general, the effective pump intensity in a laser medium is given by [Risk88]

$$I_p \approx \frac{\eta_{abs} P_{inc}}{\pi w_p^2} \qquad (5.4)$$

where η_{abs} is the absorption efficiency in the laser medium, P_{inc} is the incident pump power and w_p is the pump beam waist in the laser medium. Laser oscillation

occurs (assuming uniform pumping and extraction) when the effective pump intensity exceeds an absorbed threshold intensity I_{th}, which is given by [Risk88]

$$I_{th} = \frac{h\nu_p \left(L + T + 2 f_L N_t \sigma \ell\right)}{2\left(f_L + f_U\right)\sigma\tau} \qquad (5.5)$$

where $h\nu_p$ is the pump photon energy, T and L are the output coupler transmission and the resonator loss, N_t is the concentration of active ions in the laser host, σ and τ are the atomic cross section of the transition and the lifetime of the upper laser level, f_U and f_L are the fractional population of the Stark levels, which constitute the upper and lower laser level and ℓ is the laser rod length.

According to Giesen et. al. [Giesen94], for a high slope-efficiency operation in a quasi-three-level laser, a pump intensity of at least five times the local threshold intensity is required. The local threshold intensity, $I_{\ell,th}$, is given by subtracting the cavity losses, namely the term *(L+T)*, from equation 5.5 [Giesen94].

However, more accurate analysis for the effect of residual lower laser level population on laser operation is given by Fan at. al. [Fan87]. According to Fan et. al. [Fan87], the equation for reabsorption loss for end-pumped quasi-three-level lasers can be written as

$$\delta = f_L^P \sigma N_t \ell \frac{I_{sat}}{I_C} \ln\left(1 + \frac{2I_C}{I_{sat}}\right) \qquad (5.6)$$

where f_L^P is the fractional population of the pump Stark level. Here I_{sat} is the saturation intensity of the transition and given by

$$I_{sat} = \frac{h\nu_L}{\left(f_L + f_U\right)\sigma\tau} \qquad (5.7)$$

and I_C is the circulating intensity of the laser and given by

$$I_C = \frac{Sch\nu_L}{\pi n \ell w_L^2} \quad . \qquad (5.8)$$

In equations 5.6 and 5.7 $h\nu_L$ is the laser photon energy, n is the refractive index of the laser medium, w_L is the TEM_{00} laser beam radius, c is the speed of light, and S is the cavity photon number given by

$$S = \frac{2P_{out}\ell}{ch\nu_L\left(-\ln(1-T)\right)} \qquad (5.9)$$

here P_{out} is the output power of the laser.

From equation 5.6, it can be seen that for operation at low circulating intensity, i.e. when $2I_c/I_{sat}<<1$, the approximate value for saturable loss can be given by

$$\delta' = 2\sigma f_L^P N_t \ell \, . \qquad (5.10)$$

where N_t is the total dopant concentration. This means that at low circulating intensities the saturable loss is equal to the residual absorption because of the lower laser level population.

The analysis presented above provides a useful guide towards design of a highly efficient Ho:YAG laser. The main spectroscopic values of Ho:YAG used to calculate the above mentioned and other parameters throughout this chapter are given in table 5.3.

5.3.2. Experimental set-up

For pumping the Ho:YAG, the collimated output from the fibre laser (see figure 3.5) was focussed to a beam radius of $w_p \approx 215\mu m$, in the x-z and y-z planes, using a 200mm focal length lens, and the wavelength was tuned to the absorption peak at 1905nm in Ho:YAG. The confocal distance for the pump beam , Z, inside the Ho:YAG can be calculated via the following equation

$$Z = \frac{2n\pi w_P^2}{M_P^2 \lambda_P} \qquad (5.11)$$

where n is the refractive index of YAG given in table 5.3, M_p^2 is the beam quality factor of the incident pump beam which was equal to ~5, and λ_p is the pump wavelength. Thus with the choice of a pump beam size of 215μm the confocal distance was calculated to be $\approx$55mm. It was nearly eight times the effective pump absorption length of approximately 7mm for Ho:YAG with dopant level of 0.5*(at.)%*, ensuring good spatial overlap of the pump with the laser mode.

Property	**Value**
Laser transition frequency at 2097nm, ν_L [Hz]	1.43×10^{14}
Upper Laser $^5I_7$ Stark level Boltzman occupation factor, f_U	0.0748
Lower Laser $^5I_7$ Stark level Boltzman occupation factor, f_L	0.0113
Pump transition frequency at 1905nm ν_P [Hz]	1.57×10^{14}
Upper Pump $^5I_8$ Stark level Boltzman occupation factor, f_U^P	0.097
Lower Pump $^5I_8$ Stark level Boltzman occupation factor, f_L^P	0.157
Atomic cross section of the transition, σ [cm^2]	13.1×10^{-20}
Planck's constant, h [J/s]	6.6256×10^{-34}
Excited state storage lifetime, τ [ms]	7.2
Ho number density, N_0 [cm^{-3}]	1.38×10^{20}
Refractive index of YAG, n	1.82

Table 5.3: Some frequently used spectroscopic values of Ho:YAG.

A very simple, two mirror Ho:YAG resonator design was employed (see figure 5.5), comprising a flat input mirror with high reflectivity (>99.8%) at the lasing wavelength (2097nm) and high transmission (>95%) at the fibre pump wavelength (1905nm), and a concave output coupler with transmission, 20% at the lasing wavelength and with a radius of curvature, 300mm. A Ho:YAG crystal with Ho^{3+} concentration, 0.5*(at.)%* and length, 30mm was used as the gain medium. Both end faces were antireflection coated in the 1.8-2.1μm wavelength

regime. The laser rod was mounted in a water-cooled copper heat-sink maintained at a temperature of 18°C to allow efficient removal of waste heat, and was positioned <1mm from the plane mirror. With this arrangement, and using a total cavity length of approximately 35mm, the resonator was stable over the entire range of the pump power (see appendix A). The cavity TEM_{00} mode beam waist on the plane mirror calculated to be ≈226μm using the following equation [Koechner99]

$$w_L^2 = \frac{\lambda_L}{\pi}\left[L_{cavity}\left(R - L_{cavity}\right)\right]^{1/2} \qquad (5.12)$$

where λ_P is the lasing wavelength, R is the radius of curvature of the output mirror and L_{cavity} is the effective length of the cavity. According to resonator design calculations presented in Appendix A, the cavity TEM_{00} mode beam waist changed only by less than 5% over the length of the resonator.

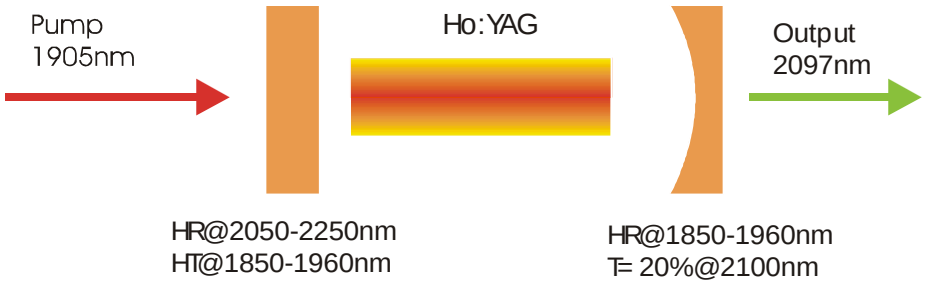

Figure 5.5: Ho:YAG set-up.

5.3.3. Results and discussion

Using the resonator design described above, we obtained room-temperature lasing at a threshold incident pump power of 1.3W, and with the maximum available Tm fiber laser power, of 9.1W incident on the Ho:YAG laser, 5.25W of output at 2097nm in a near diffraction-limited beam with M^2 value of ~1.2 (see circles in figure 5.6) was achieved. Only 80% of the incident pump power was absorbed in a single pass of the Ho:YAG crystal. However, by double-passing the pump we were able to achieve an absorption efficiency of ~96%. This results in an effective pump intensity, I_p, of ~6kW/cm^2 (see equation 5.4). This value is more than ten

times greater than the value required to overcome the absorbed threshold intensity, I_{th}, of ~0.53kW/cm^2 (see equation 5.5). Thus highly efficient cw operation should be expected.

The average slope efficiency with respect to incident pump power was ~71%. For pump power more than three times above threshold the slope efficiency increased to ~80% with respect to incident pump power. This increase is due mainly to saturation of the reabsorption loss. The circulating intensity I_c in the Ho:YAG is of the order of 18kW/cm^2 (see equation 5.8) and thereby fifteen times larger than the saturation intensity, I_{sat}, which is ~1.16kW/cm^2 (see equation 5.7). This results in a decrease of the reabsorption loss during operation (δ), calculated using equation 5.6 to be ~0.9%, by ~90% from its value for low circulating intensities (δ') of ~8.5% (see equation 5.10).

According to [Risk88], the slope efficiency with respect to pump power is given by

$$\frac{dP_{out}}{dP_{pump}} = \frac{T}{T+L}\left(\frac{\nu_L}{\nu_P}\right)\eta_{abs}\frac{dS}{dF} \qquad (5.13)$$

where T is the output mirror transmission, L is the resonator loss (including reabsorption but excluding output coupling loss), ν_L/ν_P is the quantum defect associated with transition, η_{abs} is the efficiency with which incident pump photons are absorbed and dS/dF is the efficiency with which absorbed pump photons are converted to laser photons and contains all the geometrical factors associated with the conversion of the incident pump photons to laser photons, in particular mode matching. Using the known and estimated values given above [T=20%, L=1.9% (0.9% reabsorption +1% other loss), ν_L/ν_P=0.91, η_{abs}=0.96 and dS/dF which we can approximate to be 0.95-1 in our case] the calculated slope efficiency with respect to incident pump power is ~76%-80%, which is in good agreement with the experimental value.

From figure 5.6, it can be seen that above threshold the Ho:YAG laser output power increases linearly with pump power suggesting that, for the simple laser configuration used in our experiment, the maximum output power was

limited mainly by the available pump power rather than by thermal effects. Thus, clearly there is scope for further increase in output power by increasing the Tm fibre laser power.

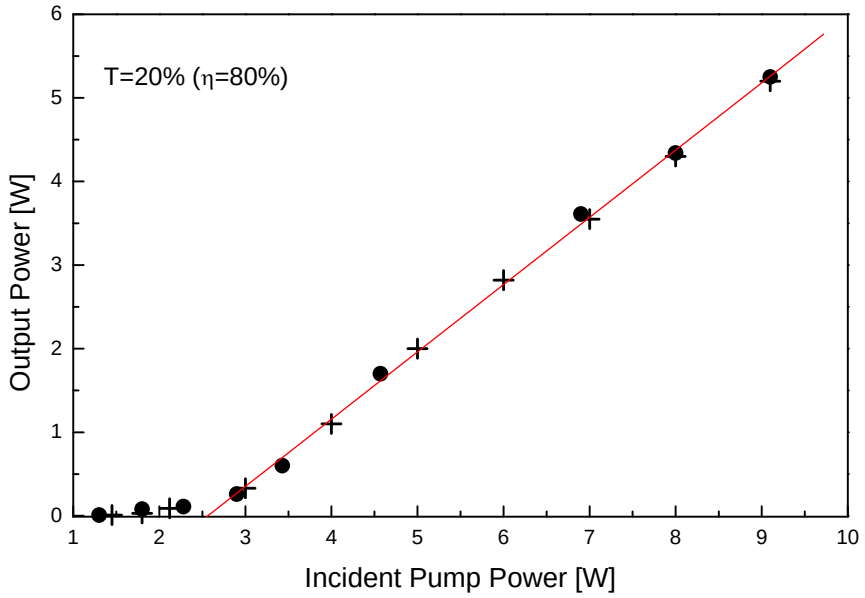

Figure 5.6: Output power versus pump power incident on Ho:YAG laser rod. The performance of the 0.5(at.%)-30mm laser rod and the 1.0(at.%)-20mm laser rod are shown with circles and crosses, respectively. The line is the best fit to the measured pointed far above the threshold. Here the experimental error was assessed to be ± 2%.

Figure 5.6 also shows (see crosses) the performance of room-temperature laser operation of a Ho:YAG laser with Ho^{3+} concentrations of 1.0(at.)% and a length of 20mm, which was investigated with the same cavity parameters as in the previous experiment. The level of performance in terms of output power (5.2W), slope efficiency (~78%) and beam quality (M^2~1.3) was comparable to that obtained for the 0.5(at.)% doped rod. The reabsorption loss during operation, at high circulation intensities, was calculated to be ~1.2% which was far below its value of ~11.3% at low circulation intensities. It has to be mentioned that for 1.0(at.%) ion concentration the obtained threshold pump power of ~1.45W, was ~10% higher than that obtained for 0.5(at%) ion concentration. This was thought to be mainly due to increase in upconversion losses for higher ion concentration which has the consequence of shortening the lifetime of the upper laser level

[Rustad96, Shaw94]. Thus one should consider the effective lifetime of the upper laser level. The value for the effective lifetime can be roughly estimated by [Mackenzie02]

$$\tau_{eff} = \frac{\tau}{KN_2} \quad (5.14)$$

where K represents the upconversion parameter for a given transition and concentration of the active medium and N_2 is the laser rod integrated excited state manifold density given by [Beach96]

$$N_2 = \frac{1}{f_L + f_U}\left[f_L N_t \ell + \frac{1}{2\sigma} \ln\left(\frac{1}{1-T}\right)\right] \quad (5.15)$$

Using equation 5.15 and taking a value of 0.25×10^{-17}cm^3/s for the upconversion parameter for the 1(at.)% doped Ho:YAG [Shaw94] results in a calculated value of ~4ms for the effective lifetime of the upper laser level. This value is ~1.35 times less than the calculated value of the effective upper laser level life time of ~5.4ms for 0.5(at.)% doped Ho:YAG. For the latter calculation the upconversion parameter of 0.12×10^{-17}cm^3/s for 0.5(at.)% doped Ho:YAG was taken from [Shaw94]. Thus, from the point of view of theory one could expect that threshold in the case of 1(at.)% doped Ho:YAG should be higher by the factor of 1.35 than in the case of 0.5(at)% doped rod. It is indeed not in the perfect agreement with the experimental values for threshold pump power, but still gives an idea of what one should expect in terms of threshold pump power.

5.3.4. Summary

In this chapter in addition to the spectroscopy of Ho:YAG, highly efficient room-temperature cw operation of a Ho:YAG laser end pumped by a cladding-pumped Tm-doped silica fibre laser was demonstrated. The Ho:YAG laser produced 5.25W of output power at 2097nm in TEM_{00} mode ($M^2\approx1.2$) for just 9.1W of incident pump power at 1905nm. This resulted in an optical-to-optical efficiency as high as ~58%. A slope efficiency with respect to incident pump power of 80%, very close to the quantum limit, was achieved. The potential for further power

scaling with prospects for high-pulse energy Q-switched operation, make the Tm-doped fibre laser pumped Ho:YAG laser suitable for various remote sensing applications.

5.4. References

[Barnes01] P. Barnes, W. A. Clarkson, D. C. Hanna, V. Matera, B. M. Walsh, " Tm:glass fibre laser pumping Ho:YAG and Ho:LuAG", Conference on Lasers and Electro-optics, paper CThV3, USA (2001).

[Barnes03] N. P. Barnes, B. M. Walsh, E. D. Filer, "Ho:Ho upconversion: applications to Ho lasers," J. Opt. Soc. Am. B, vol. 20, pp. 1212-1219 (2003).

[Basiev96] T. T. Basiev, Y. V. Orlovski, K. K. Pukhov, V. B. Sigachev, M. E. Doroshenko and I. N. Vorob'ev, "Multiphonon relaxation rates measurements and theoretical calculation in the frame of non-linear and non-Coulomb model of a rare-earth ion-ligand interaction," Journal of Luminescence, vol. 68(5), pp. 241-253 (1996).

[Beach95] R. J. Beach, "Optimization of quasi-three level end-pumped Q-switched lasers," IEEE Journal of Quantum Electronics, vol. 31(9), pp.1606-1613 (1995).

[Beach96] R. J. beach, "CW theory of quasi-three level end-pumped laser oscillators," vol. 123, pp. 385-393 (1996).

[Budni00] P. A. Budni, M. L. Lemons, J. R. Mosto, and E. P. Chicklis, "High-Power/High-Brithness Diode-Pumped 1.9um Thulium and Resonantly Pumped 2.1um Holmium Lasers," ", IEEE Journal of quantum Electronics, vol. 6(4), pp. 629-634 (2000).

[Clarkson98] W. A. Clarkson and D.C. Hanna, "Resonator design considerations for efficient operation of solid-state lasers end-pumped by high-power diode-bar,", Kluwer Academic Publisher, Dordrecht/Boston/London (1998).

[Fan87] T. Y. Fan, R. L. Byer, "Modeling and CW operation of a quasi-thrre level 946nm Nd:YAG laser," IEEE Journal of quantum Electronics, vol. 23, pp. 605-612 (1987).

[Fan88] T. Y. Fan, G. Hubber, R. L. Byer and P. Mitzscherlich, "Spectroscopy and diode laser pumped operation of Tm,Ho:YAG, ", IEEE Journal of quantum Electronics, vol. 24(6), pp. 924-933 (1988).

[Gruber91] J. B. Gruber, M. E. Hills, M. D. Seltzer, S. B. Stevens, C. A. Morrison, G.A. Turner and M.R. Kokta, "Energy-levels and crystal quantum states of trivalent holmium in yttrium-aluminium-granet," Journal of Applied Physics, vol. 69(12), pp.8183-8204 (1991).

[Giesen94] A. Giesen, H. Hugel, A. Voss, K. Wittig, U. Brauch and H. Owpower, "Scalable concept for diode-pumped high-power solid-state lasers," Appl. Phys., vol. B58, pp. 365-372 (1994).

[Henderson93] S. W. Henderson, P. J. M. Suni, C. P. Hale, S. M. Hannon, J. R. Magee, D. L. Burns and E. H. Yuen, "Coherent laser radar at 2 um using solid-state lasers," IEEE Transactions on Geoscience and Remote Sensing, vol.31 (1), pp.4-15 (1993).

[Kaminskii81] A. A. Kaminskii, Laser Crystals, 1-nd edn. (Springer-Varlag, Berlin Heidelberg New York, 1981.

[Koechner99] W. Koechner, Solid-State Laser Engineering, Springer-Varlag, Berlin Heidelberg, 1999, pp.201-205.

[Lacovara91] P. Lacovara, H. K. Choi, C. A. Wang, R. L. Aggarwal and T. Y. Fan, "Room-temperature diode-pumped Yb:YAG laser," Opt. Lett., vol. 16, pp. 1089-1091 (1991).

[Mackenzie02] J. I. Mackenzie, C. Li, D. P. Shepherd, R. J. Beach and S. C. Mitchell, "Modeling of high-power continuous-wave Tm:YAG side-pumped double-clad waveguide lasers," IEEE Journal of Quantum Electronics, vol. 38, pp. 222-230 (2002).

[Nabors95] C. D. Nabors, J. Ochoa, T. Y. Fan, A. Sanchez, H. K. Choi, and G. W. Turner, "Ho:YAG laser pumped by 1.9um diode laser," IEEE Journal of Quantum Electronics, vol. 31 (9), pp. 1603-1605 (1995).

[NASA02] NASA Langley, spectroscopic database, 2002, Website *http://aesd.larc.nasa.gov*

[Payne92] S.A. Payne, L.L. chase, L.K. Smith, W.L. Kway and W.F. Krupke, "Infrared cross-section measurements for crystals doped with Er^{3+}, Tm^{3+}, and Ho^{3+}," IEEE J. Quantum Electron, vol. 28, pp.2619-2630 (1992).

[Risk88] W. P. Risk, "Modeling of longitudinally pumped solid-state lasers exhibiting reabsorption losses," Journal of the Optical Society of America B-Optical Physics, vol. 5 (7), pp. 1412-1423 (1988).

[Rustad96] G. Rustad and K. Stenersen, "Modeling of laser-pumped Tm and Ho lasers accounting for upconversion and ground-state depletion," IEEE J. Quantum Electron, vol. 32 (9), pp.1645-1656 (1996).

[Shaw94] L. B. Shaw, R. S. Chang and N. Djeu, "Measurment of up-conversion energy transfer probabilities in Ho:YAG and Tm:YAG,", Phys. Rev. B, vol. 50, pp. 6609-6619 (1994).

[Walsh98] B. M. Walsh, N. P. Barnes and B. DiBartolo, "Branching rations, cross-section and radiative lifetimes of rare earth iones in solids: Application to Tm^{3+} and Ho^{3+} ions in $LiYF_4$," J. Appl. Phys., 83, 2772-2787 (1998).

Chapter 6

Summary of Research and Future Directions

6.1. Introduction

The desire to investigate a new approach for power scaling and, more importantly, brightness scaling of two-micron solid-state laser sources, motivated the research that has been presented in this thesis. Such sources could find many applications, with the most important one being laser remote sensing. Our strategy was based on reduction of heat generation within the laser medium. Thus, the first step was to choose a medium in which the quantum defect heating due to the difference between pump and laser photon energies is minimised. The most suitable candidate was Ho:YAG due to its favourable spectroscopic properties, long upper-laser-level lifetime, thermo-mechanical properties and finally an excellent atmospheric transmission around the 2.1μm wavelength region. The second step was to reduce heat dissipation within the laser medium by using a long laser rod with low active ion concentration. That served to reduce the extra contribution to thermal loading due to energy transfer upconversion. These requirements emphasise the need for a high-power pump source at 2μm with a good beam quality to allow focusing to small beam sizes whilst minimising the diffraction spreading of the pump beam over the long length of the laser medium. A Tm-doped silica fibre laser was just the right candidate due to its broad emission spectrum in the 2μm spectral region and its absorption line at 0.79μm for which high-power diode-bars are readily available.

Thus the work presented here was divided into two closely linked areas. The first area of research was devoted to construction of a high-power tunable two-micron source based on Tm-doped silica fibre, whilst the second part of the research was devoted to construction of a high-power two-micron hybrid laser based on a Ho:YAG crystal. In the following sections the achievements in each of these areas are summarised and some possible future directions discussed.

6.2. High-Power Tunable Two-micron Fibre Lasers

6.2.1. Summary of research

Chapter 3 and chapter 4 of this thesis were devoted to research conducted on developing a high-power tunable Tm-doped silica fibre laser. In chapter 3 a high-power cladding-pumped tunable Tm^{3+}-doped silica fibre laser with 10.5W of output power at 1921nm was presented. The laser was tunable from 1855 to 2070nm at multiwatt power levels. In this chapter the effect of cooling on the fibre performance has also been investigated.

In chapter 4, a simple way for power scaling in fibre lasers was explored. The result was a high-power beam-combined Tm^{3+}-doped silica fibre laser system with 14W of output power in the 2μm wavelength region. This output power was achieved simultaneously on four lines at wavelengths, 1926nm, 1956nm, 1981nm and 2001nm. The beam-combined system was tunable over a range of 200nm from 1.9μm to 2.1μm with multiwatt output power.

6.2.2. Future directions

Whilst the fibre laser work can be considered a success, however further power scaling would be of great interest. Given the fact that the present generation of Tm-doped fibres suffer from the disadvantage that the effective numerical aperture of the inner-cladding is significantly lower than the value of numerical aperture calculated from the effective refractive indices of pure silica inner-cladding and the outer coating, one of the research directions that follow from this work could be: Investigation of alternative cladding-pumped Tm-doped silica fibre laser designs for operation with high-power fibre-coupled diode pump

sources of low brightness. The main aim of this research would be to determine how the laser performance of the present generation of Tm-doped fibre lasers would be affected by using ultra high-power (>300W) low brightness pump sources, and to consider ways to increase the effective numerical aperture of the inner-cladding pump guide to improve launch efficiency and hence laser performance. A number of different design options could be considered including the use of lower index and/or lower loss outer coatings. Another option is the use of Tm-doped fibre with larger cores and smaller cladding-to-core area ratios. This would allow efficient pump absorption in a short device length. It will open up the possibility for core pumping of Tm-doped fibre at 1.6μm by a Yb:Er-doped fibre laser, i.e. pumping directly into the upper manifold of the laser transition. This would serve to greatly reduce the fraction of pump light converted to heat and thus highly efficient cw laser operation should be possible. On the other hand, a shorter length of the device will allow the laser oscillation to be tuned into the far wings of the laser transition. This is specially important when the emission wavelength shifts from the line centre towards the shorter wavelength limit. It has to be pointed out that a larger core size will lead to a multimode output, which could be detrimental for some applications.

Another research direction that could in principle lead on from the work presented in this section of the research could be the frequency doubling of the Tm-doped silica fibre laser to 980nm. A stable high-power source at 0.98μm with good beam quality for Er-doped fibre amplifier (EDFA) would attract a great deal of attention since current diode sources at 980nm are expensive and hard to scale. In this context one can in addition to traditional routes for frequency doubling also investigate the possibility of exploring an all fibre source based on recent advances in the poling of fibres.

Another possibility could be based on using a high-power Tm-doped silica fibre laser for cw pumping of a cw optical parametric oscillator (OPO) spanning the 3-5μm spectral region. This would be an attractive source due to the coverage of the wide mid-IR atmospheric transmission region.

6.3. Two-micron Fibre-Bulk Hybrid Lasers

6.3.1. Summary of research

Chapter 5 of this thesis were devoted to the research conducted on developing highly efficient Ho:YAG lasers end pumped by the cladding-pumped Tm-doped silica fibre laser. In this chapter, in addition to the spectroscopy of Ho:YAG, an ultra-efficient room-temperature Ho:YAG laser was presented. The Ho:YAG laser produced 5.25W of output power at 2097nm in the TEM_{00} mode ($M^2 \approx 1.2$) for just 9.1W of incident pump power at 1905nm. This resulted in an optical-to-optical efficiency as high as ~58%. The achieved slope efficiency with respect to incident pump power of 80% was very close to the quantum limit.

It is to some extent unfortunate that Ho:YAG lasers demonstrated in this thesis are both cw lasers as one of the main aims from the beginning was to develop a pulsed source based on this material. However, this was not achieved mainly due to constraints on time.

6.3.2. Future directions

There are a few research directions that lead on from the work presented here. Some of them are a logical progression of the work. For instance, investigation the merits of using alternative Tm or Ho-doped crystals in the bulk laser. This work was concentrated on Ho:YAG, but there are many other solid-state laser crystals which have attractive features for in-band pumped operation in the 1.9-2.1μm spectral region. For example, Ho:YLF has a much longer upper laser level lifetime (~14ms) compared to Ho:YAG (~7.2ms), suggesting that it may be attractive for Q-switched operation at low repetition rates.

On the other hand, upconversion related heat can have a marked effect on laser design for Q-switched lasers as the laser must operate with a high inversion density for a period before the cavity Q is switched. Thus, another line for research could be based on the thermal lensing measurements for all promising laser crystals in order to extract some information on the upconversion related heating in the laser medium. This course of research may also lead to some quantification of the aberrated thermal lens which would greatly aid laser design.

The flexibility in the operating wavelength and good beam quality afforded by high-power Tm-doped silica fibre lasers opens up a possibility for exploring radiation-balanced lasing in an end-pumped Ho:YAG laser. The idea of laser cooling within a laser medium is generally considered as a possible practical means for reducing the net heat generation and hence an attractive route towards power-scaling free from the problems associated with thermal loading [Epstein95, Epstein01, Bowman99, Hoyt00]. However, while the physical mechanism behind radiation cooling is relatively simple, the conditions for efficient laser cooling are quite demanding. Thus, a research project based on this idea could be quite challenging!

6.4. Conclusion

From the research presented in this thesis, it is evident that Fibre-Bulk Hybrid Lasers combine the advantages of fibre and bulk solid-state lasers. The focus here was on the 2µm spectral region where a high-power tunable Tm-doped silica fibre laser enable us to efficiently end-pump a number of Ho:YAG lasers. However no one could fail to have his thought turn to 1.6µm fibre-bulk hybrid lasers where a high-power tunable Yb:Er-doped fibre laser could be used to end-pump Er-doped crystals which in turn have the attraction of long upper laser level life time. In this context 1.6µm and 2µm lasers can seriously challenge the long-stabilised dominance of 1µm lasers.

6.5. References

[Bowman99] S. R. Bowman, “Lasers without internal heat generation,” IEEE J. of Quantum Electron., vol. 35, pp. 115-122 (1999).

[Epstein95] R.I. Epstein, et. al., “Observation of laser-induced cooling of a solid,” Nature, vol. 377, pp.500-502 (1995).

[Epstein01] R. I. Epstein, et. al., “Measurement of optical refrigeration in ytterbium-doped crystals,” J. of Appl. Phys., vol. 90 (9), pp. 4815-4819 (2001).

[Hoyt00] C. W. Hoyt et. al., “Observation of Anti-Stocks Fluorescence Cooling in Thulium-Doped Glass,” Phys. Rev. Lett., vol. 85 (17), pp. 3600-3603 (2000).

Appendix A

Example of Matcad Resonator Design Program: Application to Two-Mirror Cavity of chapter 5.

Define constants

$c := 2.99 \cdot 10^{8}$ $\lambda s := 2097 \cdot 10^{-9}$

$M1 := 50^{20}$ $h := 6.64 \cdot 10^{-34}$

$M2 := 300$ $\theta := 0$

$nair := 1$ Refractive index of air

$d1 := 1$ $lcry := 30$

$d2 := 4$ $ncry := 1.82$

Define the component matrices

$$L1(d1) := \begin{bmatrix} 1 & \frac{d1}{1000} \\ 0 & 1 \end{bmatrix} \qquad L2(d2) := \begin{bmatrix} 1 & \frac{d2}{1000} \\ 0 & 1 \end{bmatrix} \qquad Mcry := \begin{bmatrix} 1 & \frac{lcry}{1000} \cdot \frac{nair}{ncry} \\ 0 & 1 \end{bmatrix}$$

Define the mirror matrices

$$Mm2ta := \begin{bmatrix} 1 & 0 \\ \frac{-2}{\frac{M2}{1000} \cdot \cos(\theta)} & 1 \end{bmatrix} \qquad Mm1ta := \begin{bmatrix} 1 & 0 \\ \frac{-2}{\frac{M1}{1000} \cdot \cos(\theta)} & 1 \end{bmatrix}$$

$$Mm2sa := \begin{bmatrix} 1 & 0 \\ \frac{-2 \cdot \cos(\theta)}{\frac{M2}{1000}} & 1 \end{bmatrix} \qquad Mm1sa := \begin{bmatrix} 1 & 0 \\ \frac{-2 \cdot \cos(\theta)}{\frac{M1}{1000}} & 1 \end{bmatrix}$$

Define single pass matrices left to right from input coupler

$$LRta(d1, d2) := Mm2ta \cdot L2(d2) \cdot Mcry \cdot L1(d1)$$

$$LRsa(d1, d2) := Mm2sa \cdot L2(d2) \cdot Mcry \cdot L1(d1)$$

Define single pass matrices right to left from input coupler

$$RLta(d1, d2) := Mm1ta \cdot L1(d1) \cdot Mcry \cdot L2(d2)$$

$$RLsa(d1, d2) := Mm1sa \cdot L1(d1) \cdot Mcry \cdot L2(d2)$$

Total round trip for input coupler

$$TRICta(d1, d2) := RLta(d1, d2) \cdot LRta(d1, d2)$$

$$TRICsa(d1, d2) := RLsa(d1, d2) \cdot LRsa(d1, d2)$$

Calculate spot size at the input coupler

$$wicta(d1, d2) := \left[\sqrt[4]{\left[\frac{2 \cdot \lambda s \cdot TRICta(d1, d2)_{0,1}}{\pi \cdot \sqrt{4 - \left(TRICta(d1, d2)_{0,0} + TRICta(d1, d2)_{1,1} \right)^2}} \right]^2} \right]$$

$$wicsa(d1, d2) := \left[\sqrt[4]{\left[\frac{2 \cdot \lambda s \cdot TRICsa(d1, d2)_{0,1}}{\pi \cdot \sqrt{4 - \left(TRICsa(d1, d2)_{0,0} + TRICsa(d1, d2)_{1,1} \right)^2}} \right]^2} \right]$$

$$wicta(d1, d2) = 2.272 \cdot 10^{-4}$$

$$wicsa(d1, d2) = 2.272 \cdot 10^{-4}$$

Radius of curvature at input coupler

$$RtaIP(d1,d2) := 2\cdot\frac{TRICta(d1,d2)_{0,1}}{TRICta(d1,d2)_{1,1} - TRICta(d1,d2)_{0,0}}$$

$$RtaIP(d1,d2) = 7.186\cdot10^{14}$$

Complex beam parameter at input coupler

$$qL := \left(\frac{1}{RtaIP(d1,d2)} - \frac{i\cdot\lambda s}{\pi\cdot wicta(d1,d2)^2}\right)^{-1}$$

$w_0 := wicta(d1,d2)$ define spot size $dz := 0.001$ move 1mm

$q_0 := qL$ define beam parameter $nair = 1$ refractive i

$j := 1,2..\ d1$ define distance

$q_j := q_{j-1} + \frac{dz}{nair}$ complex beam parameter per mm over defined length

$w_j := \left(\sqrt{\frac{-\pi}{\lambda s}\cdot Im\left(\frac{1}{q_j}\right)}\right)^{-1}$ spot size for beam parameter per mm over def

$j := (d1) + 1..\ (d1) + 30$

$q_j := q_{j-1} + \frac{dz}{ncry}$

$w_j := \left(\sqrt{\frac{-\pi}{\lambda s}\cdot Im\left(\frac{1}{q_j}\right)}\right)^{-1}$

$j := (d1) + 30 + 1..\ (d1) + 30 + (d2)$

$q_j := q_{j-1} + \frac{dz}{nair}$

$$w_j := \left(\sqrt{\frac{-\pi}{\lambda s}\cdot \mathrm{Im}\left(\frac{1}{q_j}\right)}\right)^{-1} \qquad Lcav := d1 + lcry + d2$$

$$k := 0, 1 .. Lcav$$

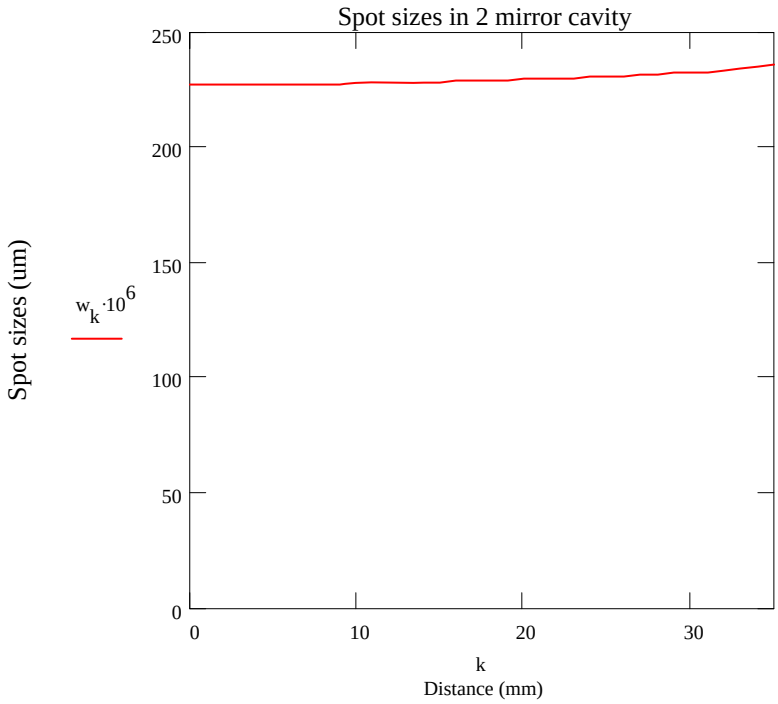

Calculate the stability

$$Ssa(d1, d2) := \frac{\left(TRICsa(d1, d2)_{0,0} + TRICsa(d1, d2)_{1,1}\right)}{2}$$

$$Sta(d1, d2) := \frac{\left(TRICta(d1, d2)_{0,0} + TRICta(d1, d2)_{1,1}\right)}{2}$$

$$L := 0 .. 100$$

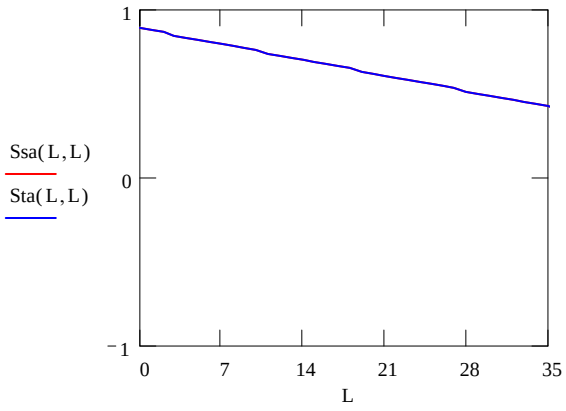

Total round trip for output coupler

$$TROCta(d1,d2) := LRta(d1,d2)\cdot RLta(d1,d2)$$

$$TROCsa(d1,d2) := LRsa(d1,d2)\cdot RLsa(d1,d2)$$

Calculate spot size at the output coupler

$$wocta(d1,d2) := \sqrt[4]{\left[\frac{2\cdot\lambda s\cdot TROCta(d1,d2)_{0,1}}{\pi\cdot\sqrt{4-\left(TROCta(d1,d2)_{0,0}+TROCta(d1,d2)_{1,1}\right)^2}}\right]^2}$$

$$wocsa(d1,d2) := \sqrt[4]{\left[\frac{2\cdot\lambda s\cdot TROCsa(d1,d2)_{0,1}}{\pi\cdot\sqrt{4-\left(TROCsa(d1,d2)_{0,0}+TROCsa(d1,d2)_{1,1}\right)^2}}\right]^2}$$

$$wocta(d1,d2) = 2.358\cdot 10^{-4}$$

$$wocsa(d1,d2) = 2.358\cdot 10^{-4}$$

Appendix B

Modeling of CW Ho:YAG Laser: Application to optimization of crystal length for a given concentration

This model is based on models presented in [Beach96] and [Mackenzie02] and includes the effect of upconversion and also consider the effect of double-passing of pump power on laser performance.

Laser 2097nm photon energy ----------hνl [J]
Laser 5I7 Stark level Boltzman occupation factor ----------fla
Laser 5I7 Stark level Boltzman occupation factor ----------flb
Spectroscopic laser emission cross section ----------σl [cm2]

Pump 1905nm photon energy ----------hνp
Pump 5I8 Stark level Boltzman occupation factor ----------fpa
Pump 5I8 Stark level Boltzman occupation factor ----------fpb
Spectroscopic pump absorption cross section ----------σp

Planck's constant ----------h [J/s]
Pump transition frequency ----------νp
Laser transition frequency ----------νl
Rod radius ----------r [cm]
Rod area ---------- a [cm2]
Rod length ----------ls [cm]
Excited state storage lifetime ----------τ [s]
Pump power ----------Pp [W]
Modefill efficiency ----------ηmode
Pump delivery efficiency ----------ηdel
One-way cavity transmission ----------T
Ho number density ----------n0 [cm-3]
Laser output coupler reflectivety ----------R
Pump reflectivity at the laser output end of the rod ----------Rp
Ho Concentration----------n%
Upconversion coefficient.....……..... K[cm3/s]

$h := 6.625610^{-34}$ $n\% := 1 \cdot 0.5$ $fll := 0.0113$ $fpl := 0.157$

$\nu p := 1.57 \cdot 10^{14}$ $n0 := n\% \cdot 1.38 \cdot 10^{20}$ $flu := 0.0748$ $fpu := 0.097$

$\nu l := 1.43 \cdot 10^{14}$ $n0 = 6.9 \cdot 10^{19}$ $\sigma l := 13.1 \cdot 10^{-20}$ $\sigma p := 13.1 \cdot 10^{-20}$

$\tau := 7.2 \cdot 10^{-3}$ $R := 0.8$ $\eta mode := 1$ $\sigma p := \sigma l$

$ls := 1, 1.5 .. 6$ $Pp := 9.1$ $\eta del := 1$ $wp := 215 \cdot 10^{-4}$

$K := 0.12 \cdot 10^{-17}$ $T := 0.98$ $\eta := 1$

$Rp := 1$

N2 is defined as the rod-integrated excited state manifold density and given by

$$N2(ls) := \left(\frac{1}{fll + flu}\right) \cdot \left[(fll \cdot n0 \cdot ls) + \frac{1}{2 \cdot \sigma l} \cdot \ln\left(\frac{1}{T^2 \cdot R}\right)\right]$$

N2l and N2p are the rod -integrated inversion densities referenced to the Stark levels coupled by the laser radiation and pump radiation

$$N2l(ls) := (fll + flu) \cdot N2(ls) - fll \cdot n0 \cdot ls$$

$$N2p(ls) := (fpl + fpu) \cdot N2(ls) - fpl \cdot n0 \cdot ls$$

In the steady state, the fraction of incident pump power delivered to the laser rod which is absorbed in a single pass though the laser rod is

$$Fa(ls) := 1 - e^{\eta \cdot \sigma p \cdot N2p(ls)}$$

The rate at which photons are absorbed out of the pump excitation beam by the lasant iones, remembering that the pump intensity that reaches the right side of the rod is reflected with reflectivity Rp back into and down the rod, is given by

$$Rex(ls) := Pp \cdot \frac{\eta del}{h \cdot \nu p} \cdot (1 - Fa(ls)) \cdot \left(1 + Rp \cdot e^{\eta \cdot \sigma p \cdot N2p(ls)}\right)$$

Effective lifetime of upper laser level

$$\tau eff(ls) := \frac{1}{\tau^{-1} + K \cdot N2(ls)}$$

$$\eta slope(ls) := \eta mode \cdot \eta del \cdot \frac{\nu l}{\nu p} \cdot \frac{(1-R)}{R} \cdot \left(1 - e^{\eta \cdot \sigma p \cdot N2p(ls)}\right) \cdot \frac{\left(1 + Rp \cdot e^{\eta \cdot \sigma p \cdot N2p(ls)}\right)}{\left(e^{\sigma l \cdot N2l(ls)} - 1\right) \cdot \left(T^2 \cdot e^{\sigma l \cdot N2l(ls)} + 1\right)}$$

$$Pth(ls) := h \cdot \nu p \cdot N2(ls) \cdot \frac{\pi \cdot wp^2}{\eta del \cdot \tau eff(ls)} \cdot \frac{1}{\left(1 - e^{\eta \cdot \sigma p \cdot N2p(ls)}\right) \cdot \left(1 + Rp \cdot e^{\eta \cdot \sigma p \cdot N2p(ls)}\right)}$$

$$Pout(ls) := \eta slope(ls) \cdot (Pp - Pth(ls))$$

Output power (W) $Pout(ls) = 6.161$

Slope efficiency $\eta slope(ls) = 0.769$

Threshold pump power $Pth(ls) = 1.092$

Absorbed pump power

$Pabs(ls) := (Fa(ls)) \cdot Pp$ $Pabs(ls) = 8.631$

0.5(at.)% Ho:YAG

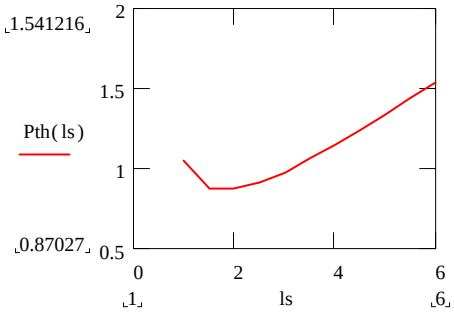

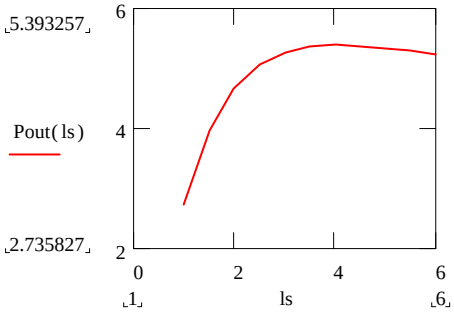

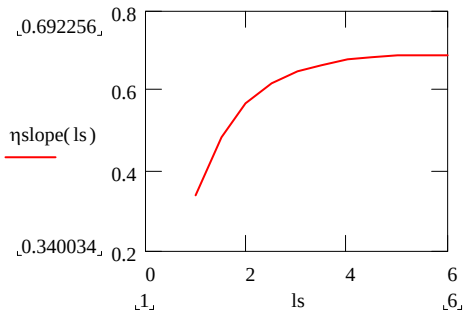

1(at.)% Ho:YAG

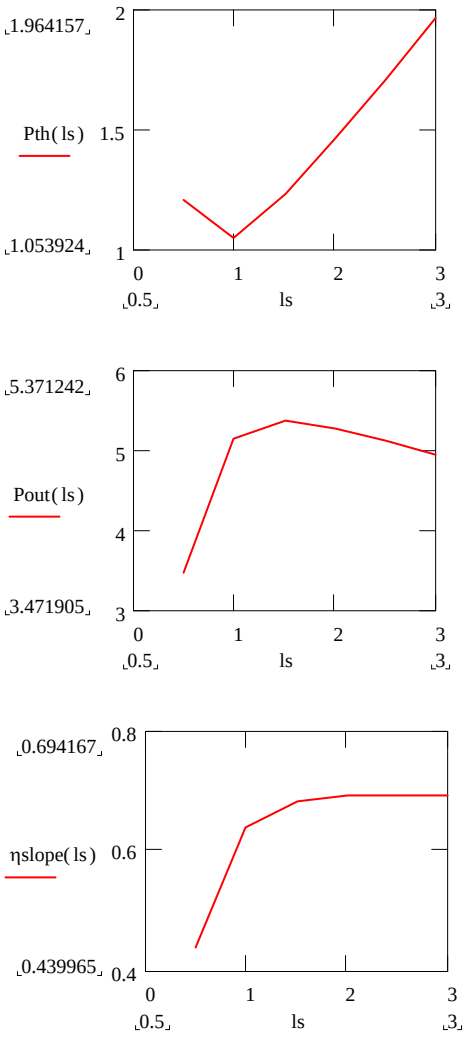

References

[Beach96] R. J. beach, “CW theory of quasi-three level end-pumped laser oscillators,” vol. 123, pp. 385-393 (1996).

[Mackenzie02] J. I. Mackenzie, C. Li, D. P. Shepherd, R. J. Beach and S. C. Mitchell, “Modeling of high-power continuous-wave Tm:YAG side-pumped double-clad waveguide lasers,” IEEE Journal of Quantum Electronics, vol. 38, pp. 222-230 (2002).

List of Publications related to this thesis

Publications in Journals & Proceedings

1. A. Abdolvand, D. Y. Shen, L. J. Cooper, R. B. Williams and W. A. Clarkson, *Ultra-efficient Ho:YAG laser end-pumped by a cladding-pumped Tm-doped silica fibre laser*, OSA Trends in Optics & Photonics, Vol. 83, pp. 7-12 (2003).

2. W. A. Clarkson, A. Abdolvand, D. Y. Shen, R. B. Hayward, L. J. Cooper, R. B. Williams and J. Nilsson, *High power two-micron fiber lasers*, SPIE Proceedings on Gas and Chemical Lasers - High Power Lasers, Vol. 5120, pp. 482-489 (2003). **Invited**

3. A. Abdolvand, V. Matera, T. M. J. Kendall, P. W. Turner and W. A. Clarkson, *High-power beam-combined cladding-pumped Tm-doped silica fibre lasers*, To be submitted to Applied Optics.

4. D.Y. Shen, A. Abdolvand, L. J. Cooper and W.A. Clarkson, *Efficient Ho:YAG laser pumped by a cladding-pumped tunable Tm:silica fiber laser*, Applied Physics B, vol. 79(5), pp. 559 (2004).

Conference papers

5. A. Abdolvand, D. Y. Shen, L. J. Cooper, R. B. Williams and W. A. Clarkson, “Highly efficient Ho:YAG laser pumped by a Tm-doped silica fibre laser,” Conference on Lasers and Electro-Optics(CLEO)/America, Maryland(2003), Paper: CThM38.

6. W. A. Clarkson, A. Abdolvand, V. Matera, T. M. J. Kendall, D. C. Hanna, J. Nilsson and P. W. Turner, “Spectral beam combining of cladding-pumped Tm-doped silica fibre lasers,” Quantum Electronics & Photonics Confrence(QEP-15)/Glasgow, pp.13 (2001).

7. W.A. Clarkson, V. Matera, A. Abdolvand, T.M.J. Kendall, J. Nilsson, P.W. Turner and D.C. Hanna, “Power scaling of cladding-pumped Tm-doped silica fibre lasers,” Conference on Lasers and Electro-Optics(CLEO)/Europe-EQEC/Munich, pp.141 (2001).

8. A. Abdolvand, D. Y. Shen, L. J. Cooper, R. B. Williams and W. A. Clarkson, “Ultra-efficient Ho:YAG laser end-pumped by a cladding-pumped Tm-doped silica fibre laser,” Advanced Solid-State Photonics (ASSP), San Antonio, Texas, Paper: MA7 (February 2-5, 2003).

9. W.A.Clarkson, V.Matera, T.M.J. Kendall, A. Abdolvand, J.Nilsson, P.W.Turner, D.C.Hanna,“High-power wavelength-combined cladding-pumped Tm-doped silica fibre lasers,” OSA TOPS Vol. 56, CWM2 (2001).